Mechanics of Organoid Formation and Repair

Alejandra Guzmán Herrera

A dissertation submitted in partial fulfillment

of the requirements for the degree of

Doctor of Philosophy

Field of study

Developmental Biophysics

Laboratory for Molecular Cell Biology

University College London

October 2023

I, Alejandra Guzmán Herrera confirm that the work presented in this thesis is my own. Where information has been derived from other sources, I confirm that this has been indicated in the thesis.

Abstract

Mechanics has an important effect on tissue morphology during development and regeneration, influencing how efficiently a tissue repairs itself. The liver is an organ with striking regenerative abilities that has been widely studied at a molecular and genetic level, however, the mechanical aspect remains unclear. While the study of such processes has recently been facilitated by the development of liver organoids that recapitulate a ductal regenerative response in vitro, the main focus has remained on the underlying molecular and genetic details. Nonetheless, the importance of tissue morphology and mechanics has become more apparent.

The aim of this project is to better understand the role mechanics play in liver regenerative morphogenesis using mouse organoids. I first characterise organoid morphology, which starts as a spherical and translucent cell monolayer that either remains spherical or becomes more complex and multi-layered upon differentiation. I then provide evidence that the final morphology of differentiated liver organoids correlates with their cell composition.

Interestingly, complex morphologies also emerge without chemical differentiation. Since the mechanoenvironment has been shown to induce and regulate cell differentiation, I investigate the effect of substrate mechanical properties (i.e. stiffness) on liver organoids. The data suggests substrate stiffness does have an important effect on organoid morphologies and their cell profile.

Finally, I examine the mechanical properties of the organoids themselves, how they change as they differentiate, and how this affects their ability to respond to further damage. The results show the fluid state of progenitor organoids changes after differentiation, impacting how the cells respond to injury.

By studying the mechanical aspect of liver regenerative morphogenesis in organoids, we hope to contribute to a better understanding of how and why the injured tissue chooses one mechanism over another amongst the numerous ways in which the liver can respond to injury.

Impact Statement

Since the introduction of organoids as a new model system, they have been used to study and replicate, to an extent, the composition and physiology of organs at different stages: development, homeostasis, and disease [1, 2, 3, 4, 5]. In recent years, there have been more efforts in developing tools to manipulate the mechanical environment in which organoids grow to control and improve their organisation, morphology, and physiology. These advances are bringing organoids closer to what it is observed *in vivo* and are working towards their used in medical applications, in particular personalised medicine [6, 7, 8, 9].

The overarching goal of this dissertation is to study the role mechanics in liver organoid formation and repair. An important step towards better understanding and improving organoid systems, as well as the bio-mechanical characteristics of liver regenerative morphogenesis and injury responses. The findings of this work will contribute to broaden the basic knowledge and understanding of tissue biophysics and liver repair, as well as potential future medical applications for organoid systems and liver regeneration.

Acknowledgements

I want to thank my supervisor, Prof. Yanlan Mao, for receiving me in her group, her mentoring, and her academic and financial support during my PhD.

My thesis committee, Dr. Julie Pitcher, Prof. Guillaume Charras, and Prof. Franck Pichaud, for their advice and guidance.

I also want to thank our collaborators, Dr. Luigi Aloia, Dr. Eileen Gentleman, Prof. Trevor Dale, and the members of their labs for sharing their knowledge and resources, and for contributing to the development and progress of this project.

Dr. Emma Rawlins and Dr. Rashmi Priya for taking the time to read and comment on this work as my examiners.

I would like to acknowledge the financial support from CONACYT Beca en el Extranjero - Gobierno de la Ciudad de México, UCL Overseas Research Scholarship (ORS), and UCL Graduate Research Scholarship (GRS). Without their financial support I would not have been able to begin and continue this PhD.

Thank you to all the previous and current staff members of the LMCB for keeping it functioning and helping with all the major and minor everyday tasks.

I want to thank all the people I have met at the LMCB and UCL for being part of this journey in one way or another. The IPLS members for amazing events and discussions about the physics of life. The pre-pandemic 'cool office' 2.23 and yoga club.

Thank you to all past and current members of the Mao lab for making it a fun place to do and talk about science (or any random topic). To the students I have supervised for their help and enthusiasm. To Rob Tetley for teaching me all about flies even though none of it made it into this thesis. To Natalie Kirkland for all the gossip and chocolate biscuits. To Ricardo Barrientos for all those water pints and constant 'positivism'. To Nargess for lovely chats over tea and cultural exchanges. To Giulia for your advice and chats about life. To Pablo for laughing and crying in Spanish with me. To Jimmy for all the TC chats and bad puns that I do not understand. To Shu En for the cute doodles and making me not hate frogs. Thank you for all the tissue tears and laughter.

To the incredible friends from around the world that I have met living in the UK. In particular Maria Pace, thank you for sharing with me the perks of living in London, all the pastini, and your banana bread! As well as Alice C. Yuen, for all those endless meals, walks, reels, and rants about everything and nothing. Thank you both for your friendship and for making me feel at home.

To my friends from home for their continued support and friendship despite the distance, and for always making time to catch up when we have the chance.

To Aldo Carmona Baez for your invaluable friendship, advice, and jokes. Thank you for continuing sharing this journey with me and for planning crazy alternative futures that will for sure happen one day.

To José Alquicira Hernández for always being there in every possible way. Thank you for sharing music, tea, and all the good and bad times throughout all these years.

Finally but most importantly, I want to thank my family. A mis hermanos, por su ejemplo y apoyo desde pequeña, por molestarme aún a la distancia, y por hacer todo lo posible para reunirnos en cualquier parte del mundo. A mis padres, gracias por todas sus enseñanzas, su paciencia, cariño, y apoyo constante. Gracias por todo lo que han hecho y siguen haciendo por mis hermanos y por mí.

Contents

List of Figures

List of Tables

Abbreviations

AFM: Atomic Force Microscopy

AJ: Adherens Junction

Alb: Albumin

BSA: Bovine Serum Albumin

CMAC: Cell-Matrix Adhesion Complex

Crb: Crumbs

DM: mICO Differentiation Medium

E-cad: E-cadherin

ECM: Extracellular Matrix

EdU: Ethynyldeoxyuridine

EM: mICO Expansion Medium

EpCAM: Epithelial Cell Adhesion Molecule

ESCs: Embryonic Stem Cells

FAK: Focal Adhesion Kinase

FBS: Fetal Bovine Serum

Ft: Fat

iPCs: induced Pluripotent Stem Cells

HSCs: Hepatic Stellate Cells

JNK: Jun N-terminal kinase

mICO: mouse Intrahepatic Cholangiocyte Organoid

MSC: Mesenchymal Stem Cell

n.s.: not significant

OJ: Occluding Junction

Par: Partitioning defective

PBS: Phosphate Buffered Saline

PEG: Polyethylene glycol

PcG: Polycomb-group

PDMS: Polydimethylsiloxane

PEG: Polyethylene glycol

RGD: arginine-glycine-aspartic acid

ROI: Region of interest

ROS: Reactive Oxygen Species

Rock: Rho kinase

RT: Room Temperature

rt-qPCR: real time quantitative PCR

s.c.: PEG hydrogel solid content

SJ: Septate Junction

TJ: Tight Junction

YAP: Yes-associated protein

Yki: Yorkie

Chapter 1

General introduction

1.1 Tissue mechanics

The components of inert and living systems, whether a particle or a cell, exhibit the same set of mechanical properties (*e.g.* viscosity, elasticity, plasticity, stiffness) and are constrained by the same physical factors. Both types of systems are exposed to the same physical forces that can affect them in different manners depending on their mechanical properties. Living tissues are composed of cells, the basic unit of multicellular systems, and an extracellular substrate or matrix. These two main elements are in constant interaction, influencing each other's composition, architecture, and mechanical properties (see section 1.3); all of which can change through time and space. Consequently, the mechanical properties of a tissue are dynamic and emerge from the properties of its cells, its substrate, and their coupling. [10, 11, 12]

Tissues and cells are in the constant presence of both internal and external forces that originate from numerous sources (figure 1.1). For example, from the cytoskeleton and its contractile properties, cell-cell and cell-substrate adhesion and interaction, substrate stiffness, osmotic pressure, compression from the microenvironment, shear stress, etc (see section 1.3) [14, 13]. Cells are able to sense and respond to such forces by integrating mechanical sig-

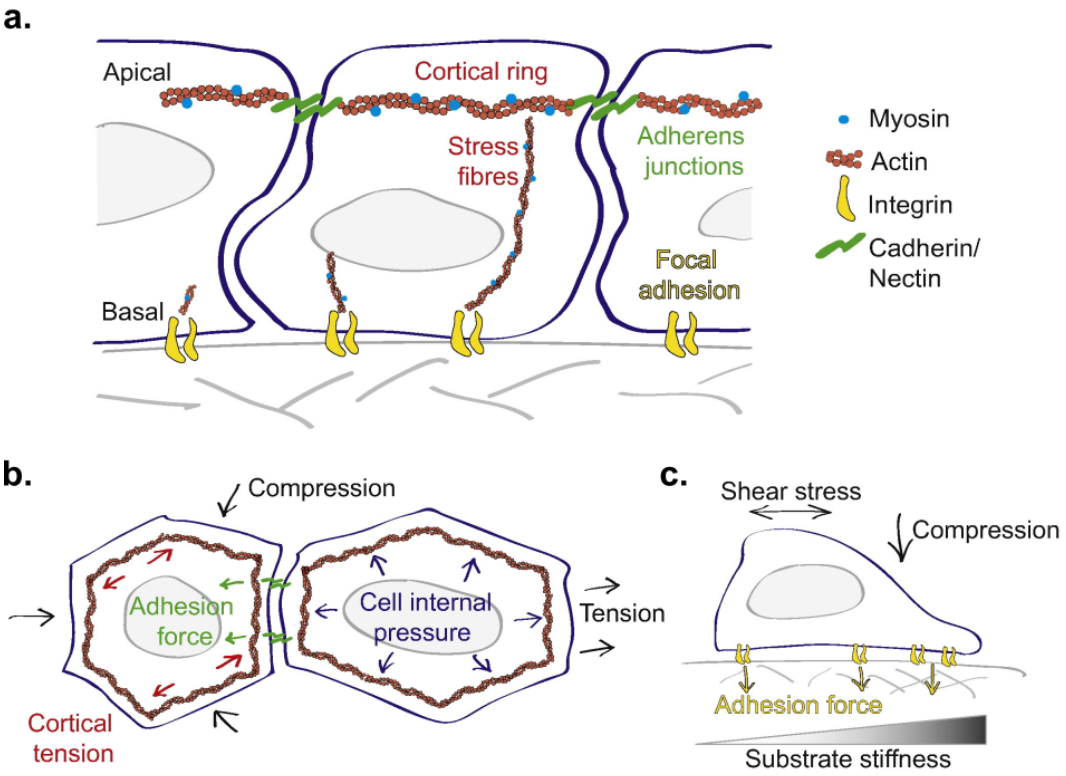

Figure 1.1: External and internal forces experienced by cells. (a.) Cell components can induce and transmit forces. **(b.)** Intrinsic and extrinsic forces from neighbouring cells induce mechanical stress. **(c.)** Extracellular sources of forces and mechanical stress. Figure from [13], reproduced with permission of the rights holder (Elsevier).

nals into biochemical and genomic pathways. This ability, known as mechanotransduction, has been of increasing interest and shown to play a key role in many biological processes. Through mechanosensing and mechanotransduction, forces can regulate cell shape, growth, proliferation, movement, and cell identity/differentiation (figure 1.2). At a multicellular level, they can regulate tissue morphology, its organisation and even function (see section 1.2) [15].

It is essential that all these dynamic forces and mechanical properties are properly regulated during development and kept in equilibrium in order to achieve and maintain homeostasis. If mechanosensing and mechanotransduction abilities are disrupted and forces unbalanced, it can lead to developmental defects, neurological disorders, cardiovascular diseases, cancer, and other pathologies [11, 15, 16, 17].

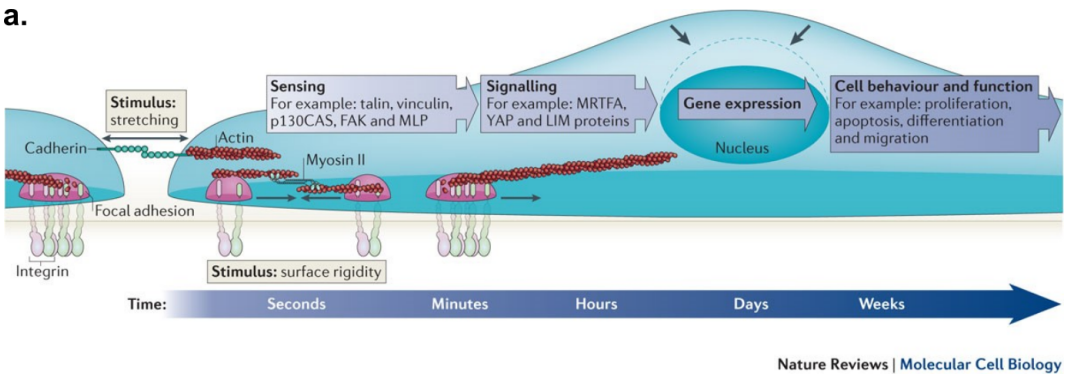

Figure 1.2: Cell mechanotransduction. Transduction process of a mechanical stimulus into chemical and physiological responses across different timescales. Figure from [15], reproduced with permission of the rights holder (Springer Nature).

1.1.1 Tissue fluidity

Inert systems (*e.g.* soft and granular materials) can sometimes behave as solids, with a more stable shape and elastic stresses, or loose these features and behave as fluids. Changing from one state to the other is known as jamming/unjamming transitions. Living multicellular systems can also exhibit such transitions depending on the ability of cells to move, exchange neighbours and rearrange [11, 18]. Cell jamming can be explained theoretically through energy barriers that are partially set by junctional tension and impede cell rearrangements in a tissue [19, 20, 21]. Junctional tension consists of two competing components: a positive contractile energy and a negative adhesive energy. When the net tension is positive (*i.e.* low adhesive energy or high contractility), cells are unable to move relative to each other and the system jams. However, the energy barriers disappear when tension is negative (high adhesive energy or low contractility), unjamming the system and allowing cells to rearrange [20, 22, 23].

Both cell adhesion and contractility have been shown to modulate tissue fluidity and cell jamming in epithelia. Relevant molecules have been suggested

to play an important role, including E-cadherin and components of the actomyosin network. Regarding cell adhesion, precise regulation of junctional E-cadherin turnover modulates tissue fluidity as observed during wing and eye morphogenesis in the *Drosophila* pupa [24, 25]. Concerning cell contractility, tuning myosin activity affects tension levels in a tissue and thus its fluid state as described in the *Drosophila* wing disc [23].

Furthermore, many other factors that are seemingly independent of these two main factors have been observed to also affect the fluid state of a tissue: crowding (*i.e.* cell density), motile forces, cell size, volume, cell and substrate stiffness, proliferation and cell death (figure 1.3a) [20, 26, 11, 27, 28, 18]. Modulating a few of these factors can trigger a jamming/unjamming transition. For example, increasing cell density, or lowering motile forces, can lead to a more jammed solid state. Conversely, a jammed cell layer can be pushed towards a more fluid state by increasing motile forces or reducing cell crowding, size or stiffness [11, 18]

Tissue fluidity is a complex dynamic property with a significant effect on collective cell behaviours. Its impact has been observed in cell monolayers grown *in vitro* [11]; tissue morphogenesis of multiple organisms, such as the process of body axis elongation in zebrafish [29] (see figure 1.3b for example) and fly [30] embryos, as well as during frog and chick development (reviewed in [31]); tissue repair [27, 23]; and in some diseases including asthma [22] and cancer [32, 33, 34]. The importance of tissue fluidity in morphogenesis and repair is of particular interest for this work and is further discussed in section 1.2.2.

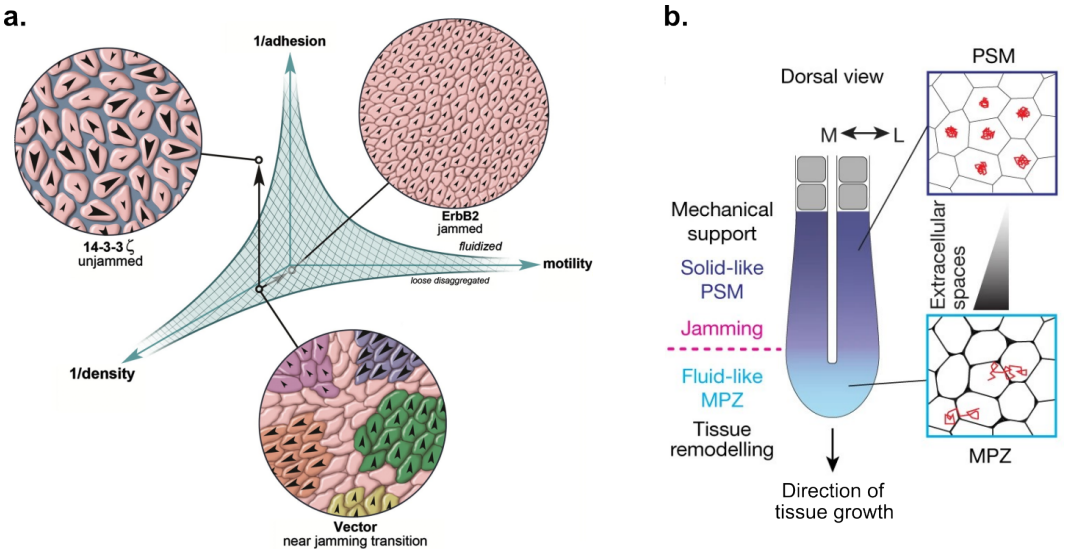

Figure 1.3: Tissue fluidity. (a.) Example of some of the factors that influence the fluid/solid (unjammed/jammed) state of cell monolayers. Arrowheads represent speed and direction of cell movement, higher in unjammed monolayers. **(b.)** Jamming transition in zebrafish body axis elongation. Extracellular spaces in the fluid region (light blue) allow cell-cell contact fluctuations, resulting in increased cell movement and rearrangements (red tracks). Cell in the solid region (dark blue) have smaller extracellular spaces and limited cell movement. (a.) adapted from [11] and (b.) from [29], with permission of the rights holder (Elsevier and Springer Nature, respectively).

1.2 Tissue morphology and repair

All multicellular structures have a well-defined morphology and spatial organisation that contributes to their particular functions. Any morphological anomalies can be detrimental, compromising their correct functioning and even survival. Hence, it is essential that tissue morphology is robustly regulated during development, maintained throughout the lifespan of an organism and, importantly, restored when damaged. Many of the mechanisms and signalling pathways that regulate tissue morphogenesis in development have been found to also play an important role in the repair process of both embryonic and adult tissues [35, 36, 37, 38]. By studying how tissue morphology is either established or recovered, we can better understand both processes at the same time.

Repairing damaged structures is a fundamental ability in order to prevent

infections, maintain homeostasis, and recover tissue integrity, as well as its original size, shape and/or function [39, 40]. Injury and repair can take place at multiple scales [41, 38], from simpler cellular structures (*e.g.* cell membranes or junctions [42]) to more complex multicellular ones (*e.g.* organs, body parts [43, 44, 45]). However, the ability to repair varies not only between species but also within the same individual and even in the same tissue, depending on the conditions at the time of injury and on the type of damage (see section 1.4.1). Some organisms can completely regenerate the damaged structure(s) while others can only close the wound to restore tissue continuity, either in a seamless or scarred manner [46, 47, 48, 49, 50, 51, 52].

1.2.1 Repair processes and mechanisms

Sealing the wounded area is a crucial first step of tissue repair, regardless of the extent and type of injury [48, 50]. The processes involved in this first step replenish lost cell populations, through oriented cell proliferation [53, 54, 27] and re-differentiation [47, 55, 56], and reduce the damaged area. To achieve the latter, cells at the wound edge come together through different mechanisms including shape changes (flattening and elongation), cell crawling or migration, and cell intercalations [57, 58, 27, 59, 23]. All these cell behaviours have been observed across different systems, which has helped to describe some of the common signalling pathways and molecular components necessary for tissue repair.

One of the most immediate responses to injury is the production of reactive oxygen species (ROS) and calcium waves. These signals activate different signalling pathways and trigger multiple cell responses essential for repair [60, 37]. The Rho kinase (Rock) and Jun N-terminal kinase (JNK) signalling pathways coordinate actomyosin-dependent cell rearrangements (*i.e.* radial cell intercalations, cell flattening, migration and elongation), the formation of actin

cables and filopodial extensions [61, 58, 51, 59]. The JNK pathway also regulates cell proliferation, induces tissue remodelling by activating matrix metalloproteinases, and promotes cellular reprogramming and re-differentiation by downregulating several genes from the Polycomb-group (PcG) [61, 62, 63]. Fat (Ft) and Crumbs (Crb) are two polarity genes that guide growth in the correct direction, by reorienting cell division, and act as sensors to prevent tissue overgrowth, by controlling the levels of the Hippo pathway effector Yorkie (Yki or Yes-associated protein (YAP) in vertebrates) [53, 54]. Other important pathways regulating cell proliferation and reprogramming are JAK/STAT, Wnt, Hedgehog, and Notch signalling [61, 62, 54, 37]. Furthermore, the actomyosin cytoskeleton is an essential component of the repair process due to its role in cell processes regulated by Rock and JNK, and in gap closure through the assembly and contraction of an actomyosin supracellular cable (*i.e.* 'purse-string') [64, 65, 54]. The roles of the actomyosin cytoskeleton during repair and its more recently described mechanical functions have highlighted the importance of tissue mechanics and some of the mechanisms through which it can regulate tissue repair (see section 1.2.2).

1.2.2 Mechanics of repair

While some mechanosensitive pathways have started to be described at the molecular level (*e.g.* Rock and Hippo pathways, see previous section), the mechanisms for transmitting and interpreting mechanical signals remain unclear. Nonetheless, there is an increasing understanding of the mechanoregulation of cell behaviours in the context of development and repair.

Mechanical forces are implicated in the regulation of many processes that are essential for tissue morphogenesis (reviewed in [66, 67, 68] across a wide variety of systems), such as cell migration [16], cell differentiation [16], cell intercalation [31], cell division rate [69, 70] and orientation [26], etc (figure 1.4). As

previously mentioned, in addition to playing an important role in shaping tissues during development, all these processes are also involved in repairing injured multicellular structures and restoring their functional morphology [13].

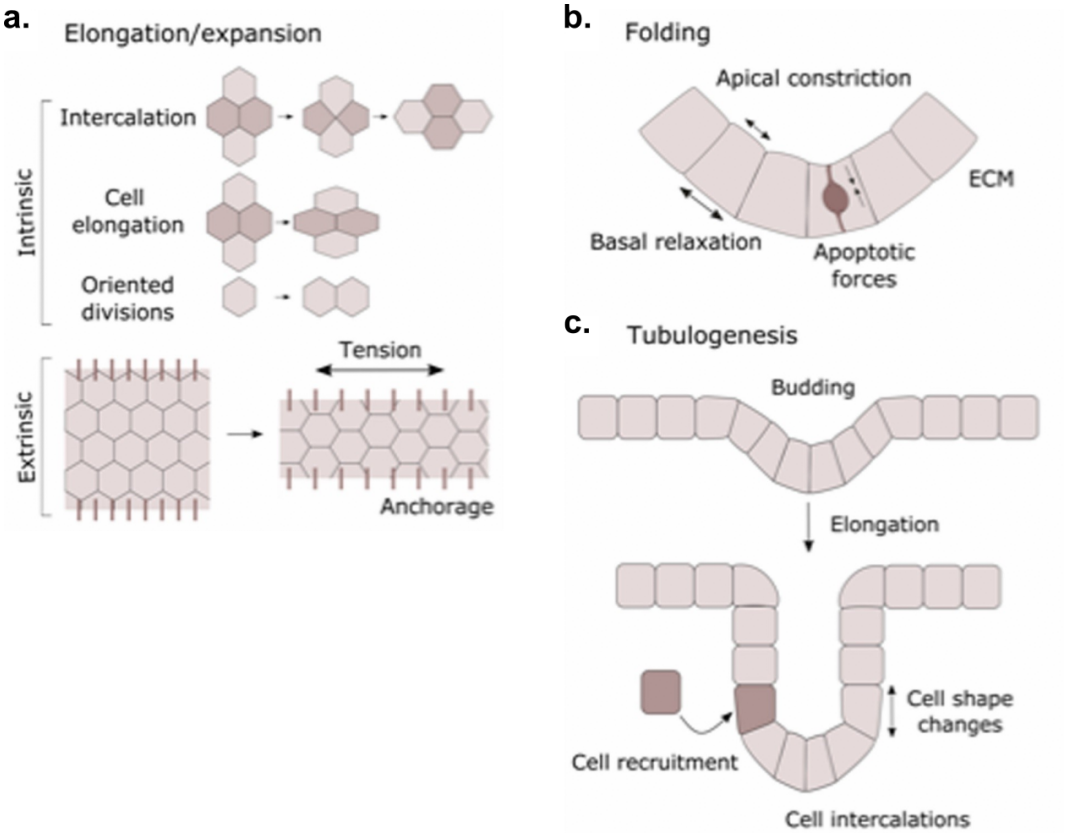

Figure 1.4: Morphogenetic processes driven by mechanical forces. Figure adapted from [68].

Some studies have provided evidence on how the mechanical properties of a tissue and its environment can influence its ability to repair. Tension is a particular property that has been shown to impact repair at multiple scales [38]. At higher scales, it has been shown that hypertrophic scars tend to occur in skin areas that are under increased mechanical stress. Studies performed in pig and human skin showed that scarring can be significantly reduced by protecting the injured area from being under constant high tension. Conversely,

when exposed to increased tension scarring was worsened [71, 72] (figure 1.5a). At the tissue level, epithelial tension affects the repair process in similar manners; as demonstrated in the *Drosophila* imaginal wing disc [23], where an overall increase of junctional tension jams the tissue and hinders repair, whilst lowering basal tension levels fluidises the tissue (see section 1.1.1). Increased fluidity allows cells at the wound edge to intercalate more, which accelerates closure and efficiently restores the original cell morphology and packing without leaving a 'scar' (multicellular rosette) behind [23] (figure 1.5b). Another example is the *Drosophila* embryo, where a local increase of tension is required only at the wound edge to stabilise the actomyosin purse-string during wound closure [73]. This is a conserved mechanism for gap closure observed in many *in vitro* and *in vivo* systems (reviewed in [74]); *e.g.* cell culture, mouse corneal epithelium, fly embryo and larvae, beetle embryos [75], etc. The actomyosin purse-string pulls together the wound edge cells and induces cell shape changes that result in the formation of multicellular rosettes [76, 57, 54, 77].

Moreover, epithelial cell junctions (see section 1.3.1) have important mechanical functions during repair. Septate junctions (SJs) impact epithelial mechanical properties and are involved in regulating wound closure in the *Drosophila* embryo [78]. Adherens junctions (AJs) are required to stabilise the actomyosin purse-string and link it intercellularly, as seen in fly [40] and chick [79, 80] embryos, cell culture [81]. Even after an epithelium has been repaired, tension is still required for new cell junctions to form and mature [82].

While mechanical forces regulate the response to injury, they can also cause damage and spread it across a larger area. Hence, tissues need to protect their morphology and cellular organisation from the internal and external forces acting on them. It has been shown both *in vitro* and *in vivo* that mechanical stress tends to accumulate at the cell-cell junctions, making them prone to breakage [83, 84, 85, 42]. Several mechanisms involving Rho signaling [85, 42]

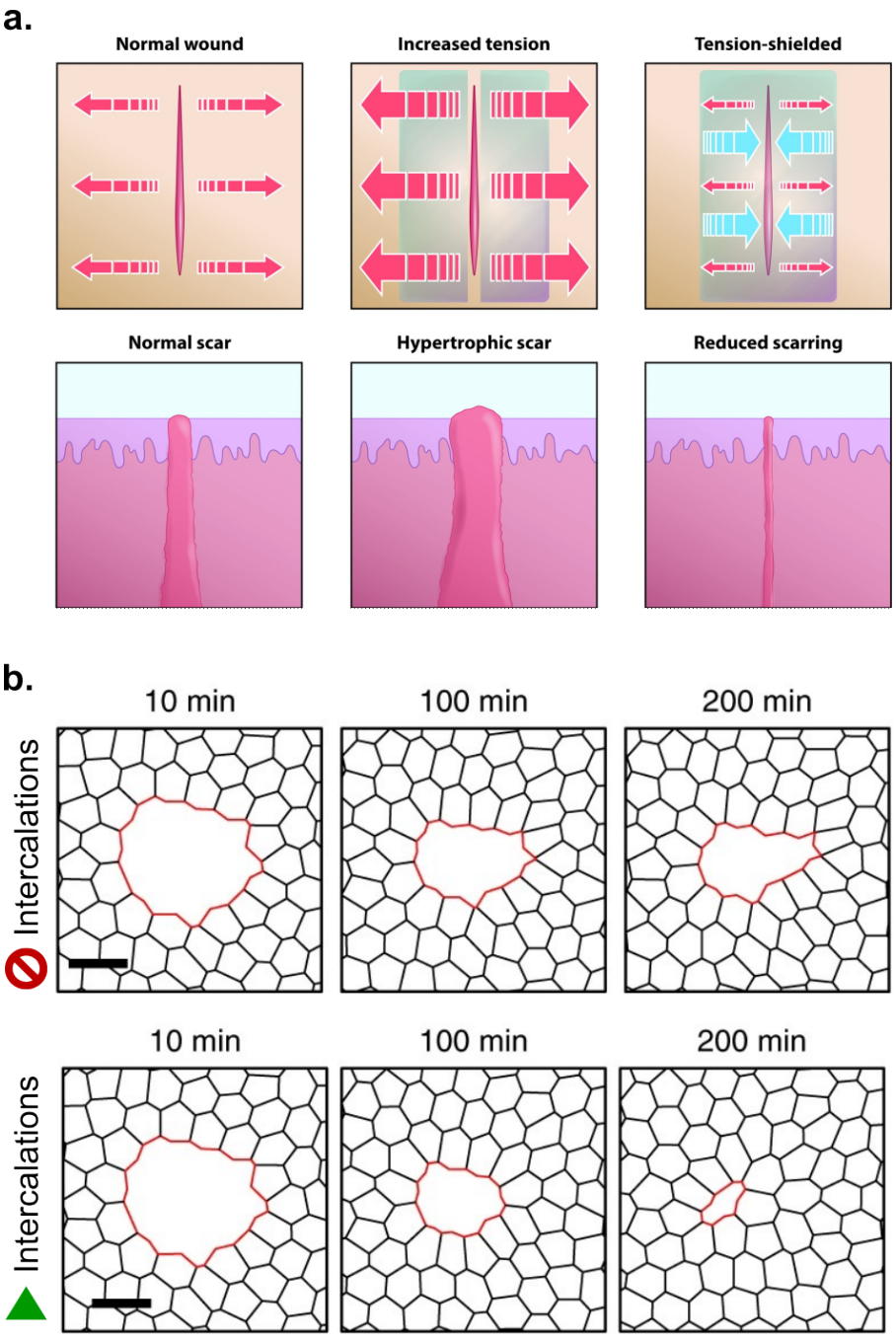

Figure 1.5: Examples of mechanical forces influencing repair efficiency. (a.) The mechanical tension sensed by the skin affects cutaneous scar formation. Tension-shielding polymers are now used for scar therapy. **(b.)** In the *Drosophila* wing disc, low tension increases efficiency of wound closure driven by cell intercalations (bottom row). Higher tension and no intercalations result in slow/unsuccessful closure. (a.) adapted from [72] and (b.) from [23], with permission of the rights holder (Mary Ann Liebert, Inc. and Springer Nature, respectively).

and repolarisation of the actomyosin network [84, 86, 87] are known to buffer mechanical stress, prevent and/or contain cell damage, and maintain tissue integrity. It has also been shown that repolarisation of the actin cable helps protect cell packing and prevent scarring during gap closure in the *Drosophila* embryo [88], while thicker actin belts help preserve cell topology and tissue architecture in the mice cochlear epithelium [89].

As mentioned in section 1.1, it is important that internal and external forces are properly regulated and balanced. Any injury event perturbs this balance and changes the state of a tissue. The forces acting on a tissue and its initial mechanical properties influence how the tissue responds and how efficiently it can repair itself.

1.3 Epithelial tissues

Epithelial tissues are continuous sheets of cells lining organs, glands, cavities and the outer surface of an organism (*i.e.* the skin). They can form a simple cell monolayer, the first multicellular structure to appear, or more complex tissues with multiple specialised cell layers (known as pseudostratified and stratified epithelia). Epithelia can be further categorised into squamous, cuboidal, and columnar based on cell shape. Regardless of the classification, the main function of an epithelium is to act as a physical and permeable barrier that separates the inside from the outside. Epithelial tissues are constantly exposed to environmental bacteria, toxins, chemical and physical stress. It is therefore essential for an epithelium to be able to overcome damage in order to maintain and restore their barrier function as well as tissue homeostasis [90, 66, 91].

1.3.1 Epithelial organisation

Cell polarity

All epithelial cells have a common organisation and characteristic polarisation that allows them to form continuous sheets of tissue and carry out their function. The typical polarisation of an epithelial cell consists of three domains that are molecularly and functionally different: apical, lateral, and basal (figure 1.6). The apical domain contains micro-villi, sometimes cilia, and is exposed to a lumen. The lateral and basal domains are in contact with and adhere to other surfaces through different molecular complexes. The lateral domain faces neighbouring epithelial cells and it is essential for cell-cell adhesion (see below). The basal domain usually faces and interacts with a basement membrane (see section 1.3.2). Apico-basal polarity is necessary to determine the external and internal surfaces of a tissue, maintain cell shape, guide molecular trafficking, and organise the cytoskeleton and other intracellular organelles [92, 93].

Epithelial cell polarity is tightly regulated by an evolutionarily conserved molecular machinery (figure 1.6, reviewed in [94, 93, 95, 96]). The Partitioning defective (Par) and Crumbs (Crb) complexes establish the apical domain and correctly position cell junctions [97]. PAR-1/MARK serine/threonine kinases and the Scribble group proteins define the basolateral domain by excluding apical proteins from it; and can also modulate polarised protein trafficking [97]. This regulation is crucial as any changes in cell organisation and polarity can propagate at the tissue scale, affecting both the structure and function of epithelial tissues [84, 85].

Cell junctions

There are two important protein complexes at the border of the apical and lateral domains (figure 1.6): the adherens junctions (AJs) and occluding junctions (OJs), also known as tight junctions (TJs) in vertebrates or septate

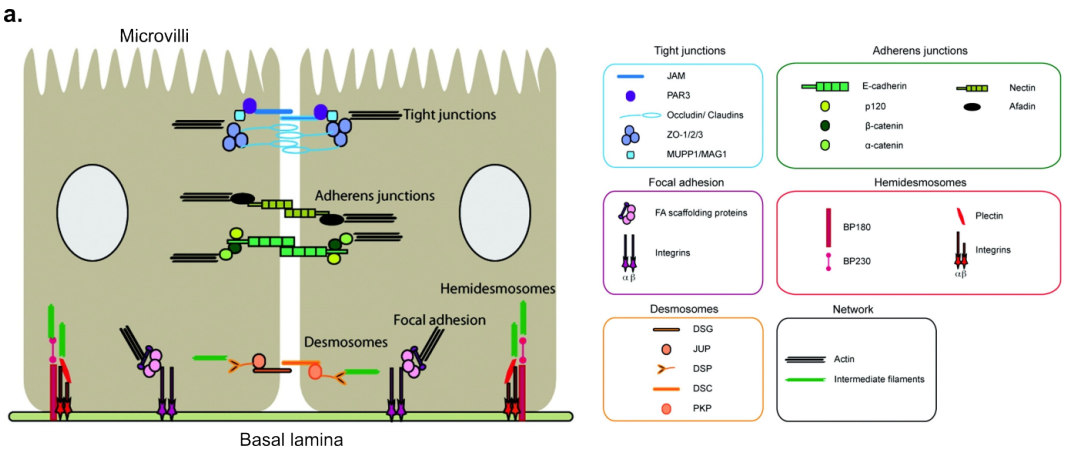

Figure 1.6: Epithelial cell polarity and junctions. Adapted from [98].

junctions (SJs) in invertebrates. AJs are highly conserved across all metazoans as they are essential for cell-cell adhesion and the maintenance of tissue integrity [99, 100, 101, 102]. The three main proteins forming an AJ are E-cadherin (E-cad), $\alpha-$ and $\beta-$catenin. E-cad establishes cell-cell adhesion by forming extracellular homodimers with neighbouring cells, and it couples the cytoskeletal network intercellularly by binding to the cell cortex through $\alpha-$ and $\beta-$catenin [103, 104, 105, 106]. OJs keep apical and basolateral compartments segregated and seal cells together at their apical side. They are crucial for controlling diffusion through the epithelial layer and its function as a permeable barrier [84, 42].

Increasing evidence has shown that cell-cell junctions have an important role in mechanosensing and mechanotransduction. Normal cell behaviours (*e.g.* cell division, shape changes, movement) can generate mechanical stress that accumulates at the cell junctions and makes them susceptible to breakage [83, 84, 85, 42] (see section 1.2.2). Therefore, junction maturation and maintenance is important for preventing cell damage and protecting epithelial integrity. High tension at the AJs [85] or the TJs [42] activates Rho signalling, promoting accumulation of actomyosin and recruitment of junctional proteins to prevent or restore any ruptures while also strengthening the junction. In

addition, intercellular coupling of the actin cytoskeleton through the AJs allows tension to be sensed and transmitted throughout the tissue, which can affect its morphology, function, and cell behaviours [20, 107, 108].

Epithelial cells are also connected through a third type of protein complex known as desmosome (figure 1.6). This complex couples intermediate filaments intercellularly through desmosomal cadherins, in a similar manner to AJs coupling actin filaments. Through this coupling desmosomes contribute to the mechanical strength of epithelial tissues, helping maintain their architecture and integrity. Desmosomes have also been shown to have an effect on cell behaviours and tissue morphology during development and repair [109, 110].

1.3.2 Role of Extracellular Matrix (ECM)

The extracellular matrix (ECM) is an organised, complex, and highly dynamic macromolecular network present in all tissues and organs. While there are different types of ECM, epithelial tissues are usually in direct contact with a particular sheet-like matrix called basement membrane. This type of ECM covers the basal surface of epithelia, providing physical support to the tissue and a platform for signalling [111, 112]. The basement membrane primarily consists of collagen, laminin, nidogen and heparan sulphate proteoglycans [112]. However, its exact composition and architecture is tissue and context specific [113, 114]. Since epithelial tissues are the main interest for this work, ECM and matrix are henceforth used as synonyms for basement membrane.

Cells adhere to their ECM through receptors that link the matrix to the cytoskeleton and enable them to communicate reciprocally [115, 116, 114] (see below). Through these connections the ECM can regulate cell signalling and, in turn, cell identity and behaviours [117, 115]. Simultaneously, cells can remodel both the composition and organisation of their matrix, two important

characteristics that determine its mechanical properties [113, 114]. The ECM is a key source of both chemical and mechanical signals for the tissue they are in contact with [113, 111]. It has been shown to have an important mechanical role in development, repair, cancer, etc [118, 119, 116, 111, 112].

Cell-ECM interaction

Interaction between epithelial cells and their ECM is mediated through mechanosensitive cell-matrix adhesion complexes (CMACs). Focal adhesions and hemidesmosomes are the two main CMACs that couple the matrix to the actin-cytoskeleton and intermediate filaments, respectively [120, 98] (figure 1.6). The principal components of these complexes are integrin receptors, transmembrane heterodimers formed by α and β subunits that allow them to recognise and bind to various ECM components [121]. The amino acid sequence RGD is the first and best described integrin binding motif that promotes strong cell adhesion [98]. Variations of the RGD peptide have been widely used for biomaterials (see section 4.1.1). Intracellularly, integrins bind to protein adaptors that can have a scaffolding, structural and/or catalytic function (*e.g.* paxillin, kindlin, talin, tensin, focal adhesion kinase (FAK), etc). Catalytic adaptors are responsible for signal transduction and propagation, while structural adaptors directly link integrins to the cytoskeleton [120].

Integrins and their adaptors are mechanosensitive proteins susceptible to mechanical forces inducing reversible conformational changes and exposing previously concealed binding sites. These changes are important for integrin activation, CMAC formation, cytoskeleton coupling and signal transduction [122, 123]. Integrins are therefore involved in both biochemical and mechanical bidirectional signalling, due to the wide variety of subunits and adaptor proteins [121, 112]. This ability is crucial for reciprocal cell-matrix communication, through which cells can influence ECM remodelling and the ECM can

influence cell identity and behaviours.

Morphogenesis and repair

The strength of cell adhesions as well as the stiffness of a substrate can have an effect on cell shape, tension, and substrate deformation. Stiffer substrates induce cell spreading and attachment, whereas softer substrates and strong cell-cell adhesion can lead to substrate reshaping around the cells. Thus, variations on strength and stiffness can result in multiple configurations of cell and tissue shapes [124, 125, 126]. Furthermore, the dynamic composition and mechanical properties of basement membranes provide cues to direct cell behaviours and tissue growth during development, homeostasis, disease, and injury. The ECM is involved in the regulation of essential processes for tissue morphogenesis, such as cell growth, proliferation, polarisation, migration, differentiation, and shape changes [127, 113, 47, 128, 111, 129].

Polarised matrix deposition directs cell polarisation in embryoid bodies and epithelial cysts and tubes [130, 131, 132, 111]. Oriented matrix fibres can also regulate tissue shape by providing patterned physical constriction in the *Drosophila* egg chamber [133], mouse salivary gland [134] and other tissues [111, 129]. The ECM is also involved in maintaining tissue architecture as observed in the *Drosophila* wing discs [135] and the *C. elegans* gonad [136]. Unexpected changes of ECM chemical and mechanical properties can severely impact tissue development [111, 129], impair repair [127, 119], and contribute to cancer development [118, 137] and disease (*e.g.* in the case of liver fibrosis [138, 139], see section 1.4.2).

The importance of the ECM for successful tissue repair has additionally been demonstrated in the field of tissue engineering and regenerative medicine. Decellularised scaffolds (tissue specific isolated matrices that preserve their orig-

inal components and architecture) have been used to grow and differentiate embryonic stem cells (ESCs) into functional organs that can be transplanted in rats and replicate rudimentary functions [140]. This technique has also highlighted the specificity of ECMs as ESCs can only differentiate into cell types that correspond to the original tissue from which the scaffold has been isolated (*i.e.* cardiomyocyte differentiation possible in scaffolds from heart and not from liver tissue [141]).

Cell fate determination

ECM properties not only influence overall cell shape and behaviours, they can also determine cell identity through chemical and mechanical regulation of cell differentiation pathways. As previously mentioned, a matrix isolated from a particular tissue induces differentiation of ESCs towards cell types that constitute that specific tissue only [141]. Remarkably, the use of artificial *in vitro* matrices has shown that mechanical cues alone can trigger cell differentiation into specific lineages, as well as other cell behaviours [6, 142, 143, 144]. Mesenchymal stem cells (MSCs) grown on matrices of low, intermediate, and high stiffness promotes differentiation towards neurons, myoblasts and osteoblasts, respectively [117] (figure 1.7). Similarly, softer gels promote MSC adipogenesis while stiffer gels favour osteogenesis [145, 146, 147].

While most of these studies have tried to manipulate the characteristics of matrices and test their effect at the cell and tissue level, it is difficult to isolate specific matrix properties and independently change them without affecting others. In recent years, more sophisticated tools have been developed to allow independent manipulation of both chemical and mechanical characteristics of 2D and, importantly, 3D matrices. One interesting example is a new synthetic hydrogel that can undergo degradation and softening at predefined regions through photopatterning. Intestinal stem cells grown on these gels acquired

spatial variations in cell shape, YAP and Notch signalling, specifying crypt-like domains with Paneth cells to the softened areas and villus-like domains with no stem cells elsewhere [148]. Synthetic matrices used *in vitro*, in particular for 3D cell culture, are further described and discussed in chapter 4 (see section 4.1.1).

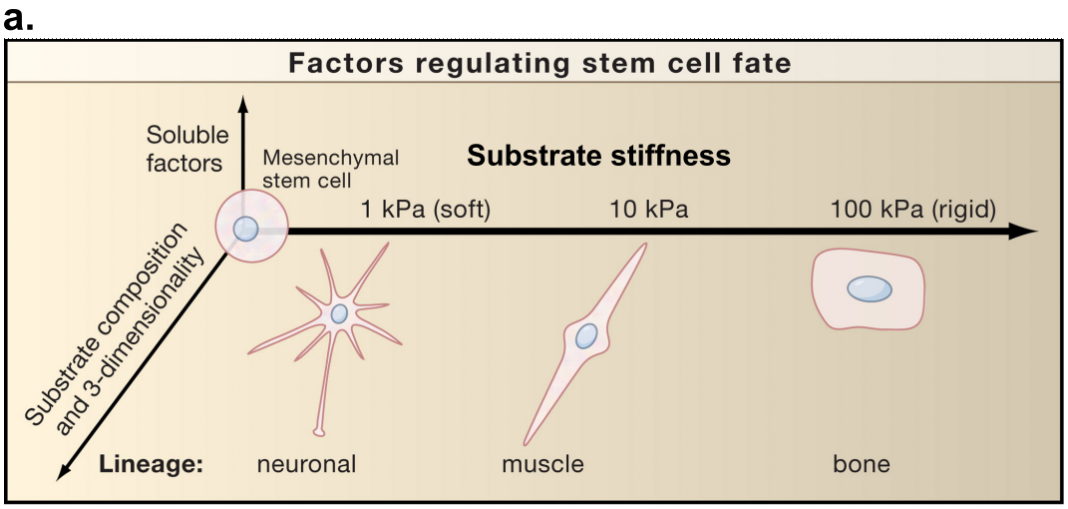

Figure 1.7: Substrate stiffness regulates stem cell fate. See [117] for experimental work. Figure from [149], reproduced with permission of the rights holder (Elsevier).

1.4 Regenerative ability of the liver

The liver is one of the most important organs with over 500 functions, including detoxification, bile production, metabolism, storage, etc. Even though the adult liver has a low cell turnover in homeostatic conditions, it has a surprising regenerative capacity as it can overcome almost any kind of damage throughout the lifespan of an individual. It is able to repair repeated microinjuries and mild damage from toxins, drugs and physical lesions. The liver can also regenerate after severe damage and fully recover its morphology and function even after removal of up to 70% of its mass (figure 1.8a). While its regenerative abilities have been widely studied, it is still highly debated which cell types

can respond to damage and how. Multiple mechanisms have been described depending on the location, source, and severity of injury (figure 1.8b) [150, 55].

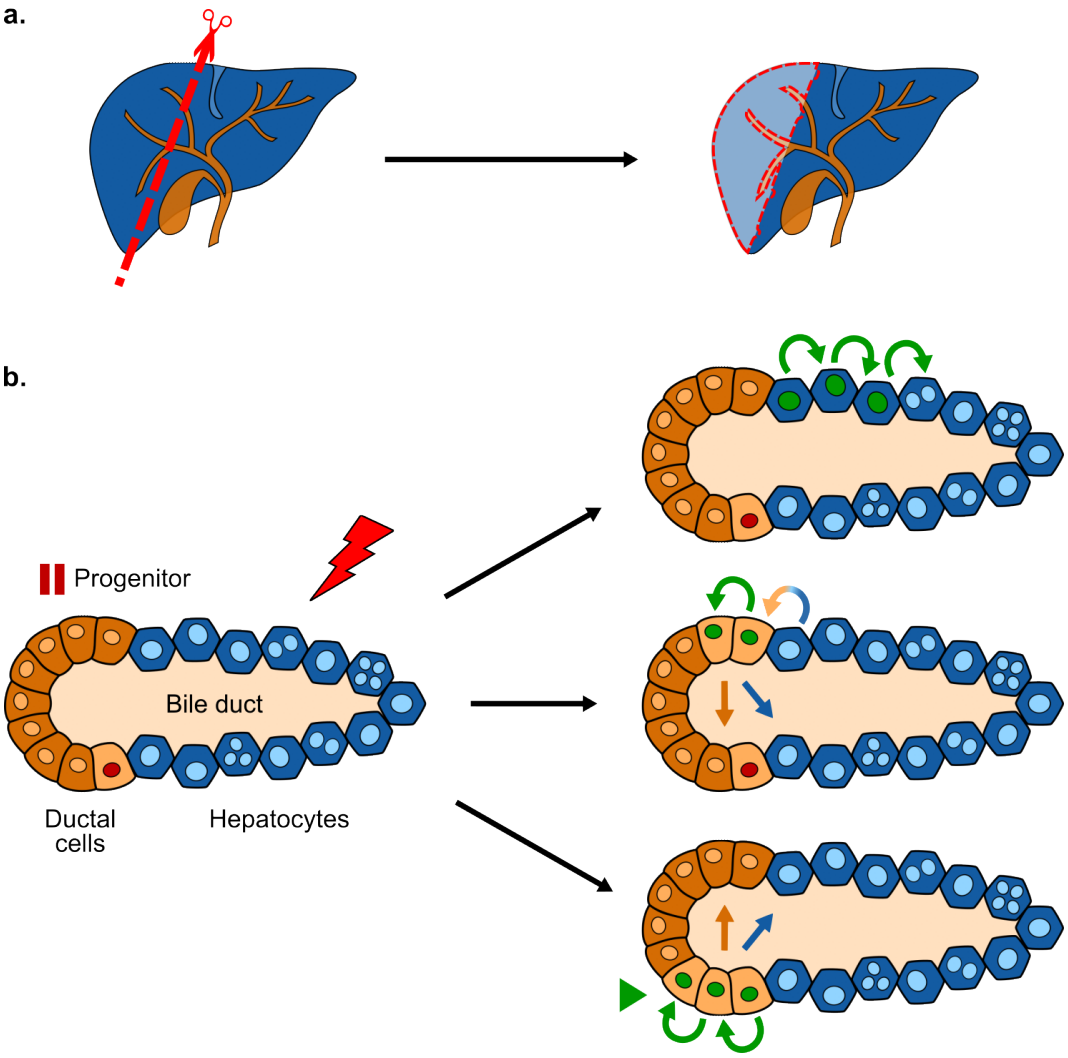

Figure 1.8: Liver repair responses. (a.) Liver regeneration (right) upon severe damage (left). **(b.)** Reported repair responses of different cells within the ductal and hepatocyte compartments. Top to bottom: hepatocyte proliferation, hepatocyte de-differentiation into bipotent cells, and re-activation of quiescent stem cells. See text in section 1.4.1 for more information.

1.4.1 Repair responses

The liver consists of mainly epithelial cells (hepatocytes and ductal cells, see section 1.4.3) and, to a lesser extent, of blood vessels (liver sinusoids), hepatic macrophages (Kupffer cells) and hepatic stellate cells (HSCs) [151, 152]. All cells present in the hepatocyte and ductal compartments (*i.e.* mature epithelial cells, progenitors and quiescent stem cells) have been reported to contribute to liver repair and regeneration in their own manner (figure 1.8b) [150, 55].

Hepatocytes are the most abundant cells and are the first ones to respond to most types of damage. Mature and immature cells from the hepatocyte compartment can re-enter the cell cycle and increase their proliferation rate to replenish lost hepatocytes [153, 154, 155]. Upon a larger loss of cell mass, they can also de-differentiate into ductal-like progenitor cells, proliferate, and re-differentiate into hepatocytes and ductal cells [156, 157]. Cells in the ductal compartment also contribute significantly to repair when damaged or when severe injury depletes the majority of the hepatocyte compartment. Ductal cells increase proliferation and quiescent stem cells within the compartment can be activated through epigenetic remodelling. These cells rapidly divide, expand, and differentiate into both hepatocytes and ductal cells to restore their respective compartments [158, 159, 160, 161, 162, 163, 164, 55, 63]. It is likely that this variety of cellular plasticity and injury responses is what makes the adult liver highly regenerative. Any alterations of cellular plasticity can lead to impaired regenerative abilities, liver disease and carcinogenesis [165].

1.4.2 ECM and liver repair

The ECM of a healthy liver is scarce compared to other epithelial tissues (<3% on a liver section). It is restricted to a few areas (*i.e.* portal tracts, sinusoid walls, and central veins) where it forms part of the border between these tissues and the blood flow [138]. The strategic and limited arrangement of ECM

within the liver mean that any changes in its properties (*i.e.* density, stiffness, flexibility, localisation) rapidly affect the structure, function and regenerative capacity of the liver [138, 166, 139], which can have deleterious consequences.

Repeated and chronic damage induce long-term activation of HSCs, a small cell population that has also been reported to play a role in liver repair. These cells regulate myofibroblast differentiation and thus fibrogenesis [150]. Prolonged HSC activation results in excessive ECM accumulation and fibrosis, characteristics that take place in most types of chronic liver diseases. Although it can be reversible, there is no standard treatment for liver fibrosis. Its progression is variable between individuals and the only successful cure is transplantation. If untreated, advanced fibrosis can lead to cirrhosis, morbidity and eventually mortality [138, 166, 139].

1.4.3 Liver epithelium

Up to ∼85% of the liver volume consists of epithelial tissue formed by two cell types: hepatocytes (∼80%) and cholangiocytes (3-5%), also known as ductal cells [167, 168]. Hepatocytes are the most abundant epithelial cell type that carry out many important functions such as bile formation, metabolic functions, detoxification, etc [150, 55]. Cholangiocytes form the intrahepatic bile duct network responsible for bile secretion and transportation [168].

Both cell types exhibit the typical polarisation of epithelial cells: an apical domain facing a lumen, lateral domains contacting neighbouring epithelial cells, and a basal domain usually facing a basement membrane (see section 1.3.1). Cholangiocytes form a monopolar epithelium with an apical domain forming the inside of bile ducts, and a basal domain resting on a basement membrane [169]. In contrast, hepatocytes tend to have more than one apical and basal domains [167, 170] (figure 1.9d). They form capillary-sized lumina

(called canaliculi) with multiple neighbour hepatocytes, making up a branched network that spans across the liver epithelium and eventually integrates into the bile duct network (figure 1.9b-c). Hepatocytes can also form multiple basal domains that face the liver sinusoids instead of a basement membrane.

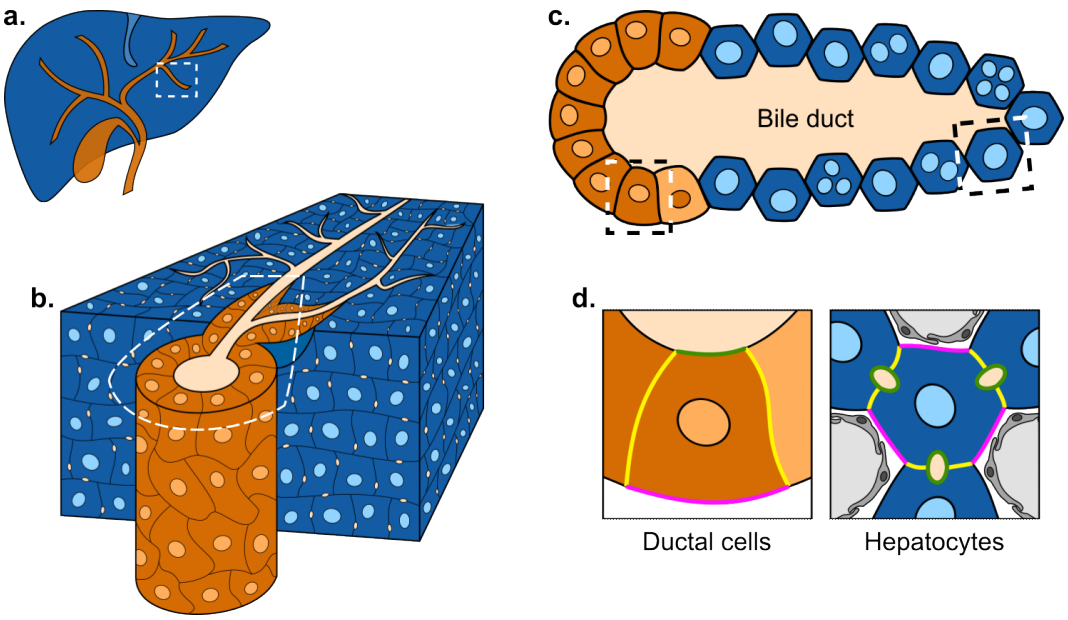

Figure 1.9: Composition and organisation of liver epithelium. **(a.)** Diagram of the liver and its intrahepatic bile duct network (dark orange). **(b-c.)** Liver epithelium consisting of a ductal compartment (dark orange cells forming ducts) that transitions into the hepatocyte compartment (dark blue cells forming a canaliculi network, illustrated as cream dots and thin branches in (b.)). **(d.)** Polarity of both epithelial cell types: apical (green), lateral (yellow), and basal (pink) domains. Liver sinusoids are in grey. Each panel is a more detailed representation of the dashed regions in its previous panel.

The hepatocyte compartment is divided into 3 zones: the periportal (zone 1), midlobular (zone 2), and pericentral region (zone 3, also called perivenous). Hepatocyte sub-populations have been described based on their position, morphology, maturation, function, polyploidy, and gene expression profiles [171, 151, 152, 172, 173]. The periportal region and the ductal compartment transition into each other throughout the biliary tract (figure 1.9b-c) [167]. Ductal cell sub-populations also exist with different levels of maturation,

proliferation, and gene expression profiles [168, 151, 152]. This heterogeneity of hepatocyte and cholangiocyte sub-populations gives the liver its characteristic cellular plasticity and variety of injury responses (see section 1.4.1).

1.5 Organoids as a model system

Organoids are *in vitro* multicellular 3D structures that recapitulate some of the characteristics and functions of a particular organ. They are derived from different kinds of stem cells: embryonic (ESCs), adult or induced pluripotent stem cells (iPSCs). Protocols for organoid culture exploit the intrinsic ability of these cells to self-assemble and organise into ordered multicellular structures from an (almost) homogeneous starting condition when grown in a 3D culture system (see section 4.1.1). Depending on the type of organoid, they can be differentiated *in vitro* into one or more cell types, or further developed through transplantation and engraftment *in vivo*. [174, 175, 1, 2, 3, 176]

This relatively new system has become popular due to its ability to better replicate the *in vivo* physiology of an organ, compared to regular 2D cell culture systems, while retaining most of the advantages of *in vitro* culture [4, 177]. Organoids can be expanded for long time periods without losing their genetic stability, differentiation potential and commitment to the tissue of origin [1, 178, 179, 2]. Manipulation techniques normally used for 2D cell culture can also be applied to organoid systems, such as genetic editing and engineering, chemical and physical perturbations, live imaging, etc. Because of the conditions in which organoids are grown, dynamical cell behaviours are preserved in a 3D tissue context [4, 177] and can be studied live with higher temporal resolution, unlike *in vivo* systems.

The field has rapidly grown and numerous types of organoids have been gen-

erated thus far, recapitulating tissues from the three main germ layers (*e.g.* retina, brain, heart, lung, intestine, liver, stomach, etc.) [1], and from multiple organisms other than mouse and human (*e.g.* apes [180], rhinoceros [181], snakes [182], etc). In translational research, they are being used to study disease and cancer progression, test new treatments, drug screening, and to advance personalised medicine by deriving organoids from human patients [175, 1, 3, 5]. In basic research they are being used to study multicellular coordination and behaviours, embryonic developmental processes, and the evolutionary differences between multiple species [3, 183, 180, 181]. Organoids can help us understand how tissues are shaped, how they respond to injury, and what dynamical processes take place during tissue repair. Furthermore, this *in vitro* system is an excellent tool to independently test and study the role of mechanical properties on tissue morphogenesis and repair.

1.5.1 Liver organoids

Various liver cell types derived from embryonic tissue, ESCs, iPSCs or adult stem cells have been used to establish 2D *in vitro* cultures: hepatoblasts, hepatocytes, and ductal cells. Bipotential hepatoblasts or hepatoblast-like cells have the potential to form hepatocytes and cholangiocytes, albeit immature ones [184, 185, 186]. Despite their regenerative ability, hepatocytes are a difficult cell type to grow *in vitro* as they develop and expand slowly, fail to retain their main functions, and have low survival [187, 188]. Adult stem and progenitor cells expressing ductal markers have been the most successful *in vitro* cultures with high expansion potential, differentiation towards hepatocyte and cholangiocyte lineage, and *in vivo* engraftment after transplantation [158, 184, 185].

In the past decade, several groups started to grow these cell types as 3D culture systems, uncovering the importance of 3D environments to better pre-

serve correct liver function and tissue organisation [189, 176]. While hepatocyte organoids have been successfully derived [190, 191], their growth rate and expansion potential remain limited. Conversely, liver organoids derived from ductal progenitor cells have a high population doubling rate (48-60 h), prolonged self-renewal capacity, high expansion potential (up to 1 year), remarkable genomic stability (only one synonymous base substitution detected in 3 months), and differentiation potential into mature ductal cells and hepatocytes [161, 162, 163, 176]. These characteristics have made them a popular system in the field.

1.5.2 Intrahepatic cholangiocyte organoids (ICOs)

One of the most commonly used protocols for growing liver organoids from ductal progenitors is the one published by Broutier *et al*, 2016 [161, 192], where they isolate intrahepatic ducts and/or cholangiocytes from the adult liver through mechanical and enzymatic disruption. This process triggers a regenerative response to acute injury in which cholangiocytes go through a transient epigenetic reprogramming in order to re-enter a proliferative progenitor state [63]. This remodelling is necessary for the cells to divide and initiate organoid formation in a 3D culture setup (see section 2.1.2 and figure 1.10a). Once formed, organoids can be passaged and cultured for over 5 months or frozen for long-term storage [161, 163, 192].

These intrahepatic cholangiocyte organoids (ICOs) [176] are a promising and convenient system to study the cellular plasticity of tissue repair. They can be maintained and clonally expanded as cholangiocytes or they can be differentiated into hepatocytes (see section 2.1.3 and figure 1.10b). Furthermore, when transplanted into mice with liver damage and impaired regeneration, ICOs can engraft and differentiate *in vivo* to regenerate the injured tissue [161, 163, 63].

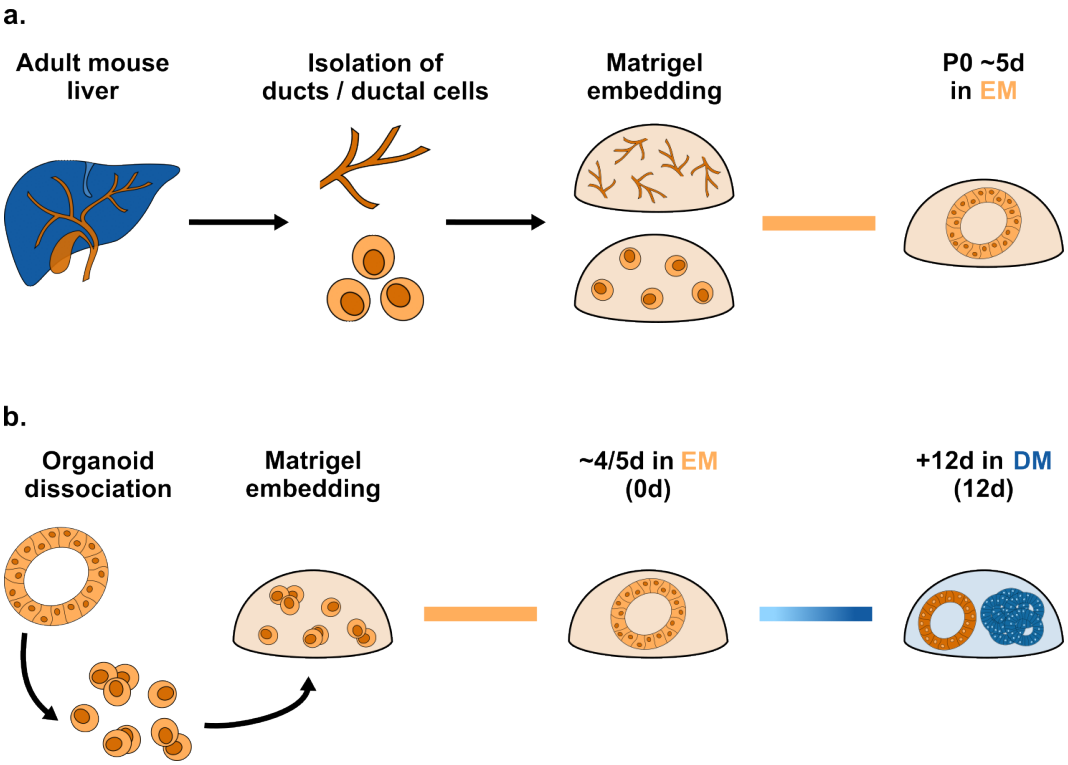

Figure 1.10: mICO isolation, culture, and differentiation processes. (a.) mICO isolation from adult mouse livers. **(b-c.)** mICO culture for maintenance, expansion, and experiments in expansion medium (EM, shown in light orange). Hepatocyte differentiation can be induced on day 4/5 by culturing mICOs in differentiation medium (DM, shown in light to dark blue). For more details on these protocols, see methods 2.1 and 2.1.3.

1.6 Questions and aims

Tissue mechanics has an important role on developmental and regenerative morphogenesis, influencing the repair efficiency of a tissue. The liver is an organ with striking regenerative abilities, even in adult individuals. While there is a general understanding of the underlying molecular and genetic processes, the mechanical aspect remains unclear due to limitations of *in vivo* systems. Similarly, since their establishment as a new model system, organoids have been mainly studied at the molecular and genetic levels. The importance of cell and tissue morphology has become more evident [193, 117, 147, 194, 195, 126, 186, 180, 144] and some groups have started to characterise organoid morphology and organisation [196, 197, 198, 199, 200, 201].

The main goal of this work is to characterise the morphological phenotypes of liver organoids recapitulating regenerative morphogenesis, and how this is affected by their mechano-environment. Furthermore, to explore the differences in mechanical properties (*i.e.* tissue tension) and how they influence the organoid repair response to injury.

The specific questions and aims addressed in this thesis are:

1. How does morphology change as organoids grow and differentiate? (Chapter 3)

    1.1 To characterise morphological changes of liver organoids as they differentiate

    1.2 To describe the correlation between morphological phenotypes and gene expression

2. How is the mechano-environment affecting organoid morphology and differentiation? (Chapter 4)

    2.1 To test the effects of substrate properties on morphological phenotypes and cell identity of liver organoids

3. Is tissue tension changing as organoids differentiate? And does it affect how organoids respond to microinjury? (Chapter 5)

    3.1 To characterise tissue tension of progenitor and differentiated organoids

    3.2 To characterise the repair response to microinjury of liver organoids through live-imaging

Chapter 2

Materials and methods

2.1 Organoid 3D culture

Mouse Intrahepatic Cholangiocyte Organoid (mICO) [176] lines were cultured at 37 °C, in an atmosphere of 5% CO_2, and supplemented with the appropriate media (table 2.1) for all conditions and experiments.

The protocols for all methods regarding organoid culture are published by Broutier *et al*, 2016 [192]. In this section, I summarise the methods I have used and include any differences or details that are specific to the work presented in this thesis.

2.1.1 Isolation, growing frozen cultures and cryopreservation

Newly isolated or frozen mICOs were embedded in 100% matrigel and cultured in isolation medium for 2-3 days. Isolation medium was then exchanged for expansion medium (EM), in which organoids were cultured for 5-6 days before splitting for maintenance and/or expansion (see sections 2.1.2).

Components	Stock Medium (2x) - 25 ml	Final concentration (1x)	Cat. No.
Advanced DMEM/F12	23 ml	-	Invitrogen 12634010
GlutaMax (100x)	0.5 ml	1x	Invitrogen 35050-038
Hepes (1 M)	0.5 ml	1x (10 mM)	Invitrogen 15630-056
N2 supplement (100x)	0.5 ml	1x	Invitrogen 17502048
B27 supplement (50x)	1 ml	1x	Invitrogen 12587010
n-Acetylcystein (NAC)	0.1 ml	1 µM	Sigma A9165-5G
Pen/Strep (100x)	0.5 ml	1x	Invitrogen 15140122

Components	Isolation Medium - 10 ml	Expansion Medium (EM) - 10 ml	Differentiation Medium (DM) - 10 ml	Final concentration	Cat. No.
Stock medium	5 ml	5 ml	5 ml	1x	-
Advaned DMEM/F12	4.936 ml	4.947 ml	4.96 ml	1x	Invitrogen 12634010
Nicotinamide	10 µl	10 µl	-	10 mM	Sigma N0636
Gastrin	10 µl	10 µl	-	10 nM	Sigma G9145.
HGF	10 µl	10 µl	-	50 ng/ml	Peprotech 100-39
FGF10	10 µl	10 µl	10 µl	100 ng/ml	Peprotech 100-26
EGF	10 µl	10 µl	10 µl	50 ng/ml	Sigma E4127.
R-spondin-1 (Rspo)	2.5 µl	2.5 µl	-	500 ng/ml	Peprotech 120-38. R&D 4645-RS-250.
Noggin	10 µl	-	-	100 ng/ml	Peprotech 250-38
Wnt3a	0.5 µl	-	-	100 ng/ml	Peprotech 315-20. R&D 5036-WN-010.
Rock inhibitor (10 mM)	1 µl			10 µM	Tocris 1254
A8301	-	-	10 µl	50 nM	Tocris 2939
DAPT	-	-	10 µl	10 µM	Sigma D5942

Table 2.1: mICO media composition. Detailed composition and concentrations for the three main media mentioned in this chapter for mICO culture.

Organoid isolation

Some organoid lines were isolated from adult mouse livers received from Dr. Luigi Aloia (LMCB-UCL then. AstraZeneca, Cambridge now) and Dr. Bethan Lloyd-Lewis (University of Bristol).

Livers were received in a 50-ml centrifuge tube with PBS up to a day after collection from the animal. They were then minced with fine scissors and subjected to several rounds of digestion (Ad DMEM/F12 + 1% FBS and 1% penicillin/streptomycin + collagenase (Sigma-Aldrich C9407) and dispase II (Life Technologies 17105-041) at a concentration of 0.125 mg/ml) with wash steps in between. Once clean duct structures were observed under a stereoscope, 50-200 of them were hand-picked with a 200 μl pipette and transferred to a 15-ml centrifuge tube with fresh digestion medium. These where then centrifuged at 100-200 g for 5 min at 8 °C, medium was removed and wash step was repeated at least once. After all supernatant was removed, the pellet was

resuspended in 100% matrigel (Corning 356238) (50 ducts per 50 μl). Duct structures were plated as described in section 2.1.2 and cultured as previously mentioned (figure 1.10a).

Newly isolated mICOs were passaged twice (see section 2.1.2) to get clean ductal cell cultures before expanding, freezing, and using for experiments. For passages 1 and 2 a couple of cryovials were frozen as backup only (section 2.1.1).

Growing frozen cultures

Most of the organoid lines used in this thesis were frozen cultures kindly gifted by the laboratories of Prof. Trevor Dale (Cardiff University, Wales), Prof. Meritxell Huch (Gurdon Institute, Cambridge then. MPCIG, Dresden now) and Dr. Luigi Aloia.

Frozen organoids were quickly thawed by gently swirling the cryovial around for 1-2 min in a water bath set at 37 °C. The vial contents were transferred to a 15-ml centrifuge tube with prewarmed Ad DMEM/F12. The tube was centrifuged at 100-200 g for 5 min, medium was removed, and wash step was repeated 1-2 times (pipetting carefully to avoid disrupting organoid fragments). The supernatant was removed as much as possible and the pellet resuspended in 100% matrigel (double the volume that was originally frozen (μl of matrigel mounds), see section 2.1.1). This was then plated as described in section 2.1.2 and cultured as previously mentioned.

Cryopreservation

To cryopreserve mICOs, organoids were grown for 5-6 days before mechanically disrupting the matrigel mounds. This was done following the same protocol for splitting (see section 2.1.2) except in this case the pellet was resuspended

by gentle pipetting to preserve organoids as much as possible. After wash steps, the pellet was resuspended in cold freezing medium (500 μl for 20-60 μl of matrigel mounds) and transferred to cryovials (500 μl per vial). Each vial was placed in a pre-cooled cell freezing container and kept in $-80\,^{\circ}\mathrm{C}$ for 24 h minimum. They were then transferred from the container to liquid nitrogen for long-term storage.

Name/ID	Genotype	Source
*2301-1	male WT	Cardiff University
Balbc	male WT	Cardiff University
0105	Axin2CRE R26-LSL-Tom	Cardiff University
*mTmG	ACTB-tdTomato,-eGFP	Gurdon Institute
MHCZ	Prom1-CreERT2/ZsGreen	Gurdon Institute
ecad-CFP	E-cadherin-mCFP	University of Bristol
*Female 40W	female WT	UCL
*Male 25W	male WT	UCL

Table 2.2: mICO lines. * indicates lines used to acquire the images and data presented in this thesis.

2.1.2 Splitting organoids for maintenance, expansion, and experiments

mICOs were passaged when fully grown (usually every 6 days) at a splitting ratio that ranged from 1:7 to 1:15, depending on organoid density. Matrigel mounds were mechanically disrupted by adding cold Ad DMEM/F12 to the well and pipetting up and down with a 1,000 μl pipette. This was transferred to a 15-ml centrifuge tube with more cold Ad DMEM/F12 and centrifuged at 100-200 g for 5 min. Medium was removed and wash step repeated twice to get rid of any matrigel left. In between wash steps the pellet was vigorously resuspended with a 1,000 μl pipette in order to break the organoids as much as possible until large cell clusters were no longer visible.

The pellet was then resuspended in the appropriate volume of 100 % matrigel based on the initial number of mounds and splitting ratio. The resuspended

cells were plated by pipetting 20 μl mounds into 24-well plates (up to 3 mounds per well) for maintenance and expansion of cultures, gene expression assays (section 2.5), morphology classification (section 2.6), and synthetic hydrogel experiments (section 2.2). For confocal imaging (section 2.3.3), tension measurements (section 2.7), and injury experiments (section 2.8), cells were plated on 8-well chambered slides as described in section 2.3.1.

Finally, the plates and/or slides were incubated for 10-15 min before adding expansion medium (550 μl for 24-well plates, 350 μl for 8-well slides). This medium was exchanged for fresh one every 2-3 days (500 μl and 300 μl, respectively) until they were ready for splitting, freezing, experiments or to begin the differentiation protocol (section 2.1.3).

2.1.3 Ductal organoid culture and hepatocyte differentiation

mICOs were grown in expansion medium (EM, table 2.1), which promotes ductal cell growth and expansion, before starting the hepatocyte differentiation process on day 4-5 (depending on how fast/slow organoids had grown because differentiating when they are too small can kill a high percentage). To induce differentiation, expansion medium was completely removed and exchanged for differentiation medium (DM, table 2.1). mICOs were then cultured for 12 more days in this differentiation medium, which was exchanged for fresh one every 2 days (figure 1.10b).

Consequently, experiments comparing 'young' progenitor (EM) and differentiated (DM) conditions correspond to organoids on day 4/5 (referred to as day 0 (EM 0d) in all figures and result chapters, see figures 1.10b and 3.1a), and day 16/17 (referred to as day 12 (DM 12d)), respectively. For experiments including the 'old' progenitor condition, organoids were cultured in expansion

medium for 16/17 days; exchanging it for fresh medium every 2 days (EM 12d, see figure 3.3a).

2.2 Organoid encapsulation in PEG-hydrogels

The synthetic hydrogel system used for this project was generated by the laboratory of Dr. Eileen Gentleman (KCL, London). We have been collaborating with her group for this part of the project and they have provided both the knowledge and the material needed for the experiments in this thesis (mainly PEG conjugates). The materials and protocols for making these hydrogels, and encapsulating organoids, are published in Jowett *et al*, 2021 [202] and Norman *et al*, 2021 [9]. Here I transcribe the protocols that were used with specific details for the experiments in this thesis.

2.2.1 Calculation of conjugates and organoids

PEG conjugate calculation

The appropriate weights of each PEG conjugate were calculated based on their molecular weight; the desired stiffness of the hydrogels (solid content, s.c.); and the ratios of inert (KDWERC), adhesive (CYAD) and degradable (DEG) PEG-peptide conjugates (figure 4.1a). To easily calculate weights and volumes, Eileen Gentleman's group generated an excel file to use as template (table 2.3 for an example). All PEG conjugates are custom ordered and conjugated by our collaborators. They provided the correct aliquots for each conjugate for every experiment, which were kept at $-20\,^{\circ}\mathrm{C}$ until used.

	Solid Content Con. of Gel w/v%	Volume added to the mold (ul)	Volume of final reaction volume (ul)	Total Solid Mass (mg, After Purification & Reaction)	Total molecular weight or PEG4VS	mmol of PEG4NPC or 1/4 peptide or PEG4VS	Molecular Weight of PEG4NPC (mg/mmol)	Purity of PEG4NPC	M(mg, PEG4NPC 10X) + 10%	KDWERC	Percentage KDWERC	Molecular Weight of Peptide (mg/mmol)	M(mg, Peptide) + 10%	CYAD	[CYAD] uM	Mass needed (mg)	Molecular Weight of Peptide (mg/mmol)	M(mg, Peptide) + 10%	DEG	[DEG]	Molecular Weight of Peptide (mg/mmol)	M(mg, Peptide) + 10%	Molecular Weight of PEG4VS (mg/mmol)	Purity of PEG4VS	M(mg, PEG4VS) + 10%
sc 2	2	30	33	0.66	38500.97	1.7E-05	10275	89.00%	0.20		0.00%	876.972	0.00		1000	50.00%	1848.95	0.06		50.00%	1872.03	0.06	20784	97.4%	0.37
sc 2.5	2.5	30	33	0.825	38500.97	2.1E-05	10275	89.00%	0.25		0.00%	876.972	0.00		1000	50.00%	1848.95	0.08		50.00%	1872.03	0.08	20784	97.4%	0.46
sc 3	3	30	33	0.99	38500.97	2.6E-05	10275	89.00%	0.30		0.00%	876.972	0.00		1000	50.00%	1848.95	0.10		50.00%	1872.03	0.10	20784	97.4%	0.55

	Solid Content Con. of Gel w/v%	Volume added to the mold (ul)	Volume of final reaction volume (ul)	M(mg, PEG4NPC-KDWERC 10X) + 10%	CYAD	DEG	M(mg, PEG4VS) + 10%
sc 2	2	30	33	0.198	0.063	0.064	0.366
sc 2.5	2.5	30	33	0.247	0.079	0.080	0.457
sc 3	3	30	33	0.297	0.095	0.096	0.549

		Con. (mg/	1	Con. (mg/	0.02641	Con. (mg/ul	0.02674	Con. (mg/	0.15242			
	Gels	M(mg) of PEG-KDWERC	Volume of PEG-KDWERC (ul)	M(mg) of PEG-CYAD	Volume of PEG-CYAD (ul)	M(mg) of PEG-DEG	Volume of PEG-DEG (ul)	M(mg) of PEG4VS	Volume of PEG4VS	Cells	HEPES	Total volume (ul)
sc 2		0.000	0.0	0.063	2.4	0.064	2.4	0.366	2.4	6.0	19.8	33.0
x6		**0.000**	**0.0**	**0.380**	**14.4**	**0.385**	**14.4**	**2.195**	**14.4**	**36.0**	**118.8**	**198.0**
sc 2.5		0.000	0.0	0.079	3.0	0.080	3.0	0.457	3.0	6.0	18.0	33.0
x2		**0.000**	**0.0**	**0.158**	**6.0**	**0.160**	**6.0**	**0.914**	**6.0**	**12.0**	**36.0**	**66.0**
sc 3		0.000	0.0	0.095	3.6	0.096	3.6	0.549	3.6	6.0	16.2	33.0
x6		**0.000**	**0.0**	**0.571**	**21.6**	**0.578**	**21.6**	**3.292**	**21.6**	**36.0**	**97.2**	**198.0**

Batches	mg	volume	x1 (2 gels each)
KDWERC			
sc 2	0.000	0.00	
sc 2.5	0.000	0.00	
sc 3	0.000	0.00	kdwerc
	0.000	0.00	0.000
CYAD			
sc 2	0.380	14.4	
sc 2.5	0.158	6	
sc 3	0.571	21.6	cyad
	1.109	42	1.109
DEG			
sc 2	0.385	14.4	
sc 2.5	0.160	6	
sc 3	0.578	21.6	deg
	1.12319	42	1.1231915

VS	Need	Weighed	Volume
sc 2	2.195		
sc 2.5	0.914		
sc 3	3.292		
	6.40148		

	vs
	6.4014814

Table 2.3: PEG conjugate calculation example for hydrogel experiment. For this example experiment, *mg* of each PEG conjugate are calculated for 3 stiffness conditions (s.c. 2, 2.5, and 3) with 50% adhesiveness (CYAD) and 50% degradability (DEG). 2 replicates per condition (x2).

Organoid calculation

Because the PEG-hydrogel reaction takes place at pH 8, organoid viability is 50-60% [202, 9]. In order to have enough organoids growing in the hydrogels, they need to be passaged at a lower ratio (1:2-1:3) and kept as large fragments rather than vigorously breaking them, as in section 2.1.2.

mICOs were always grown in 20 μl matrigel mounds (see section 2.1.2). However, the minimum volume for consistent crosslinking of PEG-hydrogels is 30 μl due to the properties of the system. To estimate how many organoids were needed and expand them accordingly, the following calculation was done for each experiment.

Hydrogel type	# of gels	µl/gel	Total µl	Buffer (µl) to resuspend cells
PEGs	6	33	198	36
mat	6	30	180	36
Total	**12**		378	**72**

Standard matrigel mound = 20 µl

378 µl / 20 µl = **18.9** mounds

19 matrigel mounds of 20 µl needed for **12** gels

Split **8** matrigel mounds minimum. Split ratio **1:2.4**

Table 2.4: Example of organoid calculation for PEG hydrogel experiment.

Organoids were then passaged and expanded once to make sure there was more than enough starting material. After 5-6 days, these mICOs were ready to be used for a hydrogel experiment.

2.2.2 Hydrogel formation and organoid encapsulation

Material setup

Before starting (or during wash steps whilst preparing the organoids, see below), the following materials were prepared.

All PEG conjugate aliquots to be used were place in a rack on ice together with sterile 1.5 *ml* low-binding reaction tubes; one for every hydrogel condition as this is the reaction tube were all hydrogel conjugates and organoids are mixed. The appropriate volume of cold Hepes/HBSS buffer pH8 was added to each reaction tube (based on the calculation from section 2.2.1).

24-well plates or 8-well slides were kept on a heating block (37 °C) to speed up the hydrogel reaction whilst all gels were being plated. A Sigmacote (Sigma, SL2-25ML) pre-treated 6 *mm* diameter glass ring was placed in the centre of a well to use as a mould for each 30 μl hydrogel.

Preparing organoids

mICOs were prepared as detailed in section 2.2.1. Once they were ready to be passaged, organoids were split following the same protocol described in section 2.1.2. To increase cell survival, organoids should remain as large fragments, instead of being broken down into small clusters of cells. Thus, the pellet was resuspended using mild to moderate force when pipetting. Wash steps were done with cold 1x HBSS solution and the pellet was kept in 0.5-1 *ml* on ice whilst preparing the PEG conjugates.

Hydrogel reaction

Low-binding 200 μl tips and tubes were used according to the protocols published in [202, 9]. For all volumes mentioned here see section 2.2.1, and tables 2.3 and 2.4.

All PEG conjugate aliquots were first spun down with a microcentrifuge and the corresponding volume of Hepes/HBSS buffer pH8 was added without pipetting up and down. Each aliquot was resuspended by vortexing for 1-2 minutes and spun down. Any powder that remained stuck to the walls and lid was collected by pipetting the buffer around, vortexing, and centrifuging. This was repeated until fully resuspended.

The organoid pellet, that was kept on ice until now, was centrifuged (100-200 g, 5 min) and the supernatant removed as much as possible. The pellet was then resuspended in the appropriate volume of Hepes/HBSS buffer pH8. 6 μl of the cell suspension were added to 27 μl of matrigel and plated on a well (no glass ring) to check cell density was high enough to proceed. If density was lower than expected, 1x HBSS was added to the cell suspension to prevent cell damage whilst more organoids were split and prepared. Once density was right, at least two 30 μl matrigel mounds were plated as positive controls before exposing cells to the reaction buffer.

The next steps for hydrogel formation and encapsulation have to be done as fast as possible, one hydrogel condition at a time, since the cells are in a pH 8 buffer and the hydrogel reaction initiates immediately upon mixing PEG-4VS with PEG-peptide conjugates. Each component (cells, KDWERC, CYAD, and DEG) was added to the reaction tube in the appropriate volume, pipetting up and down in between. PEG-4VS was then added and mixed by pipetting only. 30 μl of this hydrogel-cell suspension were pipetted inside each coated glass ring, being careful not to move or knock it over to prevent the suspension

from leaking out. The plate/slide and reaction tube were kept on the heating block whilst proceeding with the next hydrogel conditions (if more than one) or the matrigel negative controls, for which only the cell suspension was mixed with matrigel and plated directly on the well without a glass ring (figure 4.1b).

After all the replicates (minimum 2 per condition) and conditions were done, the plate/slide was carefully placed in the incubator together with the reaction tubes, which were used to determine when the hydrogels were fully formed. The leftover hydrogel-cell suspension in the reaction tubes was checked with a pipette tip 30 min after completing the first condition. If the hydrogels were not properly formed yet, they were kept in the incubator and checked every 10 min up until 1 h. When the hydrogels were ready, the plate/slide was placed back on the heating block, the rings were carefully removed with forceps and expansion medium was added (750/400 μl to cover the hydrogels). If there was more than one hydrogel condition, the time difference was considered before adding media to the rest and the matrigel controls (+ and -). After 2-3 days it became clear whether enough organoids had survived to proceed with the experiment.

2.2.3 Image and data analysis

Organoid survival

Organoid formation efficiency is usually calculated from the initial cell density or the number of cell clusters that formed organoids after several days. However, using these methods for this PEG-hydrogel system is not ideal due to a couple of reasons: (1) initial cell density cannot be reliably determined because mICOs are broken down into cell clusters; (2) one cell cluster does not necessarily equal one organoid as two or more cell clusters that are close to each other can fuse during the first days in culture (in matrigel and PEG hydrogels). Therefore, the total number of organoids in each gel (obtained

from the classification described in methods 2.6.3) were normalised to positive matrigel controls for each experiment. This total number includes organoids that were able to form even if they died later on.

Organoid size (area)

The OrganoSeg software [197] was designed to segment brightfield images of organoids and quantify morphometric features in an automated manner. While its segmentation is not clean enough for a clearer morphological classification (see section 2.6.3), it is good enough to quantify organoid area.

After optimisation with images from different conditions, the segmentation settings for all images were: 0.5 for intensity threshold, 80 for window size, and 250 for size threshold. Since organoid segmentation cannot be manually corrected in this software, four morphometric features were used to clean up merged organoids, debris, etc. using a custom R script. The features are: size threshold > 1000, eccentricity < 0.75, solidity > 0.48, and extent > 0.31. Organoid area was then extracted for each condition and imported into GraphPad Prism 7 for statistical analysis and plotting.

Morphology classification and gene expression analysis

Analysis of morphologies and gene expression were carried out as described in sections 2.6.3 and 2.5, respectively.

Data analysis

Data was analysed using custom R scripts or directly analysed and plotted with the help of GraphPad Prism 7.

2.3 Organoid imaging

2.3.1 Live sample preparation (matrigel sheet culture)

For brightfield imaging, cells were plated as matrigel mounds on 24-well plates (described in section 2.1.2). However, this set up is not the most suitable for confocal microscopy with higher resolution imaging since the working distance of the 40× objective is limited to 620 μm (section 2.3.3). Matrigel mounds are significantly taller and very few organoids end up close enough to the bottom of the plate for them to be imaged but not too close that they end up attaching to it and compromising organoid structure and cell identity. I therefore optimised a method for plating mICOs on chambered cover glasses to maximise the number of organoids located within the objective's working distance while preventing them from touching the glass bottom.

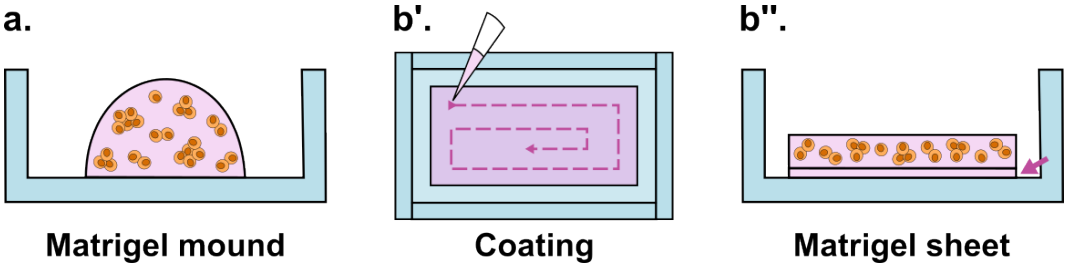

Figure 2.1: Matrigel sheet culture for live confocal imaging. (a.) Side view diagram of cells embedded in a regular matrigel mound in one well of a 8-well chambered cover glass. **(b'.)** Top view of the initial coating with a thin layer of matrigel (pink). Dotted line with arrowheads represents the pipetting motion and direction to create an even coat. **(b".)** Side view of matrigel sheet culture with the cell layer on top of the thin coat (purple arrow).

Before plating the cells, 8-well chambered cover glasses (IBL Baustoff+Labor GmbH 220.140.082) were first coated with a thin layer of matrigel. This was done by carefully pipetting 1-1.5 μl of matrigel per well, first around it to outline a rectangle without touching its walls and then slowly going around towards the centre to fill it in and create an even coat covering most of the

surface of the well (figure 2.1b'). The cover glass was then incubated for 3-4 minutes at 37 °C to set the coat, after which 14 μl of the cells resuspended in matrigel were plated by going over the coated region. To prevent any matrigel flow and achieve an even sheet with a homogeneous cell distribution, the 14 μl were slowly dispensed starting from the outside, re-drawing the outline of the first rectangle and finishing at its centre (figure 2.1b', b"). This method was used to set up mICOs for confocal imaging (section 2.3.3), tension measurements (section 2.7), and injury experiments (section 2.8).

2.3.2 Brightfield microscopy

To capture organoid morphologies, both in matrigel and synthetic hydrogel conditions, these were live-imaged using a Nikon GFP3 widefield time-lapse microscope with an incubation chamber for sample viability (37 °C, 5% CO_2) and a 4× air objective (Plan Fluor, N.A.:0.13, working distance: 17.1 mm). Four tiles (a z-stack each) were acquired per gel in order to image the entire surface of a hydrogel or most of a 20-30 μl matrigel mound. Images were taken every day, every other day or at the final timepoint only, depending on the experiment.

2.3.3 Confocal microscopy

Higher resolution images were taken using a Zeiss LSM 880 NLO microscope with an incubation chamber (37 °C, 5% CO_2) for live samples. Both live and fixed samples were imaged with a 40× oil objective (Plan Apochromat, N.A.:1.3, working distance: 0.21 mm). This microscope is equipped with a Coherent Chameleon Vision II Titanium Sapphire Multiphoton laser, tuneable from 680 nm to 1080 nm. This laser was tuned to 760 nm to perform ablations for tension measurements (see section 2.7) and injury experiments (section2.8).

Fixed samples were stained as described in section 2.4. Live samples were prepared as detailed in section 2.3.1 and stained usually with CellMask and Hoechst. Details for these and other dyes are specified in table 2.6 and in the appropriate figures.

To optimise membrane signal, in particular for injury experiments (section 2.8), organoids were incubated for 20-30 min with CellMask diluted at 1:2000-2500 (or for 10-15 min, 1:1500) in the appropriate medium. When Hoechst was used, it was added during this incubation period at 1:25000. After incubation and before live-imaging, media was changed for fresh one with only CellMask at a lower concentration (1:25000-3000).

2.4 Immunostaining

Fixing and staining organoids can be troublesome for a couple of reasons. Organoid morphology is usually compromised, mildly or severely, depending on the fixation process. Additionally, since organoids are grown embedded in matrigel, some antibodies have a harder time penetrating this matrix to reach the cells. I tried different fixing protocols to attempt to overcome these problems. Each is described below, with its specific advantages and drawbacks. Solutions, dyes, and antibodies used for fixing and staining are detailed in tables 2.5 and 2.6.

2.4.1 Protocol 1: taking organoids out of matrigel

As reported by Broutier *et al*, 2016 [192], matrigel can be removed and washed away in order to have mICOs in suspension, free of any matrix that can interfere with immunostaining. They recommend working with smaller organoids and gently handling them throughout all the steps for washing, fixing, and

staining to conserve their morphology. While this protocol allows antibodies to easily reach the cells, it has several disadvantages.

Small free organoids in suspension are harder to handle as they tend to float. Exchanging solutions becomes a finicky process, required volumes are higher, and the overall protocol is considerably longer compared to others. Moreover, matrigel cannot be fully removed without damaging the organoids and they often remain connected by a string of matrix. There are too many steps during which organoids are exposed and have to be moved around, leaving them prone to damage and even causing loss of organoids. Lastly, because mICOs are in suspension, they still need to be mounted after they have been stained. This limits the number of organoids that can be mounted and imaged in one session, as well as adding another step during which their morphology is can be damaged.

2.4.2 Protocol 2: fixing organoids in 100% matrigel

To overcome the problems that come with handling exposed organoids, I tried fixing and staining mICOs while keeping them in the same 8-well slide they were growing in (see section 2.3.1), without removing matrigel. This required some optimisation as it is a combination of the protocol used in our group to stain wing discs and the one by Broutier *et al*, 2016 [192]. The final protocol is described below.

Samples were incubated overnight at 4 °C with primary antibodies diluted at the appropriate concentrations in PBS-BSA 0.1% (see table 2.6). Organoids were then rinsed five times in PBS-BSA 0.1% (10 min washes), incubated for 2.5 h RT with secondary antibodies diluted in PBS-BSA 0.1% (covered from light), and washed again 2-3 times. If using dyes, these were diluted in PBS-BSA 0.1% and incubated for 20 min RT, followed by two 10 min wash steps.

Fluoromount G mounting medium (SouthernBiotech 0100-01) was added to each well to preserve fluorescence. Organoids were finally imaged by confocal microscopy (see section 2.3.3).

This protocol was used for all mICO stainings as it is more straightforward than others and uses the same setup established for confocal live-imaging (section 2.3.3) without having to mount the sample at the end. It takes less time and, even though bigger organoids do suffer some changes, morphology is better preserved overall without getting damaged.

Troubleshooting

I tried two more fixing strategies hoping to better preserve organoid morphology: (1) fixing with 0.25% Glutaraldehyde in Ad DMEM-F12, or PBS, for 5 min RT followed by 4% PFA for 15 min; and (2) fixing with 0.25% Glutaraldehyde + 2% PFA + 0.3% Triton in Ad DMEM/F12, or PBS, for 20 min. Samples were stained following the protocol above. However, there were no clear improvements or benefits from using these alternative fixing protocols.

Most antibodies against cell markers (cholangiocytes and hepatocytes) did not seem to work after several trials. The staining was not clear and there was a lot of background signal on the outside of the organoids. This could be due to different reasons such as matrigel being partially degraded and becoming messy when fixing and washing the sample, which could interfere with cell permeabilisation and accessibility for some antibodies. It could also be that the antibodies that were tested did not work properly, as antibodies against liver cell markers are often problematic and unstable. To solve this issue, I am currently trying a third protocol for fixing and staining recommended by Prof. Prisca Liberali (FMI for Biomedical Research, Switzerland) as well as trying other antibody options against the same or similar targets.

Solution	Dilutions	Cat. No.
Paraformaldehyde (PFA) 4%	PFA 16% 1:3 in PBS	TAAB Laboratories F017/3
Glutaraldehyde (GA) 0.25%	GA 5% 1:1000 in PBS	-
	GA 5% 1:1000 + PFA 2% 1:6 + Triton 0.3%	-
PBS-BSA 0.1%	BSA 0.01 g in 10 ml PBS	Sigma A4503
PBS-BSA 2%	BSA 0.2 g in 10 ml PBS	-
PBT 0.3%	Triton X-100 3 µl in 1 ml PBS	Sigma T8787
PBT-BSA	PBT 0.3% + PBS-BSA 2%	-

Table 2.5: Solutions used for fixing mICOs.

Dyes	Stock	Dilution	Cat. No.
CellMask	5 mg/ml	1:2000-1:2500	ThermoFisher Scientific C10046, C10045
Hoechst	50 mg/ml (in water)	1:25000	Sigma B2261
Phalloidin	200 units/ml (in methanol)	1:20-1:60	Molecular probes A34055 Life Technologies A22287
SiR Actin	1mM (in DMSO)	1:1000	Cytoskeleton Inc SC001
DAPI	1 mg/ml (in water)	1:1000	Sigma D8417-1MG

Primary antibodies	Host	Dilution	Cat. No.
ve-cadherin	Rabbit	1:300	Abcam ab33168
phospho-myosin light chain 2	Rabbit	1:50	Cell Signalling 3671S
ZO-1	Rat	1:300	DSHB R26.4C
phospho-histone H3 (PH3)	Mouse	1:1000	Millipore 05-806
alpha tubulin	Mouse	1:300	Sigma T8203
EpCAM	Rat	1:300	DSHB G8.8
oval cell marker (MIC1-1C3)	Rat	1:100	Novus Biologicals NBP1-18961
mouse osteopontin (OPN)	Goat	1:100	R&D Systems AF808-SP
Sox9	Rabbit	1:100	Sigma AB5535
human serum albumin (Alb)	Mouse	1:100	R&D Systems MAB1455-SP
Secondary antibodies	**Host**	**Dilution**	**Cat. No.**
anti-Mouse Alexa Fluor 488	Goat	1:300	Molecular Probes A11029
anti-Rabbit Alexa Fluor 488	Goat	1:300	Molecular Probes A11034
anti-Rat Alexa Fluor 488	Goat	1:300	Abcam ab150161
anti-Mouse Rhodamine red X	Donkey	1:200	JacksonImmunoResearch 715-295-151
anti-Mouse Cy5	Donkey	1:300	JacksonImmunoResearch 715-175-151
anti-Rabbit Cy5	Donkey	1:300	JacksonImmunoResearch 711-175-152
anti-Rat Cy5	Donkey	1:300	JacksonImmunoResearch 712-175-153

Table 2.6: Dyes and antibodies used for staining mICOs.

2.4.3 EdU staining and quantification

Staining

As an indicator of cell proliferation, EdU incorporation experiments were performed using the Click-iT EdU Alexa Fluor 647 Imaging Kit (Invitrogen, C10340), following a protocol optimised for the fly wing disc by Dr. Alice Roycroft, a previous postdoctoral fellow in our lab. This protocol was based on the manufacturer's instruction, only optimising the fixing, blocking and permeabilisation steps (described in Protocol 2). mICOs were first incubated for 1 h with EdU stock solution diluted 1:1000 before washing it away with PBS-BSA 0.1% for 5 min. Organoids were then fixed with PFA 4% for 25 min RT followed by two 5 min wash with PBS-BSA 2%. Samples were permeabilised with PBT 0.3% for 20 min, washed again twice with PBS-BSA 2%, and incubated in freshly prepared 1× Click-iT reaction cocktail for 30 min RT. After incubation, samples were washed once with PBS-BSA 2%, three times with PBT 0.3% for 10 min, and three more with PBT-BSA for 10 min. Organoids were ready for further staining with antibodies and/or dyes as described in 2.4.2.

Quantification

EdU^+ and EdU^- cells were manually counted using the multi-point and counters tool on Fiji [203]. Percentage of positive cells [EdU^+ / ($EdU^+ + EdU^-$)] was calculated and plotted on RStudio [204] and GraphPad Prism 7.

2.5 Gene expression assay (rt-qPCR)

2.5.1 Sample preparation

For organoids grown in matrigel, mICOs were passaged as described in section 2.1.2 and plated as 20 μl matrigel mounds in 24-well plates (3 mounds per well). Every condition had at least 2 replicates (2 wells) per experiment. For experiments where organoids were sorted by morphology, see section 2.6.1. PEG-hydrogels are harder to dissociate and RNA yield is usually quite low, probably due to PEG molecules interfering with the extraction process. Sorting organoids by morphology was impossible for these experiments and replicates had to be pooled together in order to extract enough RNA.

2.5.2 RNA extraction

PicoPure RNA Isolation Kit (Applied Biosystems KIT0204) was used for all experiments in this thesis since it is able to give a reasonable yield even when working with a few organoids. All samples were disassociated with the extraction buffer from the kit (50 μl for 2 wells with matrigel mounds or for 2 hydrogels), transferred to 1.5 ml tubes and homogenised by continuously pipetting up and down. Each tube was then flash frozen in dry ice sprayed with 70% ethanol and kept at $-4\,^{\circ}\mathrm{C}$, this step helps reduce RNase activity and improve RNA stability.

For matrigel conditions, wells were rinsed with PBS for 5-10 min before adding the extraction buffer. For experiments where organoids were sorted by morphology, samples were processed as described in section 2.6.1 before extraction buffer and flash freezing. PEG-hydrogels were also rinsed with PBS before adding Trypsin-EDTA (50 μl for 2 gels) to dissociate them, as recommended by Eileen Gentleman's group. Gels were transferred to a 1.5 ml tube and incubated at $37\,^{\circ}\mathrm{C}$ for 20-30 min, pipetting up and down every 10 min with

a 200 μl tip to help break the gels down. After incubation, extraction buffer was added to each tube (50 μl for 2 gels) and mixed by pipetting to dissociate hydrogels as much as possible. These were then flash frozen as described above.

All frozen samples were thawed in a water bath at 37 °C and processed according to the manufacturer's instructions for RNA extraction.

Initial attempts

When first implementing these experiments, I tried two other kits for RNA extraction. RNeasy Plus Mini Kit (QIAGEN 74134) had a very low RNA yield, which was probably due to low organoid numbers and their Micro Kit might have worked well. The second one, PureLink RNA Micro Kit (Invitrogen 12183016) using Trizol for the extraction, was recommended by a neighbouring lab (Alison Lloyd group). This kit worked well but took longer and required more additional reagents compared to PicoPure, which gave similar or even better yields.

2.5.3 Reverse transcription quantitative real-time PCR (rt-qPCR)

cDNA was synthesised from 100 ng to 1 μg of extracted RNA using the SuperScript II Reverse Transcriptase kit (Invitrogen 18064-014) and random primers (Invitrogen N8080127), according to the manufacturer's protocol. The cDNA was then amplified using MESA Blue qPCR MasterMix Plus kit (Eurogentec RT-SY2X-03+NRWOUB) and specific primer pairs (see table 2.7) on a CFX Connect Real-Time PCR Detection System (Bio-Rad). The cycling conditions used were (1) 95 °C for 5 min; (2) 45 cycles of 95 °C for 15 sec, 60 °C for 20 sec and 72 °C for 40 sec; (3) 95 °C for 10 sec; and (4) a melting curve from 65 °C to 95 °C with an increase of 0.5 °C. The housekeeping gene Hprt1 was used as

a control for all conditions and negative controls using water instead of cDNA were added for every primer pair. All conditions and primer pairs had at least 2 replicates.

Gene	Forward	Reverse	Reference
Housekeeping			
Hprt	AAGCTTGCTGGTGAAAAGGA	TTGCGCTCATCTTAGGCTTT	Aloia *et al,* 2019. Broutier *et al,* 2016.
Progenitor / Stem cells			
Axin2	TGTCCAGCAAAACTCTTC	CTTCTCTTGAAGGACCTGA	Aloia *et al,* 2019.
Ki67	CCTTTGCTGTCCCCGAAGA	GGCTTCTCATCTGTTGCTTCCT	Aloia *et al,* 2019.
Lgr5	ATTCGGTGCATTTAGCTTGG	CGAACACCTGCGTGAATATG	Sorrentino *et al,* 2020.
Sox9	CTCCTAATGCTATCTTCAAG	GCTTCAGATCAACTTTGC	Aloia *et al,* 2019.
Trop2 (Tacstd2)	CACGGCTCAGAGCAACTGTA	AATACCTGTGAGCCCATTGC	Aloia *et al,* 2019.
Cholangiocytes			
Hnf6 (Onecut1)	AGCATCCCACAGGCCATCTT	CCCGTGTTCTTGCTCTTTCC	Broutier *et al,* 2016.
Epcam	GACGACGTGGACATAGCTGA	GCTCTCCGTTCACTCTCAGG	Aloia *et al,* 2019.
Hepatocytes			
Albumin	GCGCAGATGACAGGGCGGAA	GTGCCGTAGCATGCGGGAGG	Broutier *et al,* 2016. Sorrentino *et al,* 2020.
Cyp3a11	CCTTCCAGCCTTGTAAGGAA	CCGTGGCACAACCTTTAGAA	Aloia *et al,* 2019.
G6pc	GAATTACCAAGACTCCCAGG	TGAGACAATACTTCCGGAGG	Aloia *et al,* 2019.
Glul	CAAGTGTGTGGAAGAGTTACCTGAGT	TGGCAACAGGATGGAGGTACA	Sorrentino *et al,* 2020.
Hnf4a	GCTAAGGCGTGGGTAGGG	AGGCTGTTGGATGAATTGAGG	Broutier *et al,* 2016.
Ttr	ATGGTCAAAGTCCTGGATGC	AATTCATGGAACGGGGAAAT	Broutier *et al,* 2016. Sorrentino *et al,* 2020.

Table 2.7: Primers used for rt-qPCR.

Data analysis

Gene expression levels (Ct values) were normalised to the expression of the housekeeping gene Hprt1 and analysed using a custom R script.

2.6 Morphology classification

2.6.1 Sample preparation

Organoids were grown either in matrigel (as described in section 2.5.1) or PEG-hydrogels (see section 2.2). Samples were imaged using a widefield microscope (section 2.3.2) and/or processed for gene expression analysis (section 2.5) when mICOs were ready to be collected (section 2.1.3).

In order to collect and process organoids, each condition was rinsed with PBS for 5-10 min before digesting matrigel with collagenase (Worthington LS004194, 0.0208 g/ml, 1:5 dilution) for 10 min at room temperature, gently pipetting up and down a couple of times with a sterile Pasteur pipette (cut tip). Once organoids were released form the matrix, all wells for each condition were pooled together in a 90 mm petri dish filled with Ad DMEM/F12 to dilute collagenase and stop digestion. mICOs were then hand sorted by morphology (see section below) into three 1.5 ml tubes using a Pasteur pipette (cut tip) under a stereoscope (figure 3.6a). All tubes were spun down to remove as much media as possible before adding 50 μl of extraction buffer and proceeding as described in section 2.5.2.

2.6.2 Classification criteria

mICOs were classified by morphology into 3 main categories for gene expression analysis (see figures in chapter 3 for representative images):

1. ***Spherical***: translucent organoids with a clear big lumen enclosed by a cell monolayer; mostly of spherical shape, sometimes with a more elongated ellipsoid-like morphology but still smooth and translucent. Darker, less translucent, organoids that remained smooth with a big lumen and a spherical/ellipsoid shape were also included. When an organoid of these characteristics had a small, almost negligible bulge or wrinkle, it was also considered as spherical. All organoids from a 'young' progenitor condition (EM 0d) had a spherical morphology, except for a few that were unclear and not enough to separate and extract RNA from.

2. ***Folded***: these organoids were not translucent anymore and did not have one clear big lumen. They were darker with cell layers folding into the previous luminal space, sometimes forming bilayered bridge-like structures. The cell layer outlining the organoids looked thicker and irregu-

larly folded instead of smooth.

3. ***Unclear(mix)***: for gene expression experiments, when a cluster of organoids was not properly disassociated and had a mix of morphologies, all of them were included in this category. Organoids that had as many characteristics of spherical as well as folded morphologies were also classified as unclear/mix. For both gene expression and image analysis, organoids that were too small to determine whether the outlining cell layer was thicker because it was folded or because it was too small in size were also considered as unclear. For image analysis, organoid that were not entirely visible within the image were also counted as unclear.

For image analysis, three more categories were added for further specificity. Categories 4 and 5 were quantified separately but grouped together as ***intermediate*** to facilitate analysis and comparison across conditions. Similarly, categories 3 and 6 were grouped as ***unclear*** for analysis since they are significantly different from *folded* and *spherical* organoids. Representative images of these morphologies are included throughout chapter 3.

4. ***semi-Spherical***: any organoid that had a clear lumen and was mostly spherical except for a couple folded features such as an obvious bulge, wrinkle or any 'imperfection' that compromised the spherical shape but was insufficient to consider the organoid as folded.

5. ***semi-Folded***: any organoid that was mostly folded except for a couple small regions with clear spherical characteristics such as a smooth surface, a lumen considered big for the organoid size and/or more translucent but with a highly wrinkled/folded surface. Any spherical feature that compromised the folded shape but was insufficient to consider the organoid as spherical.

6. ***Bulging***: this category included organoids that retained a translucent morphology but had several bulges protruding, resembling a blebbing cell. They had no cell layers folding in and the outlining layer remained thin and smooth even though it was bulging. These organoids were a minority and not always present.

7. ***Dead***: dead organoids were easy to distinguish as both cells and luminal space darken significantly and their outline becomes fuzzy with debris on the outside, as if they were disintegrating. Spherical organoids have an almost black cell outline and a very dark lumen filled with dead cells. Folded organoids turn black overall and it is almost impossible to discern their complex internal structures (*i.e.* folds and bridges). For gene expression experiments, dead organoids were discarded.

2.6.3 Image and data analysis

Manual classification

As described in section 2.3.2, four z-stacks per gel were acquired. These were stitched together using a custom Fiji macro. The multi-point and counters tool on Fiji [203] was used to manually classify organoids into the categories described above. The points were marked and saved on the average projection of every stitched image but its z-stack was used as reference.

Semi-automated classification

The software OrganoSeg [197] was designed to segment brightfield images of organoids and quantify morphometric features in a more automated manner. Initial data from mICO images ran through this program seemed promising. However, more optimisation needs to be done in order to obtain reliable data. In addition, all the morphometric information needs to be analysed more care-

fully to be able to interpret it. This is work in progress.

Data analysis

Data acquired from manual classification was analysed using a custom R script and plotted with the help of GraphPad Prism 7. Data acquired through semi-automated classification was preliminary analysed using a custom R script.

2.7 Tissue tension measurements

2.7.1 Sample preparation

mICOs were plated on 8-well slides as described in section 2.3.1. When ready for experiments (section 2.1.3), organoids were stained with CellMask for live-imaging and ablation (see section 2.3.3).

2.7.2 Laser ablation

Organoids were imaged on a confocal microscope equipped with a 2-photon laser for ablation. Digital zoom was set to 5×, using a 40× oil objective, and laser power to 35-45% after optimisation (see section 2.3.3 for details). Only one junction per organoid was ablated by drawing a thin perpendicular ROI across it. A timelapse was acquired for every junction, starting prior to ablation and finishing up to 5 min after ablation with a pixel size of 83.0266 nm (for x and y), and a time interval of 0.64 sec.

2.7.3 Image and data analysis

Junction displacement was measured in Fiji [203] by drawing a straight line from the centre of each vertex right before and after ablation. The first was subtracted from the latter and divided by the time interval to calculate the instant recoil (*i.e.* initial velocity). Microsoft Excel was used for this calculation and the data was plotted on RStudio [204] and GraphPad Prism 7.

Plateau curves were obtained by measuring junction displacement every 3.2 sec for 1.5 min. However, junctions would often heal and shrink beyond their initial length, making curves hard to interpret. As a result, curves were not included here and instant recoil was used to compare conditions.

2.8 Injury experiments

2.8.1 Sample preparation

mICOs were plated on 8-well slides as described in section 2.3.1. When ready for experiments (section 2.1.3), organoids were stained with CellMask and Hoechst for live-imaging and injury (see section 2.3.3).

2.8.2 Laser ablation

Organoids were imaged on a confocal microscope equipped with a 2-photon laser, which was used to induce injury following a similar protocol to the one established by Dr. Robert Tetley, a previous postdoctoral fellow in our group [31]. Cells chosen for ablation were targeted by drawing small circular ROIs around their tricellular junctions (10-12). This ensures cell death of only the targeted cells while avoiding autofluorescence and cavitation issues induced by large ROIs. Ablation was also restricted to a single Z-plane in the sub-apical

region. Digital zoom was set to 1×, using a 40× oil objective, and laser power was set to 70-80% after optimisation (see section 2.3.3 for details).

A timelapse was acquired for 1-4 h, starting prior to ablation/injury, with a pixel size of 0.2 μm (for x and y), and a time interval of 1-6 min (longer intervals after 1 h post-injury). To avoid phototoxicity when using Hoechst, the blue channel was only acquired at the beginning of a timelapse and at the end as a final Z-stack for reference. Z-stacks were defined with a 0.4-0.75 μm depth resolution.

2.8.3 Image processing and analysis

Timelapses were first reduced to a more manageable size by choosing timepoints at the following intervals to keep them as uniform as possible (depending on the initial acquisition intervals): the first 2 timepoints are right before and after ablation, subsequent timepoints were taken every 4 min from 4-60 min, every 8 min from 68-108, and 12 min from 120 until the end of the movie. These substacks were then used for the following analyses.

Wound closure time

Reduced timelapses were manually checked to determine the timepoint at which the wound had closed. Recently, evidence has shown that apical and basal surfaces of epithelia can behave differently and even independently [205]. Therefore, to gain insight into apical vs. basal behaviour of injured mICOs, two final timepoints were registered for each movie: apical (t_a) and basal (t_b) closure time.

Pipeline for wound closure and tissue dynamics

I tried several pipelines to optimise processing and analysis of injury movies and extract information about wound and tissue dynamics. These pipelines included different software such as Imaris, Huygens, Ilastik [206], and EpiTools [207]. This optimisation, together with the help of other lab members (Dr. Robert Tetley, James Van-Hear, and Dr. Pablo Vicente-Munuera), led to the pipeline now used in our group as the current standard for analysing organoid injury movies:

a. ***Cleaning/prepping movie (Fiji)***: background subtraction, gaussian blur, and 3D registration on reduced timelapses. A custom Fiji macro (written by James Van-Hear) splits and inverts every single timepoint to prepare them for the next step.

b. ***Peeling layer of interest (Fiji)***: surface peeler plugin (from https://github.com/DaleMoulding/SurfacePeeler) identifies the upper surface of the 3D structure on the image, which can then be moved along the Z-axis to extract a particular layer with a specific thickness. For injured mICOs, the surface was moved to the sub-apical layer for extraction, which allows removal of most of the unwanted membrane and debris signal from other planes. This is an important step for a clearer 2D adaptive projection, downstream analysis and tracking.

c. ***Projecting curved layer of interest in 2D (Fiji)***: localZprojector plugin [208] generates a cleaner adaptive 2D projection by calculating a height-map and only incorporating the signal of interest. This results in sharper cell outlines that make segmentation less prone to errors and therefore reduces the time spend on manual corrections.

d. ***Image segmentation (Fiji)***: Tissue Analyzer plugin [209, 210] segments cell membranes for all images in a timelapse in a semi-automated way. The resulting skeletons were then manually corrected to remove any mistakes.

e. ***Timelapse tracking (ICY)***: 2D-projected timelapses and their hand-corrected skeletons were then imported into ICY for cell tracking using EpiTools plugins [207]. The 'CellGraph' module was run with the 'stable_marriage' algorithm, a propagation limit of 5 frames, cutting 0 border lines, and using ICY-SwimmingPool. Any tracking mistakes were corrected using the 'Test' tool in the 'CellOverlay' module. Further information and detailed instructions on these modules and tools can be found in the Icy Plugins section from EpiTools Wiki Pages (https://epitools.github.io/wiki/) and the supplementary information from Tetley *et al*, 2019 [23].

f. ***Data extraction (ICY)***: 'CellOverlay' and 'CellExport' modules were used to extract relevant data , which was then exported as Excel files for analysis (details below).

Wound closure dynamics

Because the analysis pipeline is very time-consuming, an initial analysis was done to look at the wound dynamics only. Steps d-f were performed focusing only on the wound and the first cell row around the wound. Wound area and polygon number (*i.e.* number of cells around the wound) were extracted for every timepoint to look at wound closure dynamics and wound-edge cell intercalations as an indicator of tissue fluidity [23].

Tissue dynamics

For tissue dynamics, steps d-f from the analysis pipeline were performed including at least the first two rows of cells around the wound. So far, only cell elongation and polygon number have been properly analysed to look at tissue behaviour. However, a lot more data can still be extracted from tracked

timelapses and analysed to collect more information.

2.8.4 Data analysis

For wound closure dynamics, wound area was expressed as a percentage of the total area of ablated cells. Wound-edge cell intercalations were also expressed as a percentage of the initial number of cells (polygon number) around the wound.

For tissue dynamics, spatial distribution of cell elongation was calculated using the distance between the centres of the wound and each cell (custom R script).

Pre-injury timepoints were easier to process and segment. Thus, polygon numbers can be extracted from all visible cells to use as indicators of cell packing distribution and tissue fluidity [211, 212, 20].

All data was analysed using custom R scripts and plotted with the help of GraphPad Prism 7.

2.9 Data and statistical analysis

Data analysis

Specific details regarding image and data analysis are provided in the appropriate sections within this chapter. All data was processed and analysed using Microsoft Excel, custom R scripts, and/or GraphPad Prism 7. Custom Fiji macros and R scripts are all available upon request.

Statistical analysis

Statistical tests were performed in either RStudio [204] or GraphPad Prism 7. Specific details and p-values are provided in the corresponding figures and tables throughout chapters 3, 4, 5, and appendix A.

Chapter 3

How does morphology change as organoids grow and differentiate?

3.1 Introduction

Research on liver organoids has mostly been at a molecular and cellular level, comparing changes in gene expression and cell identity to a developing or regenerating liver *in vivo* (reviewed in [176] and discussed in 1.5). Although morphology and cell organisation has been generally overlooked in the organoid field, they have become of increasing interest in recent years in other organoid systems [196, 197, 198, 199, 200, 201].

The aims of this chapter are (1) to characterise the morphological changes of liver organoids as they go from progenitor cells to a mature/differentiated state; and (2) to describe the correlation between changes in morphology and cell identity.

3.2 Organoid morphology becomes more complex as they differentiate

3.2.1 Morphological changes in differentiated cultures

mICOs are initially grown and maintained as progenitor cells in expansion medium (EM) (see methods 2.1.3 and [192]), where they normally form epithelial cysts with a spherical morphology. When hepatocyte differentiation is induced by exchanging EM for differentiation medium (DM) for 12 days, I noticed these spherical structures often acquire a more complex 'folded' morphology (figure 3.1). Some of the features organoids develop are: turning darker; their cell monolayer enclosing a big lumen becomes thicker and/or wrinkled; cell bilayers appear, sometimes bridging opposite ends of an organoid across its lumen; the main lumen is reduced in size and small lumina form within multilayered regions (figure 3.1b" and 3.2).

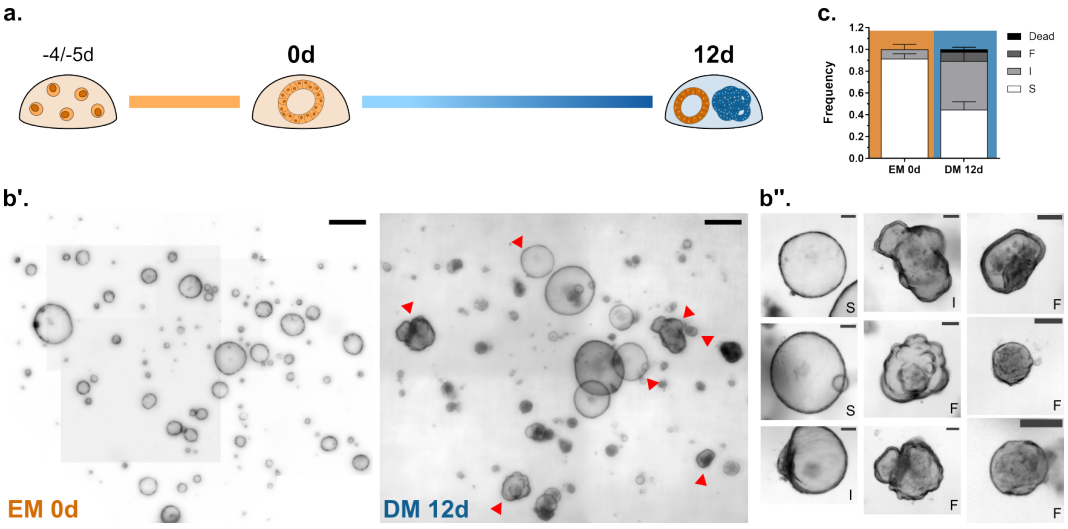

Figure 3.1: Morphological changes upon differentiation. (a.) Differentiation protocol for mICOs. Expansion Medium (EM) in orange, Differentiation Medium (DM) in blue. **(b'.)** Brightfield images of representative matrigel domes. 500 μm scale bars. **(b".)** Individual organoids from b' (red arrows) showing morphological variety. 100 μm scale bars. S: spherical, I: intermediate, F: folded. **(c.)** Quantification of morphology frequencies. n=4 independent matrigel mounds (456 organoids) for EM 0d. n=7 mounds (254 organoids) for DM 12d. Error bars represent mean and s.d. See table A.1 for statistical analysis and p-values.

Quantification of these morphologies per matrigel mound (figure 3.1c) shows that progenitor organoids, before differentiation is induced (EM 0d), are ∼90% spherical (S) with a minority starting to acquire folded features (intermediate, I). After the differentiation process (DM 12d), less than 50% remain spherical and over 50% of organoids have folded characteristics to varying degrees. While ∼40% exhibit a mix of spherical and folded features (I), around 10% acquire a distinct folded (F) morphology.

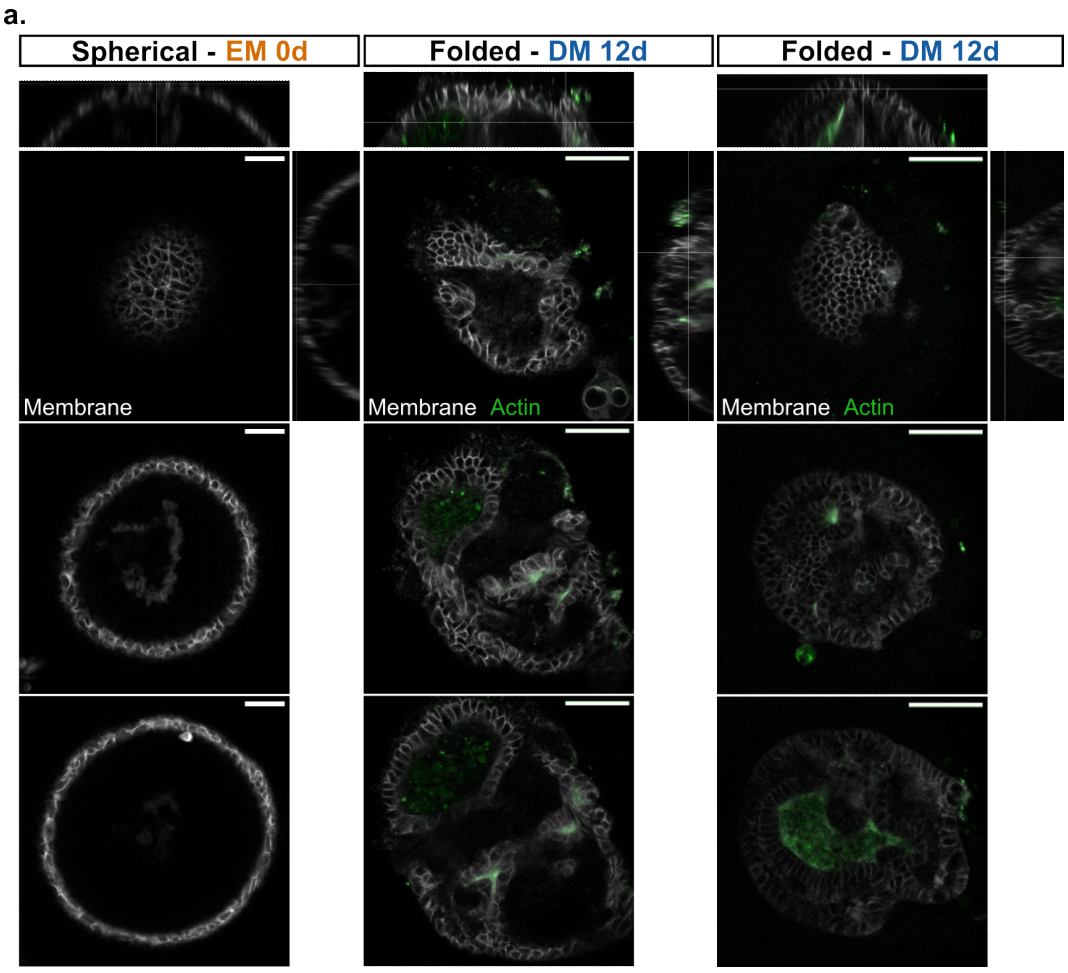

Figure 3.2: Representative confocal images of spherical and folded morphologies. XZ (top) and XY (right) views, as well as 3 different XY views for each organoid. Spherical organoid from progenitor conditions (EM) is representative of spherical organoids in differentiated conditions (DM). Folded organoids in DM show cell thickening, multilayered regions and multiple big and small lumina (labelled in green with Phalloidin). 50 μm scale bars.

3.3 Changes in morphology and gene expression profiles take place without chemical differentiation

3.3.1 Morphological changes in older cultures

Interestingly, mICOs kept in EM for longer than 6 days also start to acquire a complex folded morphology even though chemical differentiation has not been induced and fresh EM being replenished every 2 days (figure 3.3a and b). In order to compare these changes in morphology to differentiated conditions, I cultured mICOs in EM for the same amount of time (12 days) and quantified the frequency of each category as in section 3.2. Similar to DM 12d, organoids in older EM cultures (EM 12d) are ∼60% spherical, less than 40% show folded features, and ∼10% are distinctly folded (figure 3.3c).

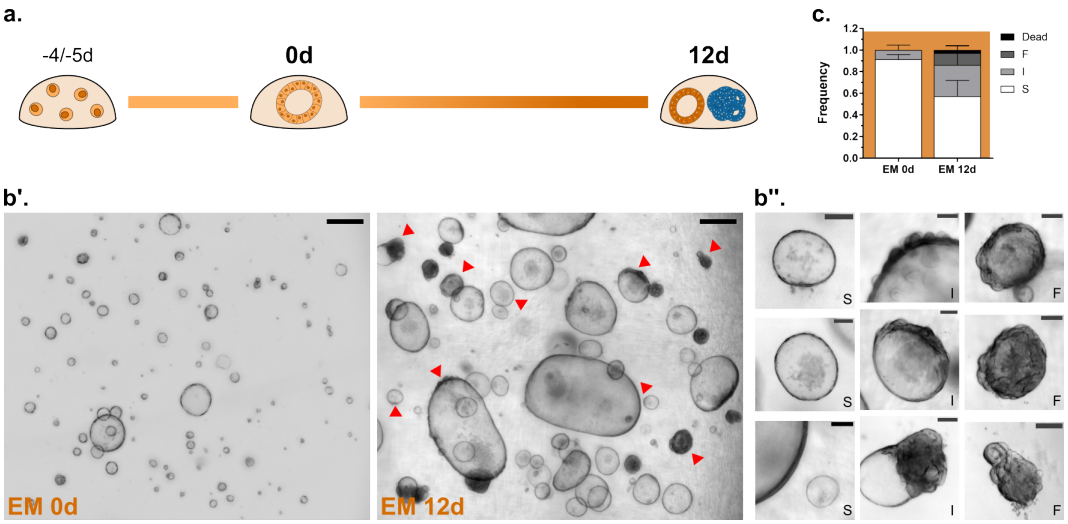

Figure 3.3: Morphological changes in older organoid cultures. (a.) Culture protocol for mICOs. Expansion Medium (EM) in orange. **(b'.)** Brightfield images of representative matrigel domes. 500 μm scale bars. **(b".)** Individual organoids from b' (red arrows) showing morphological variety. 100 μm scale bars. S: spherical, I: intermediate, F: folded. **(c.)** Quantification of morphology frequencies. n=4 independent matrigel mounds (456 organoids) for EM 0d. n=7 mounds (281 organoids) for EM 12d. Error bars represent mean and s.d. See table A.1 for statistical analysis and p-values.

The fact that these proportions are a lot more variable than those in differentiated cultures, and that comparable morphologies have been observed in other studies using mICOs [161, 213, 163, 192], raise two questions. The first one is whether older cultures are differentiating despite being kept in progenitor medium (EM), which I address in the next section. The second question is if these morphological changes are related to successful hepatocyte differentiation, addressed in section 3.4.

3.3.2 Gene expression profiles

To answer the question of 'spontaneous' differentiation taking place in older expansion cultures, I first quantified cell proliferation through EdU staining of organoids in young progenitor/expansion conditions (EM 0d), chemically differentiated cultures (DM 12d), and expansion cultures of the same age (EM 12d) (figure 3.4a and c). EdU+ cells per organoid show that proliferation levels are higher in young organoids and are significantly lower in both differentiated and older organoids (figure 3.4c). I then examined changes in gene expression across the same 3 conditions by measuring mRNA levels of canonical markers for progenitor/stem cells, cholangiocytes, and hepatocytes through RT-qPCR (figure 3.4b).

Gene expression profiles of EM 0d and DM 12d agree with what has been reported before for mICOs [161, 163, 192, 63] (figure 3.4b). Lower expression of markers for cell division (Ki67), stem cells (Lgr5, Sox9, Axin2 (n.s.)), and cholangiocytes (Epcam (n.s.)) in DM 12d compared to EM 0d. Conversely, DM 12d organoids have significantly higher expression of hepatocyte markers: albumin, a protein expressed throughout the entire hepatocyte compartment with highest levels in zone 1 hepatocytes (periportal region) [172] (see section 1.4.3); Hnf4α, a transcription factor that antagonises β-catenin to promote

zone 1 hepatocytes [171, 173]; and Cyp3a11, an important enzyme involved in drug metabolism, produced by mature hepatocytes in zone 3 [214, 172]. Trop2 expression, a conventional proliferative marker, is also higher in DM 12d. However, while Trop2 is known as an oncogene with a role in cell proliferation [215], it is normally expressed in healthy liver tissue and there is evidence showing decreased expression of this gene in liver carcinomas. Trop2 is also expressed in the bile duct and it is associated with bipotent hepatic stem cells and organoid formation (reviewed in [216]). These changes in gene expression confirm that hepatocyte differentiation is taking place in DM 12d mICOs to an extent, as it has been shown that *in vitro* hepatocyte differentiation of mICOs is not 100% efficient. Ductal phenotypes remain present, hepatocyte markers are expressed in up to 30-40% of cells, and only $\sim$1% feature hallmarks of mature hepatocytes [161, 192].

In addition to being less proliferative (EdU in figure 3.4c and Ki67 in figure 3.4b'), organoids from older cultures (EM 12d) have lower expression of cholangiocyte markers (Hnf6 (n.s.), Epcam). Even though Hnf4α and Cyp3a11 levels are not that different from EM 0d, Albumin expression is 10$\times$ higher, a ubiquitous marker for all hepatocytes. Similar to DM 12d, EM 12d also shows higher expression of Trop2 indicating the presence of potential bipotent hepatic stem cells. These observations are evidence that, as the culture grows older, some organoids start to 'spontaneously' differentiate into hepatocytes. Differences between DM 12d and EM 12d are expected as differentiation is more directed when chemically induced (using differentiation medium, see methods 2.1.3) instead of occurring 'spontaneously'.

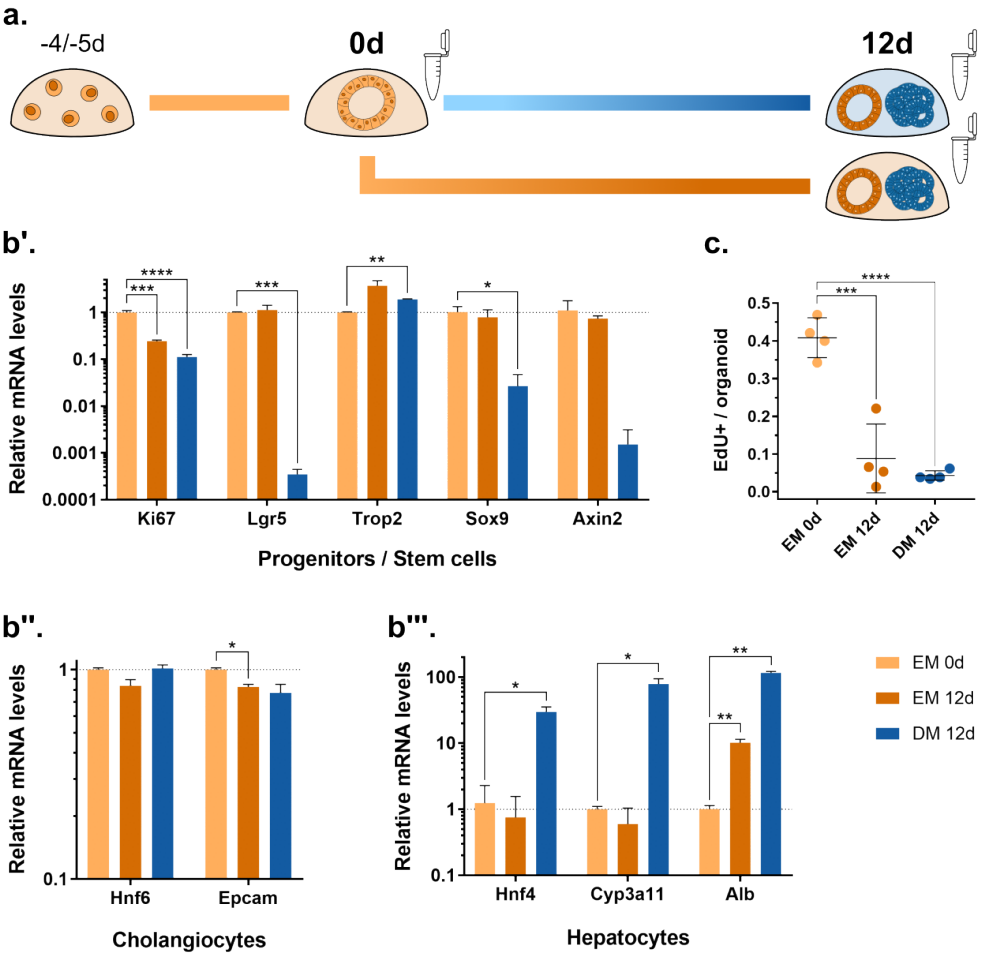

Figure 3.4: Changes in gene expression profiles of older and chemically differentiated cultures. (a.) mICOs growth conditions for gene expression analysis. **(b.)** mRNA levels of (b'.) progenitor/stem cell markers, (b".) cholangiocyte/mature ductal cell markers, and (b"'.) hepatocyte markers. All mRNA levels are shown in log scale and relative to EM 0d. n=2 for all conditions. Unpaired two-tailed multiple t-tests with False Discovery Rate approach (FDR using the two-stage linear step-up procedure of Benjamini, Krieger and Yekutieli, with Q=1%) to compare 12d conditions against EM 0d. **(c.)** Quantification of cell proliferation from EdU stainings. n=4 for all conditions. One-way ANOVA analysis with Tukey's multiple comparisons test to compare all conditions against each other. Colour labels on the bottom right are the same for all panels. Error bars represent mean and s.d. p-values are * <0.05, ** <0.01, *** <0.001, and **** <0.0001. n.s. are not shown.

3.4 Gene expression profiles of organoid morphologies confirm differences in cell composition

3.4.1 Morphological features suggest differences in cell composition

Organoid morphology can vary depending on the tissue and cell type they are derived from. In the past decade, several studies on liver organoids from either hepatocyte or biliary duct origin have been published (see [161, 213, 163, 192, 217, 190, 191, 218, 219, 220, 221, 222]). Even if not directly addressed, these studies provide evidence that ductal and hepatocyte organoids tend to have different morphological features that somewhat resemble their *in vivo* anatomy. At the cell level, ductal and hepatocyte polarisation have significant differences (figure 3.5c). These differences allow ductal cells/cholangiocytes to form biliary ducts with tubular structures, and hepatocytes to form a network of bile canaliculi that spreads throughout the liver epithelium (see section 1.4.3 and [186]).

All of this indicates that organoid morphology is likely to be determined by its cell composition. Since *in vitro* differentiation of mICOs towards hepatocytes is heterogeneous and up to 30-40% efficient (as discussed in 3.3.2), I propose the following hypothesis to explain the morphological differences observed in sections 3.2 and 3.3. The organoids that remain spherical upon differentiation retain a ductal phenotype and cell identity (figure 3.5b,c, top panels), those which acquire a complex folded morphology are the organoids that are able to progress further in the hepatocyte differentiation process and are mostly composed of immature and/or mature hepatocytes (figure 3.5b,c, bottom panels, and a).

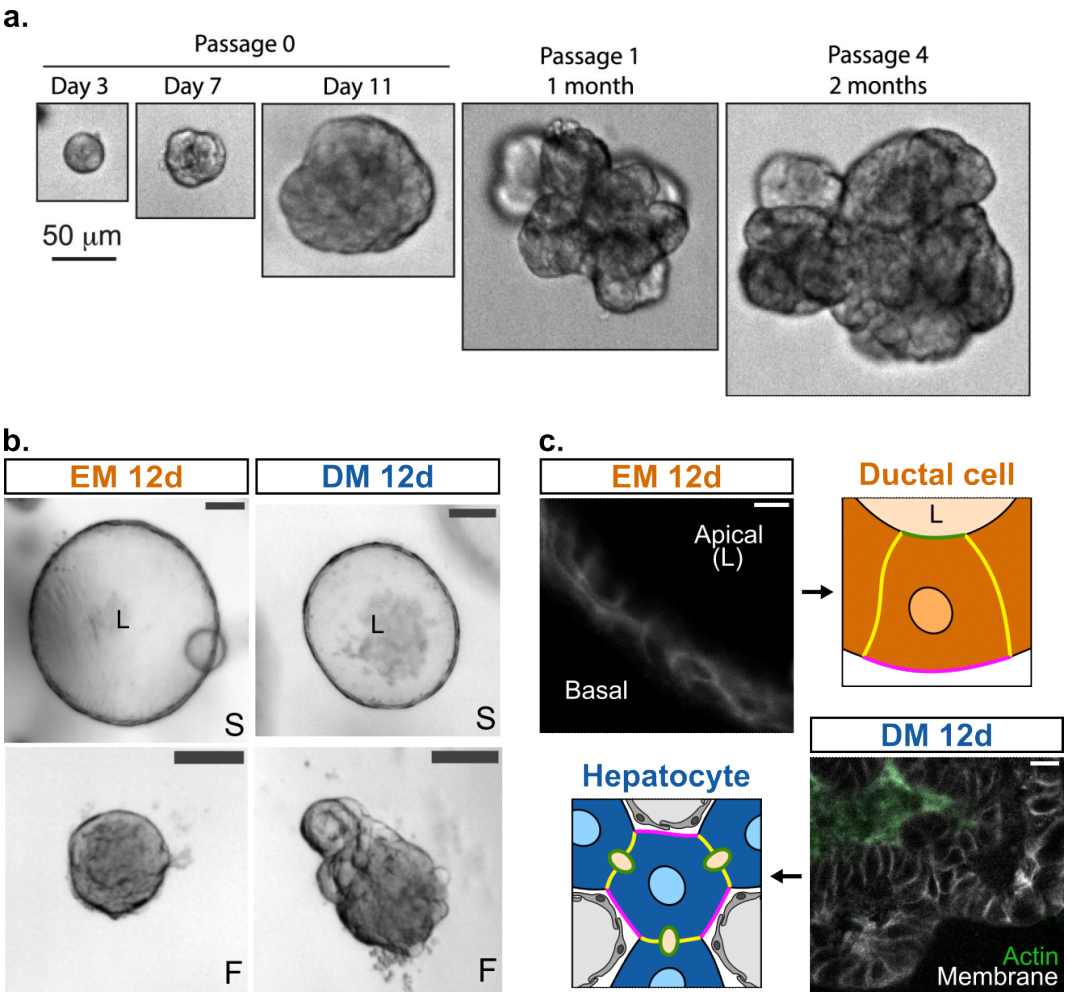

Figure 3.5: Different organoid morphologies resemble organisation of ductal cells or hepatocytes. Morphology hypothesis: Spherical (S) organoids **(b)** result from ductal polarity, resembling ductal structures **(c, top panels)**. Folded (F) organoids **(b)** result from hepatocyte-like polarity **(c, bottom panels)**, resembling morphologies of hepatocyte derived organoids **(a)**. **(a.)** 3D culture of primary mouse hepatocytes as organoids. Image from Peng *et al*, 2018 [191], reproduced with permission of the rights holder (Elsevier). **(b.)** Brightfield images from figures 3.1 and 3.3. 100 μm scale bars. **c.** Confocal images zoomed in from figure 3.2 showing cell organisation in spherical (top) and folded (bottom) mICOs. 10 μm scale bars. Diagrams indicate polarity of both epithelial cell types in the liver: apical (green), lateral (yellow), and basal (pink) domains. Liver sinusoids are in grey. L, lumen.

3.4.2 Gene expression profiles of organoids sorted by morphology

To test the proposed hypothesis, I cultured mICOs as in section 3.3 and manually sorted organoids from EM 0d, EM 12d, and DM 12d into 3 categories: spherical, folded, and mix (to include organoids that did not clearly belong to the first two, see methods 2.6 for details). I then quantified gene expression levels of markers for ductal cells (Ki67, Sox9 for proliferative; Hnf6 for mature) and hepatocytes through RT-qPCR (figure 3.6).

Overall, the 3 conditions follow a similar trend to that observed in section 3.3.2. DM 12d organoids have lower levels of ductal genes and higher levels of hepatocyte markers compared to EM 0d and EM 12d. Further interesting differences are observed when comparing spherical vs. folded morphologies across all conditions (figure 3.6b). Folded DM 12d (solid blue) have decreased expression of Hnf6 and an increase in Hnf4α and Albumin compared to spherical DM 12d (blue outline); suggesting folded morphologies do have a more hepatocyte-like profile than spherical morphologies. On the other hand, folded and spherical organoids from older cultures (solid and outlined orange, respectively) have seemingly similar levels for most genes, except for Sox9 and Cyp3a11. While it is possible that both organoid morphologies in EM 12d might have the same number and type of ductal cells vs. hepatocytes, these results could also be explained by the contribution of four factors considering expansion medium (EM) is not actively inducing differentiation: (1) the total numbers of each cell type; (2) whether similar cell types always express these genes at the same or varying levels; (3) the state of cells along the hepatocyte differentiation/maturation process; and (4) the presence of bipotent cells and/or the natural gradual transition observed *in vivo* between ductal and hepatocyte compartments, with ductal sub-populations expressing some hepatocyte markers and vice versa (see section 1.4.3).

The fact that gene expression profiles of EM 12d spherical and folded mICOs are so similar despite having very different morphologies is intriguing. An additional explanation could be that morphological changes precede gene expression changes that eventually take place in a permissive chemical environment, which might be delayed or absent in EM 12d given that cell maturation and differentiation are 'passive' and unregulated compared to DM 12d. It would be interesting to look at these gene expression profiles when folded organoids first appear in DM 12d conditions, as well as 1-2 days later, to test whether organoid morphology changes before hepatocyte markers are clearly expressed. To further confirm this hypothesis, the effect of a possible heterogeneous starting population would need to be ruled out as these organoids are not grown from single cells. This could be done following a similar protocol to Serra *et al.* [199], where they grow intestinal organoids from truly single cells and follow them individually until they form cystic or budding structures. Although the starting heterogeneity should be much lower in liver compared to intestinal organoids due to differences inherent to each organ, the number of epithelial cell types each is normally comprised of and the way in which they are isolated.

Moreover, spherical DM 12d organoids remain more hepatocyte-like compared to both spherical and folded EM 12d. This could be due to the four factors discussed above, as well as the chemical conditions in DM driving cell differentiation in a more regulated manner while EM promotes ductal progenitors (with a constant supply of Rspo1 triggering the Wnt pathway). In addition, hepatocytes present in spherical DM 12d mICOs could be closer to those found in zone 1 *in vivo*, which tend to show a more ductal-like morphology, unlike hepatocytes from zone 2 and 3 (described in section 1.4.3).

Complementary approaches are therefore needed to further distinguish between ductal and hepatocyte sub-populations within organoids of different morphologies, as RT-qPCR is limited by the number of genes that can be tested

at once and the overlap between cell sub-populations. I have tried antibody stainings of different markers to visually confirm folded regions correspond to hepatocytes; however, these stainings have not been successful and are possibly more limited than RT-qPCRs for similar reasons. Electron microscopy could provide more information at the cellular level since there are distinctive characteristics that identify ductal cells from hepatocytes. This is a technique that I am currently testing and seems promising, although at the moment there are no results that can be included in this thesis as preliminary. Furthermore, bulk and/or single-cell, as well as fluorescent *in situ*, RNA sequencing would be powerful tools to discern cell sub-populations within organoids of specific morphologies in more detail. These would also help identify the type of hepatocytes in spherical and folded DM 12d organoids, and whether they correspond to zone 1 and zones 2-3, respectively, as discussed above.

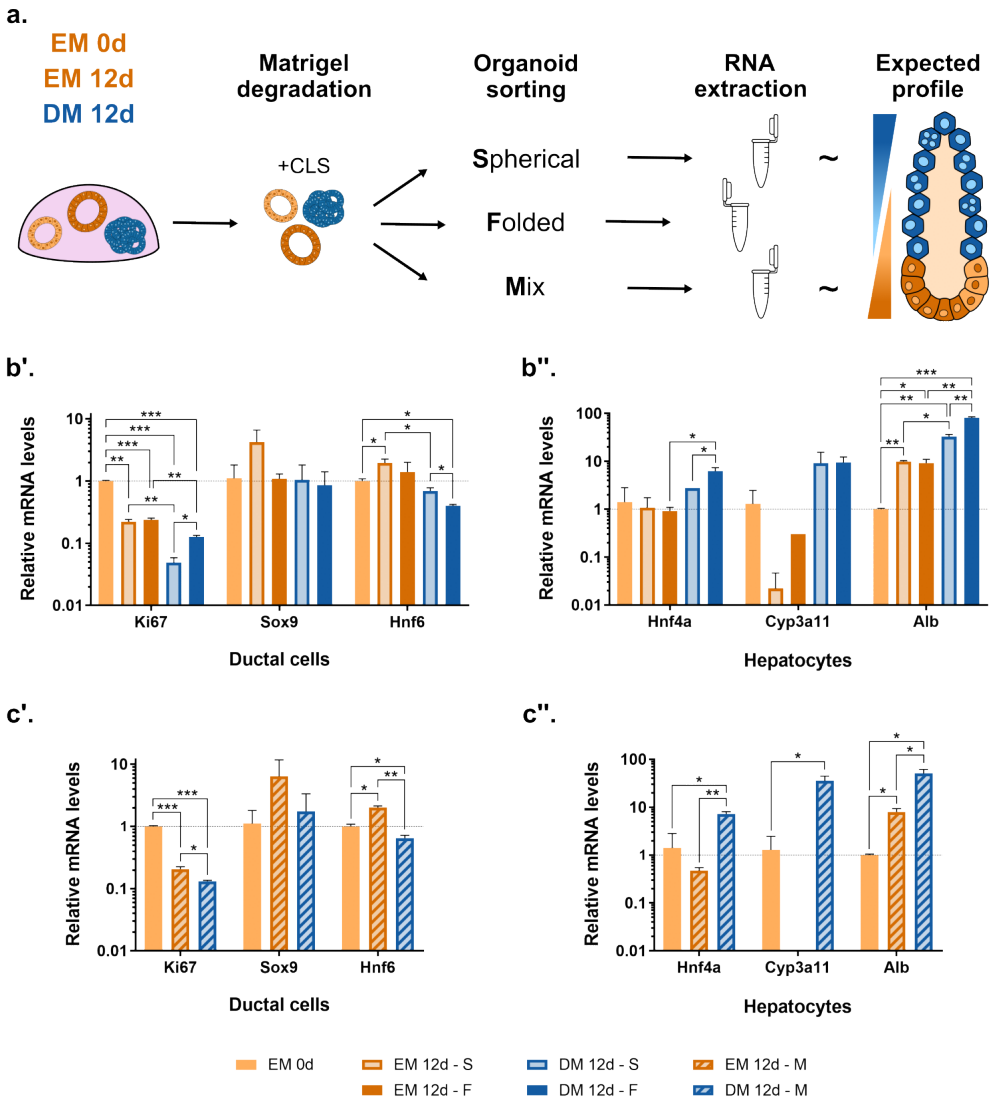

Figure 3.6: Morphological phenotypes have different gene expression profiles. **(a.)** Experimental procedure. **(b.)** mRNA levels of spherical and folded organoids, as well as **(c.)** organoids with mixed morphologies for (b',c'.) ductal cell markers (proliferative (Ki67, Sox9) and mature (Hnf6)), and (b",c".) hepatocyte markers. All mRNA levels are shown in log scale and relative to EM 0d. n=2 for all conditions. Unpaired two-tailed multiple t-tests with False Discovery Rate approach (FDR using the two-stage linear step-up procedure of Benjamini, Krieger and Yekutieli, with Q=1%) to compare all conditions against each other. Colour labels at the bottom are the same for all graphs. Error bars represent mean and s.d. p-values are * <0.05, ** <0.01, *** <0.001, and **** <0.0001. n.s. are not shown.

3.5 Discussion

In this chapter I focused on two main aims. The first one was to characterise changes in morphology of mICOs as they go from a progenitor to differentiated state; for which I grouped organoid morphologies into 3 main categories: spherical, folded, and intermediate. At first (EM 0d), ∼90% of organoids have a clear spherical morphology, with none being properly folded. After 12 days of chemical induction of hepatocyte differentiation (DM 12d), the 3 morphology categories repeatedly appear (figure 3.1). This takes place not only in DM 12d, but also in older cultures grown in progenitor conditions for the same number of days (EM 12d) (figure 3.3). When examining these older cultures in more detail, I observed they are less proliferative, they have lower levels of ductal markers and start expressing Albumin, a classical hepatocyte marker for hepatocytes (figure 3.4).

The second aim was to determine the correlation between changes in morphology and cell identity. Morphological features of spherical and folded organoids resemble characteristics of ductal and hepatocyte cells, respectively (figure 3.2 and 3.5c). Folded morphologies are also very similar to those formed by hepatocyte derived organoids (figure 3.5a,b). Additionally, evidence from other groups working with different types of liver organoids (reviewed in [176] and discussed in section 3.4.1) support the hypothesis that spherical mICOs are mostly composed of ductal cell types, and folded mICOs are mainly composed of hepatocyte-like cells and/or differentiated hepatocytes.

To address this hypothesis, I quantified changes in gene expression of spherical and folded organoids from actively differentiated (DM 12d) and older cultures (EM 12d). While results show that folded DM 12d organoids have a more hepatocyte-like profile than spherical DM 12d, they are less clear for the other categories. This uncertainty can be explained by the high variability in 'spontaneous' or passive differentiation of older cultures (comparing figure 3.4 and

3.6, as well as 3.1c and 3.3c). As discussed in section 3.4.2, the presence of immature and other sub-populations of each cell type due to the gradual transition of ductal and hepatocyte gene expression *in vivo* also make it difficult to fully distinguish between sub-populations with a single technique. These results and potential interesting explanations are discussed in depth in the same section, as well as additional experiments and alternative approaches to gather more detailed information on the differences between spherical and folded organoids.

Nonetheless, we can conclude from the work in this chapter that actively differentiated folded organoids (DM 12d) display a more hepatocyte-like phenotype; and that hepatocyte differentiation can happen 'passively' as mICOs are grown for longer periods of time, even in conditions that favour progenitor cells (EM 12d). The latter suggests other mechanisms must be inducing morphological changes and cell differentiation independent of medium composition, which I seek to better understand in chapter 4.

Chapter 4

How is the mechano-environment affecting organoid morphology and differentiation?

The synthetic PEG hydrogel system used in this chapter was developed by our collaborators from Dr. Eileen Gentleman's group at King's College London [202, 9]. They have provided the material and background knowledge needed for these experiments. Shirine Merlo-Nikpay, a then summer student in our group, helped with initial hydrogel experiments and morphology quantification.

4.1 Introduction

In chapter 3, I showed that differentiated mICOs exhibit a wide range of morphologies that seem to correspond to the main cell type present in the organoid. However, this is a variable phenotype that is not fully regulated by the controlled composition of the media and thus must be influenced by other factors. It is generally known that the substrate of a tissue has an important mechano-

chemical role in morphogenesis and differentiation (see section 1.3.2 for more detail). The liver is particularly susceptible to changes in ECM levels and composition due to its strategic and limited arrangement *in vivo*, practically absent in the hepatocyte compartment (see section 1.4.2). Hence, changes in the mechanoenvironment of liver organoids can potentially affect their morphology and induce cell differentiation.

Organoids are usually grown in matrigel, a natural soft hydrogel that can be degraded and remodelled by the cells. While there are many benefits of using matrigel, its composition is highly variable and its mechano-chemical properties cannot be independently controlled, making it a significant source of heterogeneity in organoid culture. Moreover, when growing mICOs for maintenance and experiments, I noticed that the matrigel domes slowly get degraded after a week in culture, becoming looser and possibly softer. These observations, together with the results from chapter 3 and previous evidence of substrate stiffness regulating cell differentiation (discussed in section 1.3.2), hint at the prospect of changes in the substrate properties influencing organoid morphology and cell composition. Matrigel heterogeneity and irregular degradation could also be contributing to the variability in organoid morphologies and gene expression profiles in older mICO cultures.

The aim of this chapter is to test the effects of substrate properties on the morphology and cell identity of liver organoids. To overcome the disadvantages of matrigel and address this, I make use of a synthetic PEG-hydrogel system [202, 9] that permits independent manipulation of its mechano-chemical properties. These experiments are discussed in this chapter after an introduction on synthetic matrices (section 4.1.1) and PEG hydrogels (section 4.1.2).

4.1.1 Synthetic Matrices

An important component of *in vitro* cell culture is the substrate provided for the cells to grow. The plastic or glass surfaces of a culture dish are a common and simple substrate that enables cell attachment and growth. However, their non-physiological chemical and mechanical properties (*i.e.* lack of ECM components and high stiffness) affect cell behaviours, growth rate, morphology, and identity (see section 1.3.2 and [117, 6, 223, 142, 143, 144]). To overcome this problem and replicate some of the physiological characteristics of substrates *in vivo*, ECM proteins have been used to coat these stiff surfaces (*e.g.* collagen, fibronectin, laminin, matrigel, etc.).

Matrigel is a 'natural' hydrogel with a rich mixture of ECM proteins and growth factors that mimic the extracellular environment of many tissues *in vivo*. It provides a more physiological *in vitro* 3D microenvironment in which cells can have complex behaviours and form complex 3D structures. Its liquid state at $4°C$ facilitates cell embedding before polymerising at $37°C$. Because of these characteristics, matrigel has been established as the standard natural gel for 3D cell culture and organoid growth. Although there are many benefits of using natural gels, there are also several drawbacks that limit the potential and applications of organoids. In particular, matrigel is produced by a mouse sarcoma cell line, which results in compositional and structural variability from batch to batch, in addition to making it unsuitable for therapeutic use. Furthermore, its physical characteristics cannot be independently manipulated. Matrigel is already a soft substrate (20–450 Pa, depending on protein concentration and temperature conditions [224, 225]) that cannot be softened nor stiffened without simultaneously changing its biochemical properties.

To address some of the limitations of natural gels, synthetic ones have been developed from inert polymers that can be functionalised with ligands, peptides, or ECM proteins to control cell-substrate interaction. Polyacrylamide

and polydimethylsiloxane (PDMS) hydrogels have been mostly used for 2D cell culture [117], while polyethylene glycol (PEG) hydrogels have become of interest for 3D culture in recent years [6, 8, 202]. In addition to the advantages of synthetic gels discussed below, their optical properties make them suitable for live cell imaging.

4.1.2 Polyethylene glycol (PEG) hydrogels

Polyethylene glycol (PEG) is a biocompatible hydrophilic polymer that can be synthesised in multiple geometries (*i.e.* linear, branched, Y-shaped, and multi-arm) with a broad range of molecular weights. PEGs are inert polymers resistant to biodegradation and protein adhesion, a perfect 'blank canvas' that can be modified with reactive functional end groups to conjugate them with different ligands that allow interaction with the cells. After being functionalised, PEGs are physically or covalently crosslinked to form hydrogels consisting of polymer networks with well-defined molecular architecture, biochemical composition, and physical properties. [6, 226, 7, 223]

Multi-arm PEG hydrogels (typically 4, 6, or 8 arms) are commonly used for drug delivery and tissue engineering. More recently, new PEG based hydrogels have been developed for 3D cell culture due to their high modularity, which allows independent manipulation of their physical and biochemical properties. For example, the molecular weight of the chosen PEG molecules determine the mesh size and network architecture; changing either PEG size or polymer density controls hydrogel stiffness and elasticity; the shear modulus is affected by the degradation rate, which can be manipulated via polymer density (passive, long-term, degradation) or the type of degradable peptides used (active, short-term, degradation) [226, 202, 227, 9].

The biochemical properties of a hydrogel are defined by the ligands used

to functionalise the polymer, which are usually known to play a role in cell signalling (*e.g.* growth factors, receptor ligands), cell-cell interaction (*e.g.* transmembrane or junctional proteins) or cell-substrate interaction (*e.g.* adhesive (RGD) or degradable peptides). These ligands can be modified to react passively, via enzymatic reactions or user-directed methods (*e.g.* light exposure). More advanced techniques (such as photopatterning, bioprinting and microfluidics) have allowed ligands activation or incorporation in a specific spatial micropattern before or after hydrogel crosslinking and polymerisation, further controlling and manipulating the cells microenvironment. [6, 228, 226, 7, 229, 230]

4.1.3 Tetra-PEG hydrogel system for culture of mICOs

The synthetic hydrogels used in this project consist of two PEG molecules: a PEG-peptide conjugate (A_4) and a PEG-4VS (B_4). This A_4+B_4 system was developed and characterised by Dr. Eileen Gentleman's group [202, 9] with the purpose of avoiding primary looping to increase crosslinking efficiency and network connectivity. The inert PEG-4NPC is functionalised with a degradable (DEG), adhesive (CYAD) or non-functional (KDWERC) peptide. These PEG conjugates are then combined with PEG-4VS in a 1:1 ratio to trigger crosslinking and polymerisation (see methods 2.2). Thus, stiffness is determined by total polymer concentration (characterised through AFM by Dr. Michael Norman [9]), while degradability and adhesiveness are independently controlled by adjusting the ratio of the corresponding conjugates. [202]. Stiffness and mesh size can also be altered with bigger or smaller PEG molecules, however this was kept constant for the experiments of this chapter, using only 20 kDa PEGs.

4.2 Characterisation of substrate properties that affect organoid growth and morphology

4.2.1 PEG system and experimental setup

To investigate how substrate properties affect mICO morphology and cell identity independently from medium composition, I cultured organoids in synthetic PEG hydrogels with varying mechano-chemical characteristics while keeping medium composition constant (*i.e.* expansion medium, EM) and organoids grown in matrigel as controls (see methods 2.2 and figure 4.1).

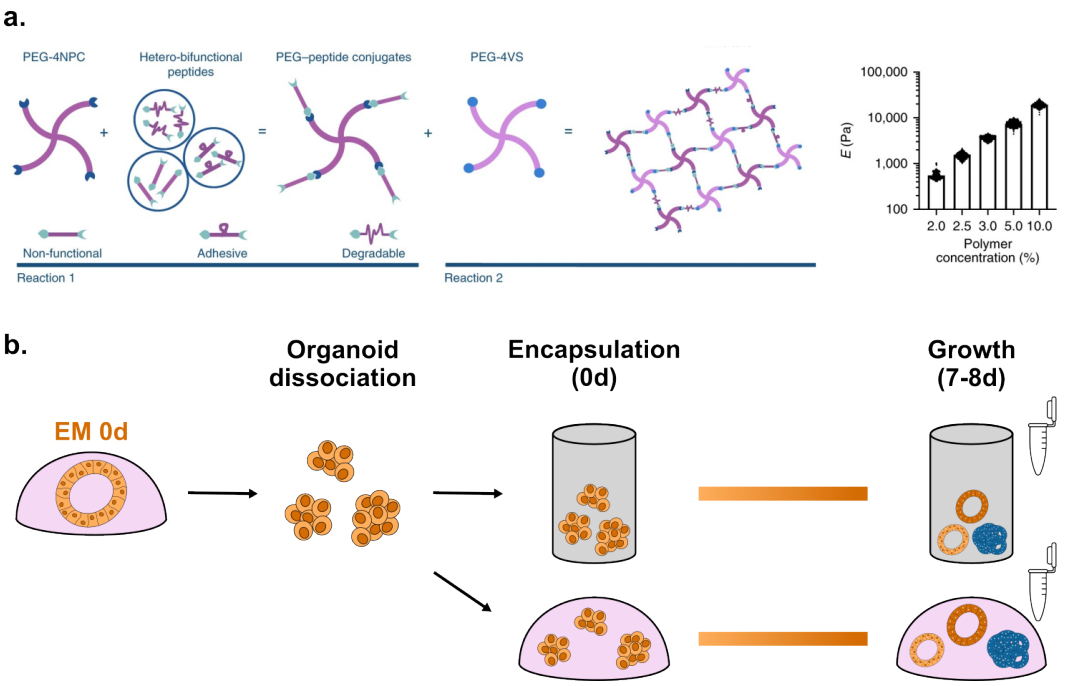

Figure 4.1: PEG hydrogel system and experimental setup. (a.) Representation of the components and the reaction that takes place to form PEG hydrogels. Graph shows hydrogel stiffness when varying PEG polymer concentration (log scale). Diagrams and graph from Jowett *et al*, 2021 [202], reproduced with permission of the rights holder (Springer Nature). **(b.)** Experimental pipeline for growing mICOs in PEG hydrogels (grey) and their corresponding matrigel control (pink). See methods 2.2 for detailed protocols.

There are four main mechano-chemical characteristics that can be independently tuned with this PEG system: stiffness, mesh size, adhesiveness, and degradability (figure 4.1a). Through discussions with our collaborators and running a couple of test experiments, it was reasoned that the most relevant variables are stiffness and adhesiveness. Thus, I explored a matrix with 3 different levels of each variable without changing mesh size, degradability, and culture medium.

Stiffness is determined by PEG polymer concentration as tested and established by the Gentleman lab [202, 9] (figure 4.1a, right panel). The three stiffness levels I explored are 2% = 0.5 kPa, 2.5% = 1.6 kPa, and 3% = 4 kPa. The reasoning behind these conditions is that 0.5 kPa is the softest gel we can make with this system without compromising its crosslinking efficiency and it is similar to what has been reported for matrigel (up to 0.45 kPa, see section 4.1.1). 1.6 kPa falls within the range of what has been reported as physiological liver stiffness (1.3-1.7 kPa [231, 232]). Finally, 4 kPa is the stiffest condition that can be still considered as physiologically healthy in some studies [233], although others have reported it as a diseased condition [231, 232].

Adhesiveness is controlled by changing the percentage of the PEG conjugate with adhesive peptides (RGD). We decided to test 0%, 25%, and 50% as the highest RGD concentration in order to avoid compromising degradability, which was kept constant at 50% for all 9 conditions. Organoid survival and morphology frequencies were quantified for all conditions; the results are discussed in the following sections.

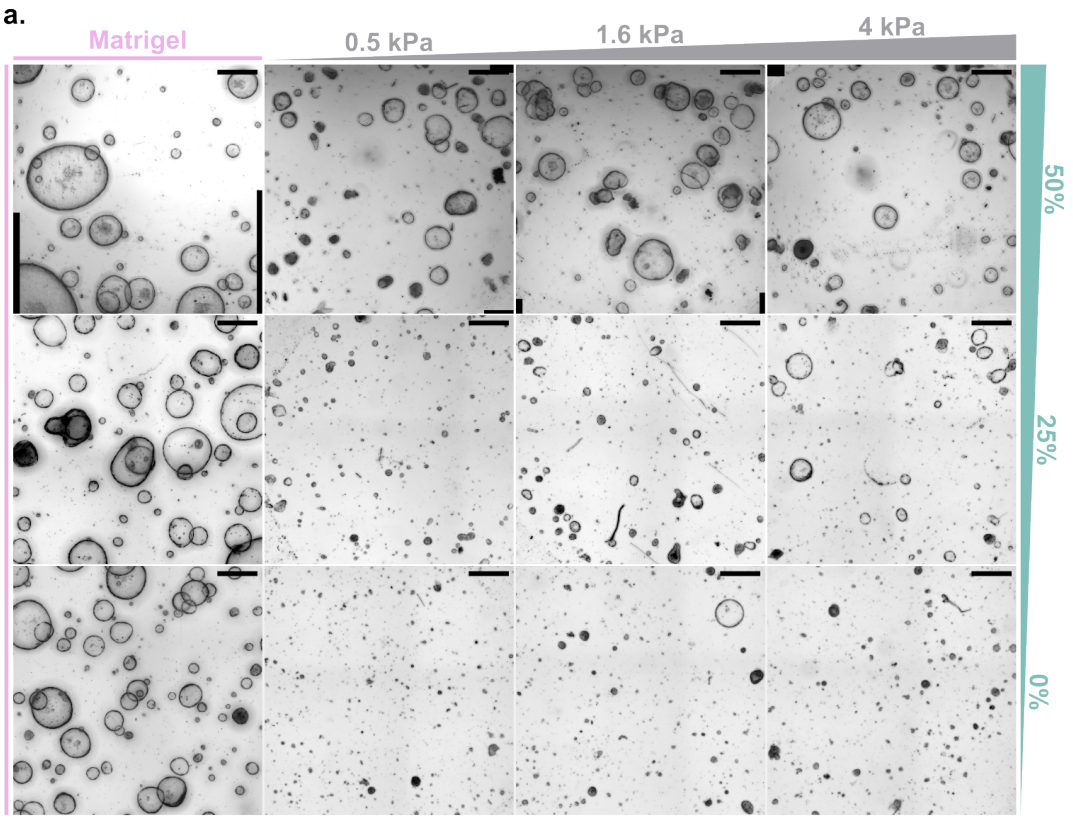

Figure 4.2: Matrix of PEG hydrogel conditions. Representative brightfield images of every hydrogel condition. Each row represents 3 independent experiments with their corresponding matrigel control on the left. Stiffness is indicated in grey at the top and adhesiveness in teal on the right. 500 μm scale bars. n=3 for 50%. n=2 for 25% and 0%.

4.2.2 Effects of hydrogel adhesiveness

Organoid survival

The chemical reaction to form these hydrogels requires a buffer with pH8 to take place. This non-physiological pH is unfavourable for cell survival and already reduces organoid viability regardless of the characteristics of the hydrogel [202, 9]. To discern the effects of the pH from hydrogel conditions, positive and negative matrigel controls were included; in which organoid fragments were embedded before (M+) and after (M-) resuspension and exposure to the buffer, respectively.

Quantification of organoid survival (figure 4.3a) shows the gelling reaction has a variable effect, decreasing viability by 40-80% (M- in 0% and 25% adhesiveness). Nevertheless, substrate adhesive levels clearly have a high impact on mICO survival and growth. Only ∼15-20% of organoids grown in non-adhesive hydrogels (0%) are able to form without growing in size (figure 4.3a-b and 4.2, bottom panels). Organoid formation improves in 25% adhesive gels, although their growth remains compromised in comparison to their matrigel control (middle panels). 50% adhesive levels seem to be the most optimal for organoid formation; up to 60%, similar to 50-60% survival reported by our collaborators [202, 9]. Even though some small organoids are still present, others are able to keep growing and reach bigger sizes similar to those grown in matrigel (top panels).

Organoid morphologies

Overall, higher substrate adhesion seems to support spherical organoid morphologies; going from being absent in non-adhesive gels to over 40% in high adhesive levels (50%) (figure 4.3). A possible explanation is that a clear basal surface adhering to the substrate is an important feature for normal epithelial cells to polarise and form spherical or ductal/tubular morphologies [169, 213]. In contrast, epithelial cells with atypical polarity (such as hepatocytes) have reduced basal surfaces and favour increased cell-cell interactions in order to form other types of morphologies and structures [167, 170, 186]. These characteristics can be some of the reasons behind non-spherical morphologies (*i.e.* intermediate, folded, and unclear) being the most prevalent in low and medium adhesive hydrogels.

Non-spherical organoids dominate even in 50% adhesive conditions when compared to matrigel (figure 4.3c, top panel). This could be due to a considerable difference in the abundant and varied adhesive proteins within matrigel and

the lower concentration of a single adhesive peptide (RGD) in these PEG gels. These differences would result in matrigel allowing more cell-ECM interactions, which could be tested through antibody stainings of focal adhesions in matrigel and PEG gels. Moreover, it would be interesting to test hydrogels with higher adhesiveness (75-100%) to compare focal adhesion formation and to potentially increase the ratio of spherical morphologies; albeit hydrogel degradability would be compromised and its effect on mICO growth and morphology would need to be further investigated. Embedding fluorescent beads in matrigel and hydrogels to track their movement as the organoids form and grow would also provide some insight into how the cells are interacting with the different substrates and remodelling them. Other possible experiments are discussed in the section below (4.2.3, *Organoid morphologies*) as they pertain to substrate stiffness compensating for substrate adhesiveness.

4.2.3 Effects of hydrogel stiffness

Organoid survival

Survival is at least 10% higher in soft and medium gels with 25% and 50% adhesiveness (figure 4.3a). The trend is reversed in 0% hydrogels, where survival is ∼5% higher in stiff gels. As discussed in the previous section, organoid survival is severely affected in 0% adhesiveness, making any subtle effects of stiffness hard to interpret. Considering the effects of 25% and 50% gels, increased substrate stiffness does seem to have an impact on organoid formation; however, this is less apparent than the effect of hydrogel adhesiveness.

Organoid morphologies

Once again, the effect of 0% adhesiveness on organoid survival and growth limit any interpretations regarding organoid morphology despite the significant reduction of spherical organoids for all stiffness levels (figure 4.3, bottom

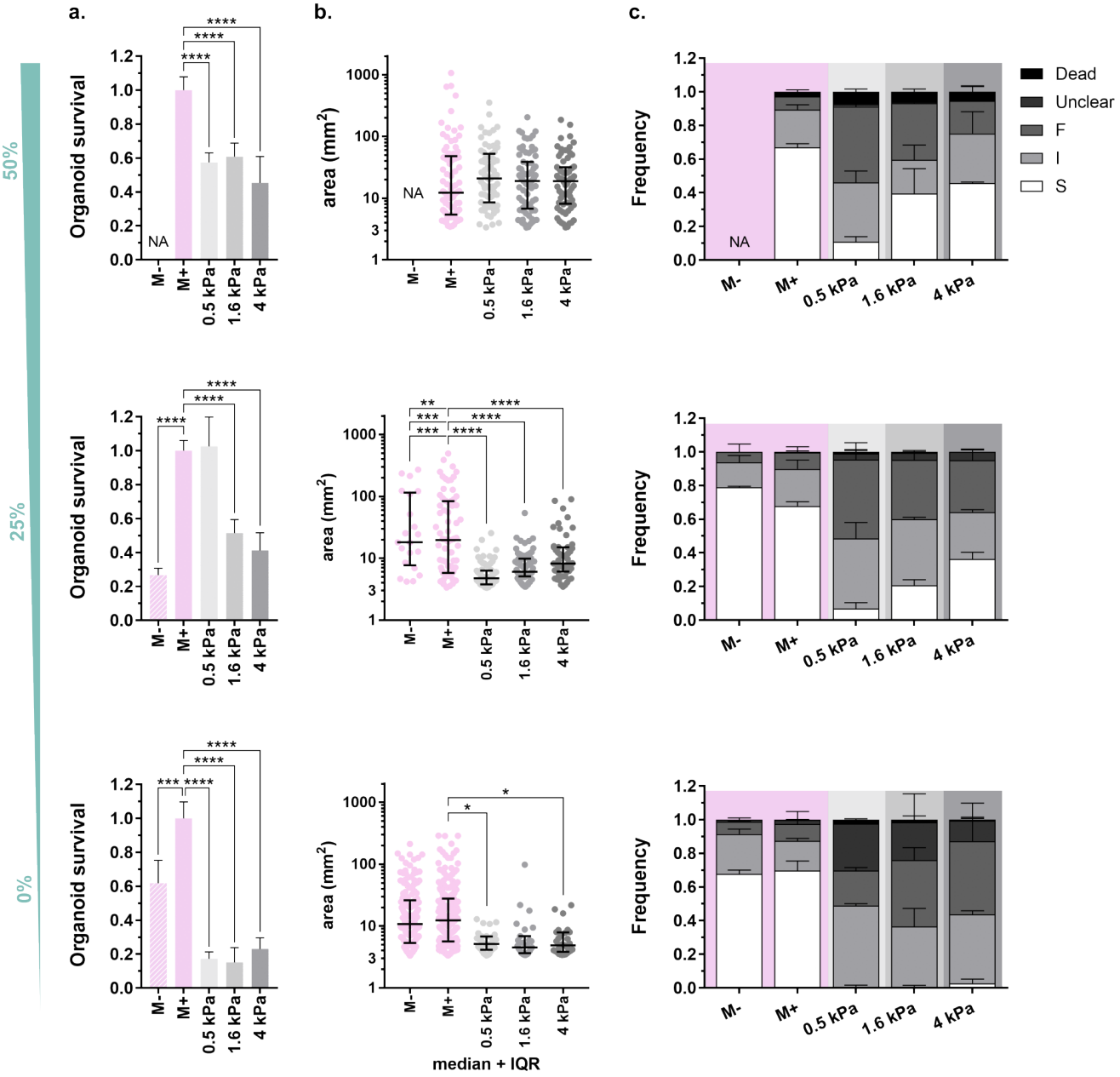

Figure 4.3: Organoid survival, size, and morphology quantifications. Graphs correspond to the images shown in figure 4.2. They indicate **(a.)** organoid survival, **(b.)** area distribution representing organoid size shown in log scale, and **(c.)** morphology frequencies in soft, medium and stiff hydrogels for each of the 3 adhesive % conditions. Adhesive levels are indicated in teal on the left. Stiffness levels are indicated in light to dark grey and matrigel in pink (bars in **(a.)** and background colours in **(c)**). Colour labels on the top right correspond to all graphs in **(c.)**. F=folded, I=intermediate, S=spherical. **(a.)** Organoid survival statistical analysis using 2-way ANOVA with Dunnett's multiple comparisons, comparing all conditions to M+. Error bars represent mean and s.d. **(b.)** 1-way ANOVA with Tukey's multiple comparisons, comparing all conditions to each other. Error bars represent median and the interquartile range (IQR). **(c.)** See table A.2 for statistical analysis and p-values. Error bars represent mean and s.d. p-values are * <0.05, ** <0.01, *** <0.001, and **** <0.0001. n.s. are not shown. n=3 for 50%. n=2 for 25% and 0% as in figure 4.2.

row). Nevertheless, substrate stiffness does have a significant effect on organoid morphologies in 25% and 50% adhesive hydrogels (figure 4.3c, top and middle panels). A similar trend is observed for both adhesive conditions, where non-spherical morphologies are dominant in soft gels with less than 10% of spherical organoids. This percentage increases to ∼20% and ∼35% in medium and stiff gels for 25% adhesiveness, and up to 40% in 50% adhesiveness. Consistently, folded organoids are less prevalent in stiff gels compared to soft ones.

While no condition resembles the morphology ratios observed in matrigel, stiff hydrogels are surprisingly the closest. A recent study on hPSC-derived hepatocytes grown *in vitro*, in 2D and 3D, provides evidence for cells being able to sense both stiffness and adhesive ligand concentration through β-1 integrins; suggesting that higher substrate stiffness can compensate for low adhesive levels to an extent [234]. This could be an explanation for the observed morphologies in matrigel, soft and stiff gels. Even though matrigel is the softest substrate (<0.5 kPa), it consists of multiple adhesive proteins in higher concentrations that support cell-substrate interactions and spherical morphologies (as discussed in section 4.2.2. Conversely, PEG hydrogels have a lower concentration of only one adhesion ligand. Stiff gels, however, provide an additional variable for the cells to sense and interact with their substrate, contributing to an increase in spherical morphologies with a clear basal outer surface. Soft gels, similar to low adhesive gels (section 4.2.2), would favour cell-cell interactions instead, promoting non-spherical organoids. This could be confirmed through immunostainings of polarity markers in soft and stiff gels and their localisation within organoids of different morphologies. In addition, it would be worth testing hydrogels with even higher stiffness and adhesiveness to further explore these effects and try to replicate matrigel conditions and morphology frequencies.

4.3 Substrate stiffness induces gene expression changes in progenitor organoids

The effects of substrate stiffness on organoid morphology and the results from chapter 3 led to further inspection of any changes in gene expression that might be happening. From the hydrogel conditions I explored in section 4.2, it was clear that 50% adhesiveness was the most optimal for mICO growth. Thus, I focused on this set of soft, medium and stiff gels to isolate mRNA and look at expression of relevant markers (also used for experiments in section 3.4).

Unfortunately, using this PEG hydrogel system has two big limitations. The first one is that organoids cannot be removed from the gels without harsh treatments that disintegrate both, making it impossible to sort organoid morphologies for RNA extraction as it was carried out in section 3.4. The second limitation is that the chemistry of the gels interferes with RNA extraction protocols, resulting in low yields. As a consequence, from the 8 genes that were tested through RT-qPCR, only 4 had Ct values that could be analysed and compared. These are shown in figure 4.4 and discussed below.

Compared to matrigel controls, organoids in soft gels (where non-spherical morphologies are more abundant) have lower levels of the proliferation marker, Ki67, and mature ductal marker, Hnf6; which agrees with similar observations in figures 3.4 and 3.6. Conversely, stiff gels with ∼45% of spherical organoid, express Ki67 and Hnf6 at higher and lower levels, respectively. Surprisingly, all hydrogels have increased expression of Ttr, a robust marker of early hepatocyte specification [235]; with soft and medium conditions having higher levels than stiff gels. Trop2, a stem cell marker, follows a similar trend with lower levels in the stiff condition.

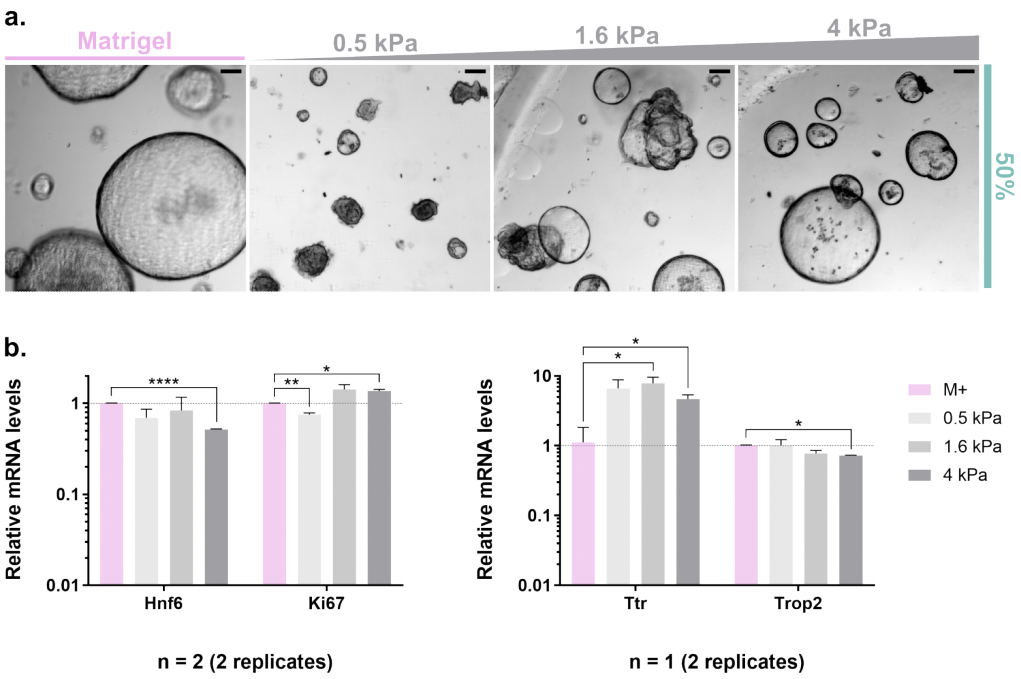

Figure 4.4: Gene expression in PEG hydrogels. (a.) Close up images from figure 4.2 showing spherical and folded morphologies. 100 μm scale bars. **(b.)** mRNA levels of relevant genes relative to matrigel condition (shown in log scale). n=2 for graph on the left. n=1 for graph on the right. Unpaired two-tailed multiple t-tests with False Discovery Rate approach (FDR using the two-stage linear step-up procedure of Benjamini, Krieger and Yekutieli, with Q=1%) to compare all conditions against matrigel (M+). Colour labels on the right are the same for all graphs. Error bars represent mean and s.d. p-values are * <0.05, ** <0.01, *** <0.001, and **** <0.0001. n.s. are not shown.

While these experiments are currently being repeated with more replicates to extract enough RNA and provide more conclusive results, these preliminary results suggest that substrate stiffness does affect gene expression in mICOs. Organoids start to express a hepatocyte specification marker and its levels follow the same trend as the percentage of non-spherical morphologies in soft, medium and stiff gels.

4.4 Discussion

The main objective of this chapter was to test the effects of substrate properties on mICO growth, morphology, and cell composition. Using a synthetic PEG hydrogel, I first explored a set of conditions where I manipulated two mechano-chemical characteristics of the substrate in which organoids are growing: stiffness and adhesiveness (figure 4.2). The results from this exploration demonstrate that mICO survival and growth are severely affected by low substrate adhesiveness and possibly, to a minor extent, by stiffness (figures 4.2 and 4.3).

Concerning morphology, non-spherical organoids are highly abundant (over 90%) in softer gels; whereas high adhesive and stiffness levels are required to support spherical morphologies. As discussed in section 4.2, this could be due to cell-cell interaction and adhesions being favoured in soft or low adhesive gels, allowing cells to form more complex folded morphologies; a requisite that has been observed in hepatocyte *in vitro* culture [186]. Conversely, substrates with high stiffness or adhesion levels stimulate cell-substrate adhesion, promoting typical epithelial apico-basal polarity [129] and supporting a ductal-like spherical morphology [169, 213, 186]. In the same section (4.2) I proposed additional experiments that can help confirm these ideas and validate the differences in adhesive levels between matrigel and PEG hydrogels.

Although the results from gene expression analysis (section 4.3) are not yet conclusive, they do suggest mICOs profile begins to change with decreased expression of a stem cell marker and increased expression of a marker for early hepatocyte specification (figure 4.4). Furthermore, folded morphologies resemble those observed in chapter 3 and of hepatocyte derived organoids (figure 3.5). Morphology frequencies in stiff gels are similar to those in older and differentiated mICO cultures (sections 3.2 and 3.3), while soft gels have a more homogeneous non-spherical population. These findings provide promising sub-

strate conditions with reproducible characteristics (unlike matrigel) that can be further explored in conjunction with media composition to make mICO *in vitro* differentiation more efficient, homogeneous, and reproducible.

It is worth highlighting that all experiments in this chapter were carried out in progenitor conditions. All gel conditions were grown in expansion medium (EM) for only 8 days since organoids do not grow and survive in PEG hydrogels as efficiently and for as long as they do in matrigel. Hence, the effects on morphology and gene expression described in this chapter are taking place earlier than those described in chapter 3. Morphological changes are particularly early as folded organoids appear after only a couple of days of culture in hydrogels, when it takes >5 days in matrigel (figures 3.1a and 3.3a). This is an interesting observation as it could suggest that substrate stiffness (a mechanical cue) has an initial considerable effect on organoid morphology before triggering changes in gene expression and cell identity.

In this chapter I focused on exploring the effects of the mechanoenvironment on mICOs. However, the mechanical properties of the organoids themselves can change as they differentiate and form complex morphologies. The next chapter begins to elucidate tissue mechanics of mICOs and how it can affect cell behaviours.

Chapter 5

Is tissue tension changing as organoids differentiate? And does it affect how organoids respond to injury?

Three group members have contributed to the analysis of some of the experiments included in this chapter. Shirine Merlo-Nikpay, summer student, helped with quantification of junction ablations. James Van Hear, PhD student, helped improve the image analysis pipeline for cell segmentation, wound and tissue dynamics. Jing Ying Lin Quan, master student, has been and is currently helping with processing and analysing injury movies.

5.1 Introduction

In chapter 4, I investigated the effects of two properties of the microenvironment (*i.e.* substrate adhesiveness and stiffness) on mICO morphology and potentially cell composition. However, the mechanical properties of the tissue itself are extremely important and typically change during morphological

transformations and differentiation processes. Moreover, previous work from our group [31] and others (covered in sections 1.1.1 and 1.2) has shown that tissues with lower tension, in a fluid-like state, repair more efficiently than those with higher tension.

The fact that the mechanical characteristics of a tissue influence its ability to repair is particularly relevant for mICOs as the liver is a highly plastic and regenerative organ with the ability to respond in various manners to different types of damage (covered in section 1.4.1). Understanding the dynamics and details of liver repair responses is still a challenge due to the limitations of *in vivo* models. Organoids are a good system that escapes those limitations and allows us to study regenerative responses *in vitro* (see section 1.5 and [63]).

In this chapter I set to determine tissue tension of progenitor and differentiated mICOs (sections 5.2 and 5.3). Subsequently, I characterise their repair response to injury through live-imaging to test whether differences in tension correlate with distinct responses (section 5.4). Due to the wide variety of organoid morphologies (described in chapter 3), I first focus on spherical organoids from progenitor and differentiated conditions (EM 0d and DM 12d). In the last section (5.5), I look into what might be happening in folded differentiated organoids.

5.2 Tissue tension increases in differentiated organoids

To directly measure tension in the tissue, I used a 2-photon laser to ablate individual cell junctions at the sub-apical level in progenitor (EM 0d) and differentiated (DM 12d) organoids with spherical morphologies (one junction per organoid, see methods 2.7). Quantification of the instant recoil after ablation

indicates progenitor mICOs have almost no junctional tension in the tissue and that this increases upon differentiation (figure 5.1a).

Actin stainings confirm this increase in junctional tension given that its organisation and localisation is different in organoids from EM 0d and DM 12d conditions (figure 5.1b). Actin forms a clear mesh network and what seem to be supra-cellular cables in progenitor organoids. However, in differentiated organoids the mesh network disappears and actin localisation becomes junctional, labelling the cell outlines more clearly.

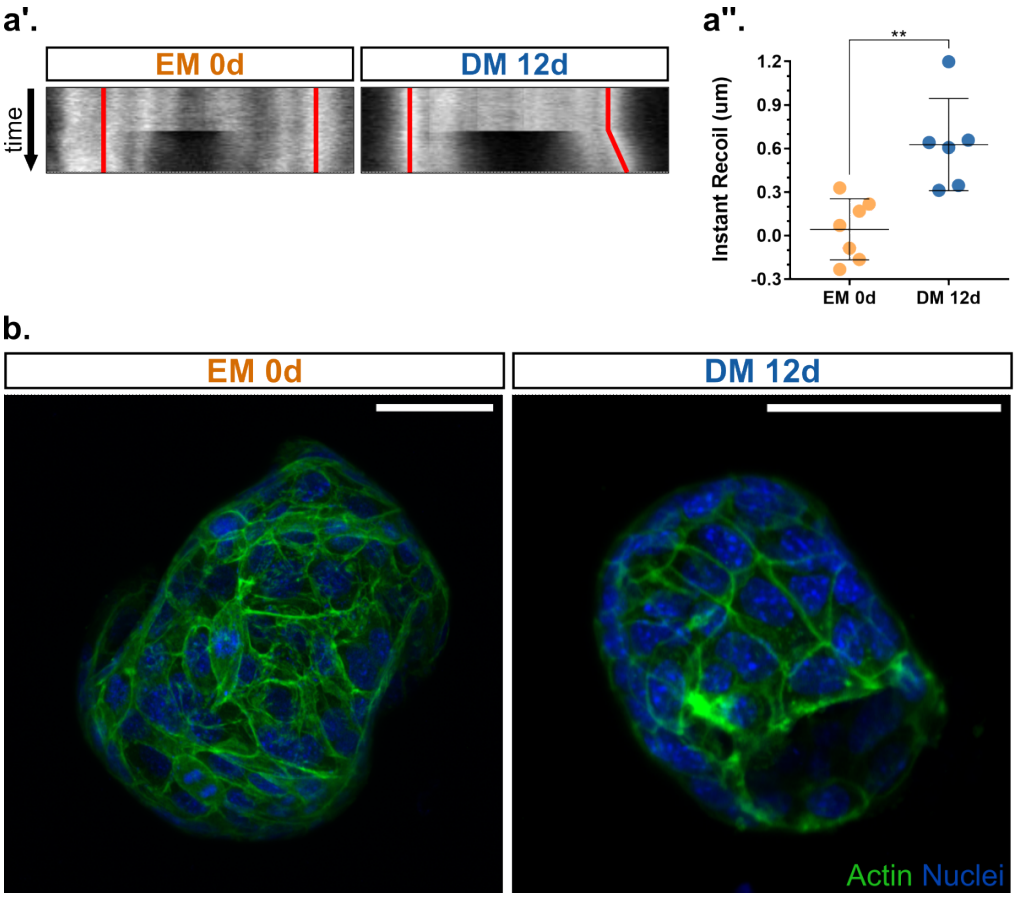

Figure 5.1: Tension in progenitor vs differentiated spherical organoids. (a.) Junction ablations for measuring tension. (a'.) Representative kymographs and (a".) instant recoil of ablated junctions. n=7 for EM 0d. n=6 for DM 12d. Unpaired two-tailed t-test to compare EM 0d against DM 12d. Error bars represent mean and s.d. p-values ** <0.01. **(b.)** Representative confocal images of actin staining in spherical organoids. 50 μm scale bars.

Tissue tension is a common indicator of its fluidity state (covered in section 1.1.1). Fluid tissues tend to have lower tension while higher tension is observed in solid tissues. It can therefore be concluded from these results that mICOs undergo a fluid to solid (jamming) transition during the differentiation process. Additional essays that could complement these results are stainings against phospho-myosin and cell adhesion proteins (*e.g.* e-cadherin, see section 1.1.1), as well as AFM measurements to probe organoid stiffness at the tissue level. Another complementary characteristic that is often used to determine jamming/unjamming transitions in epithelial tissues is their cell packing [211, 212, 20], which is quantified and discussed in the following section.

5.3 Cell packing transitions from fluid to solid-like state in differentiated organoids

Image acquisition and analysis

Pre-wound images from injury movies (section 5.4) were used for cell segmentation and quantification of cell packing. Processing and analysis of these images is not a straightforward procedure due to the curvature of spherical organoids and the nature of the membrane dye used to stain them (see methods 2.8.3). The dye binds to and labels membranes lipids, which means cell vesicles and any debris inside or outside the organoids are also labelled. This adds noise to the acquired image and, together with the curvature of the tissue, complicates normal 2D projection and segmentation of the 3D image stack as all the signal from the apical, lateral, and basal membranes are included. Organoid lines expressing an endogenous membrane marker had similar problems. I tried isolating and imaging an mICO line expressing Ecad-CFP, which would mainly label the apical domain. However, its expression and signal were too weak and impossible to use for segmentation.

After optimising membrane staining to minimise vesicle labelling, and trying several software and plugins, a processing and analysis pipeline was established to generate cleaner projections, segmentations, and to reduce hand-corrections. The entire protocol is described in detail in methods 2.8.3. At the end of this pipeline, many cell characteristics can be extracted and analysed. For the purpose of this section, I focus on polygon class.

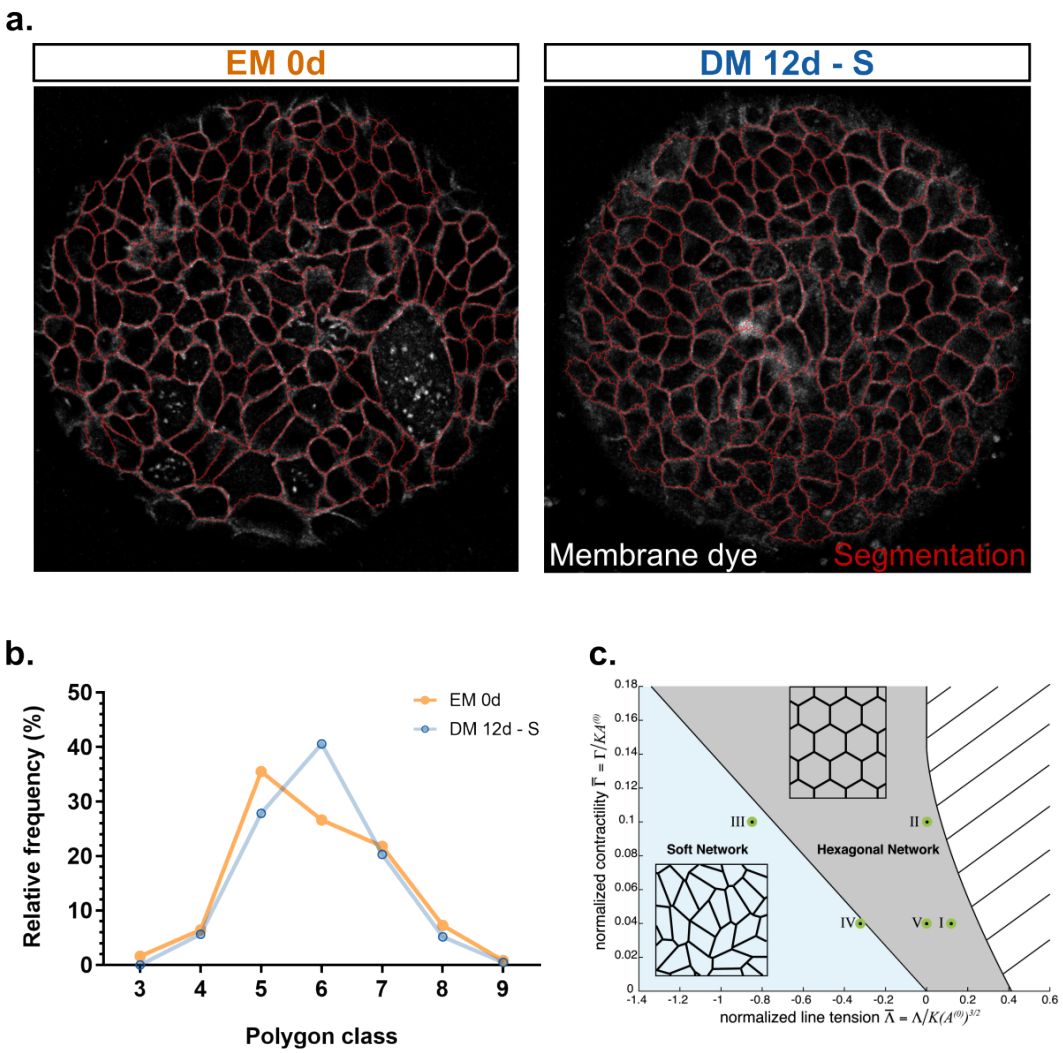

Figure 5.2: Cell segmentation and packing distribution of spherical organoids. **(a.)** Examples of cell segmentation. **(b.)** Cell packing (polygon class) distribution. n=124 cells for EM 0d, mean=5.855. n=212 cells for DM 12d - S, mean=5.929. **(c.)** Diagram representation of tension and contractility determining soft or hexagonal cell packing. Image from Farhadifar *et al*, 2007 [20], reproduced with permission of the rights holder (Elsevier).

Cell packing

It has been shown that epithelial tissues tend to have a hexagonal packing when looking at the polygon distribution of the cells [211, 212]. Any deviations from this distribution are due to perturbations such as changes in cell division, apoptosis, or even cell tension and contractility [212, 20]. Hexagonal distributions correlate with tissues in solid-like states and pentagonal distributions with softer, more fluid-like tissues [20] (figure 5.2c), which is what I observe in mICOs. Progenitor organoids have a pentagonal distribution that becomes hexagonal in differentiated organoids (figure 5.2b) as actin relocalises to the cell junctions and tension increases (section 5.2). There is a caveat, however, to using cell shape to infer the fluid state of a tissue. This readout has usually been used for cells with straight edges, normally epithelial cells with a junctional instead of a membrane marker [212, 20, 21]. Cells or markers than look "messier" do not tend to correlate with the established cell shape index [21], for example, and polygon shape distribution might face a similar issue. While this result does suggest EM 0d organoids are more fluid than DM 12d, junctional tension measured through laser ablations is the main readout for the fluid state or these organoids (section 5.2).

5.4 Organoids with different tension levels respond differently to injury

As already covered in sections 1.1.1, 1.2, and 5.1, it is known that tension levels in a tissue impact its ability to repair. Tetley *et al*, 2019 [23] demonstrated in the *Drosophila* wing disc that changing tension affects healing rates by altering the cells ability to intercalate away from the wound edge, an important mechanism driving fast and seamless wound closure.

Since differentiated organoids have higher tension than progenitor ones, I

tested whether they also respond differently to injury by inducing targeted cell death with a 2-photon laser (methods 2.8). Acquisition and analysis of injury movies exhibited the same problems encountered and described in section 5.3, with the additional issue of dying cells interfering with the signal of the wound edge cells as they are being extruded and even after wound closure. Thus, a simpler initial quantification of wound closure times was done before looking at wound and tissue dynamics using the pipeline described in methods 2.8.3 with manual optimisation of steps b-c, as well as more extensive hand-correction for clean segmentation of the wound and wound edge cells.

5.4.1 Wound closure time

To have a general idea of the differences in repair abilities between progenitor and differentiated organoids, apical and basal wound closure times were manually recorded. Closure times of individual organoids vary greatly within the same condition: 65-115 min (t_a) and 35-85 min (t_b) for differentiated, 70-140 min (t_a) and 25-105 (t_b) for progenitors (figure 5.3a"). There were no significant differences between conditions, which could be due to a couple of reasons: (1) *Variations in initial wound area.* Even though the number of targeted tricellular junctions was maintained between 10-12 to account for variability in cell size across organoids, this range might not have been enough for those with significant differences or high variability of cell sizes. Similarly, while the size of injured organoids was kept within a range of 200-250 μm in diameter, cell size variability could have resulted in a bigger organoid with a smaller wound or vice versa. These initial differences might not be obviously different but could still affect the total time it takes for a wound to close in organoids of the same condition. (2) *Cell heterogeneity within and across organoids.* Although all injured organoids have a spherical morphology, cell composition can still be heterogeneous with different ductal and hepatocyte sub-populations; even more so since hepatocyte differentiation is 30-40% efficient (see section 3.3.2)

and variable each time [161, 192]. This is probably the main reason behind closure time variability as repair responses could differ depending on the type of cells within the injured region.

To circumvent the first complication, wound area can be set by an ROI that is proportional in size to organoid diameter and the laser targeted to the tricellular junctions that are found within this determined area. Alternatively, the range for organoid diameter can be narrowed down and an ROI of constant area can be used to determine the cells targeted for ablation. The problem with cell heterogeneity is harder to resolve. Live reporters of stem cells, cholangiocytes, and/or hepatocytes would be ideal but I have struggled to find organoid lines or mice with a reversible marker that could reliably label specific cell types. Another option would be to generate a specific reporter and transfect wild type mICOs. However, adult stem cells are notoriously hard for gene editing and cell types would not be as well defined given the natural overlap in gene expression of ductal and hepatocyte sub-populations (see section 1.4.3). Organoids grown from single cells could also be an option to work around or at least minimise cell heterogeneity, as discussed in section 3.4.2.

Apical vs. basal wound closure

Curiously, for most of the movies from both organoid conditions, wound closure is first observed basally before apically with a few exceptions closing at the same time as the apical domain but never after. This is an interesting observation as differences between apical and basal closure rates and tissue dynamics have not been described in detail, at least to our knowledge. Although several studies have indeed described molecular mechanisms that take place in the basal (cell crawling through lamellipodia and filopodia) or apical (contraction of a supracellular actomyosin ring) domains of epithelial cells, simultaneously or independently [79, 236, 81, 237]. Thus, wounds would first

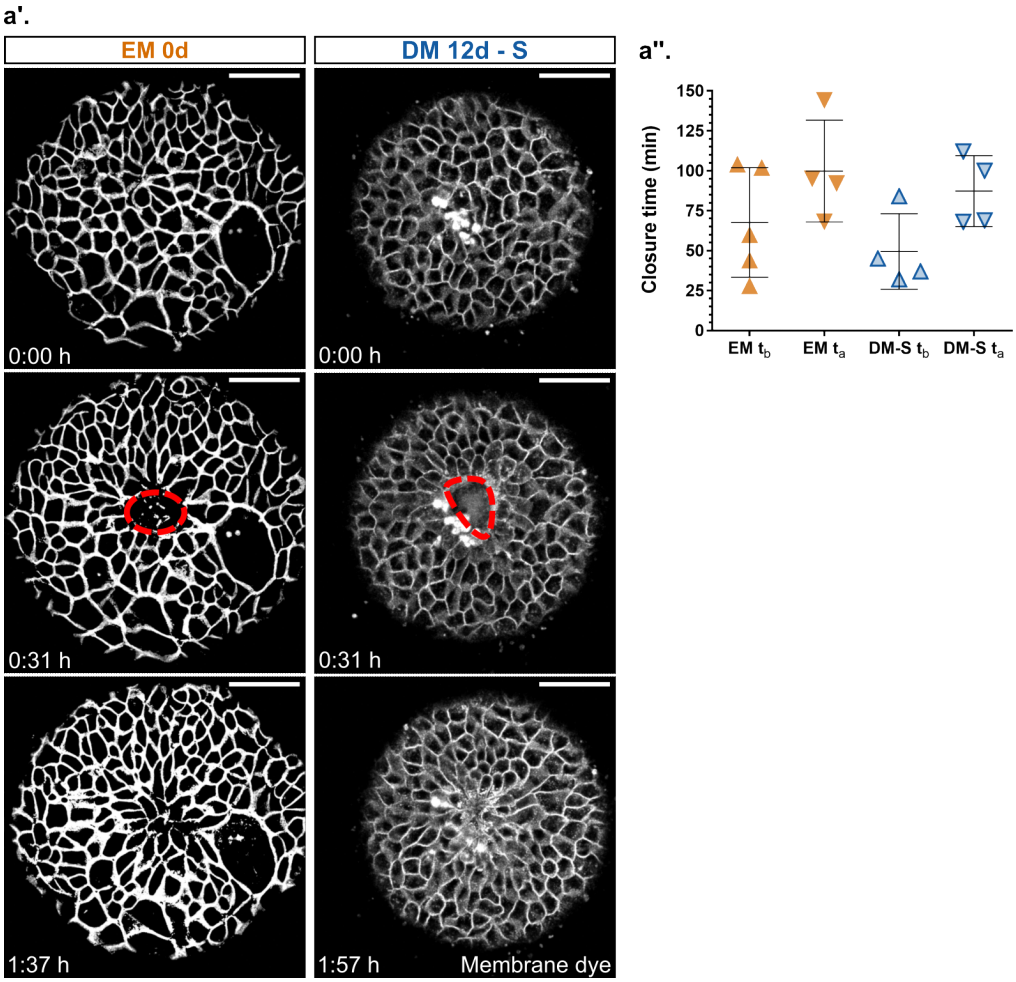

Figure 5.3: Injury of spherical organoids and wound closure times. (a'.) Confocal images of spherical organoids before injury (top), 31 min into wound closure (middle), and after repair (bottom). 50 μm scale bars. **(a".)** Apical (t_a) and basal (t_b) closure times. n=4 for EM 0d and DM 12d - S. One-way ANOVA analysis with False Discovery Rate approach (FDR using the two-stage linear step-up procedure of Benjamini, Krieger and Yekutieli, with Q=1%) to compare t_a and t_b closure across all conditions against each other (EM 0d and DM 12d - S in this figure and DM 12d - F in figure 5.6). Error bars represent mean and s.d. p-values n.s., not shown.

close on either surface depending on the context and the mechanisms involved, similar to single cells being able to extrude apically or basally [238]. Recent evidence confirms that apical and basal behaviours of epithelial tissues are uncoupled [239, 205] and more groups are now looking at the basal surface in detail, comparing it to what it is already known about the apical surface during morphogenesis and repair. Hence, it would be worth further examining the differences between basal and apical cell behaviours during wound closure in mICOs. Actin dyes could also be used during live imaging to determine if cell crawling and/or an actomyosin ring are behind wound closure in EM 12d and DM 12d organoids. For now, the work discussed in the following sections focuses only on apical closure and apical tissue dynamics.

5.4.2 Tissue dynamics

To examine the dynamics of repair beyond just closure times, I quantified wound edge intercalations, cell movement, and elongation ratios throughout the wound closure process (figure 5.4). It is important to point out that due to the laborious process of analysing injury movies and extracting this type of data, the results discussed here are preliminary.

When examining these cell behaviours, progenitor and differentiated organoids do seem to respond differently to injury. Wound edge cells of injured progenitor organoids intercalate out into the tissue as the wound closes, a key characteristic of fluid tissues [23]. Cells also seem to respond in a local manner with those closer to the wound moving towards it and elongating more whereas the cells further away do not elongate as much or at all (figure 5.4a and c, left panels). On the contrary, differentiated organoids respond in a collective manner with all cells moving towards the wound (figure 5.44b). They also elongate to a lesser extent until the wound is almost closed, when the cells closer to it suddenly become more elongated, which correlates with wound edge intercalations

taking place at the end of the repair process to resolve and close the wound (100 min, figure 5.44b and c, right panels).

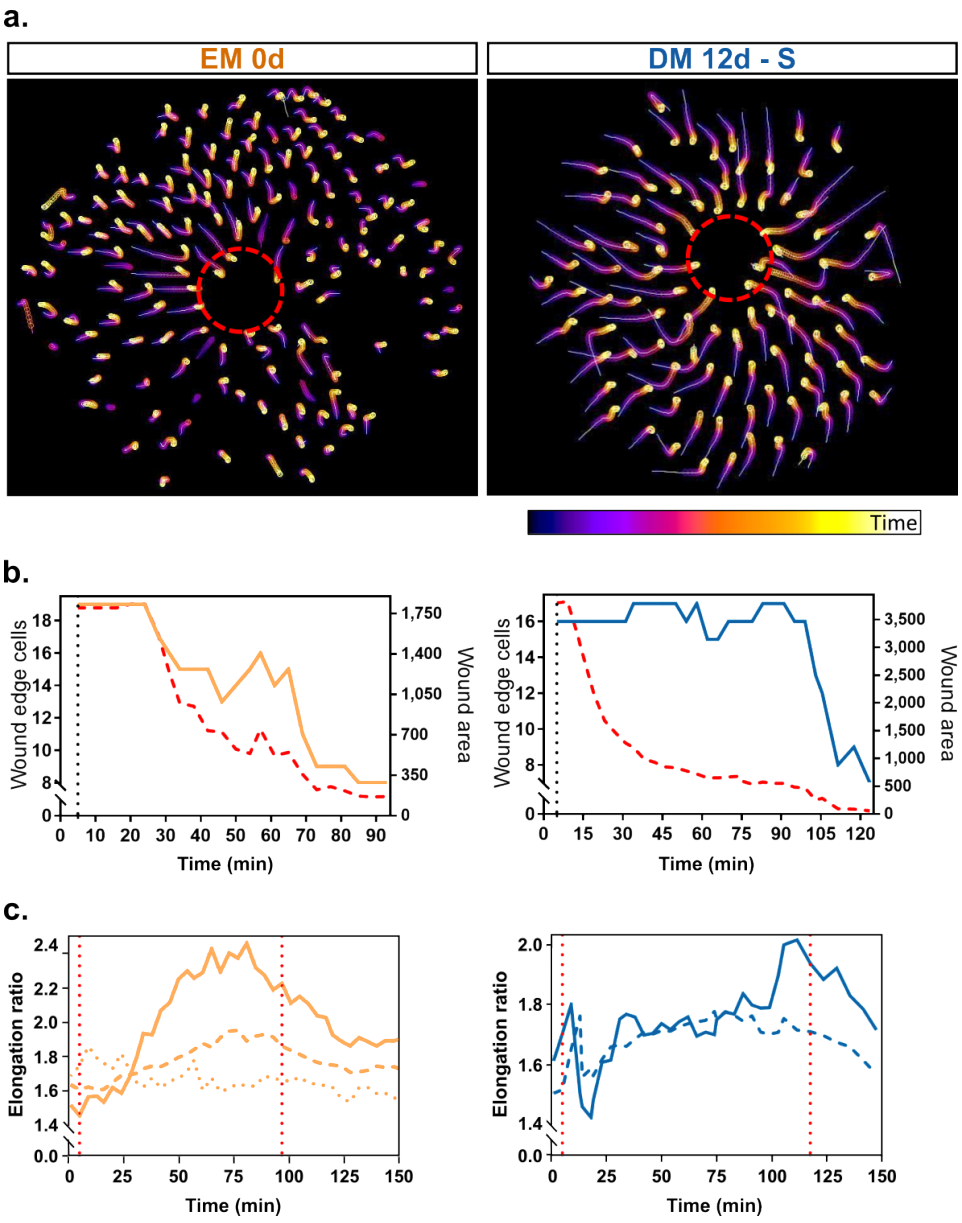

Figure 5.4: Wound and tissue dynamics of spherical organoids during repair. **(a.)** Movement of cell centres during wound closure. **(b.)** Wound closure dynamics. Red dashed line represents wound area. Solid lines represent wound edge intercalations. **(c.)** Elongation ratios of cells close to the wound (solid lines), further away (dashed lines), and most outer cells (dotted line). n=1 for EM 0d and DM 12d - S.

Although more movies need to be included in this analysis, the preliminary wound and tissue dynamics are in line with the observation of progenitor mICOs having lower tension and being more fluid while differentiated mICOs are more solid, preventing cells from leaving the wound edge until the end when it is almost closed. Additional preliminary results shown and discussed in section 5.5.3 further support these observations.

5.5 Injury of differentiated organoids with different morphologies

Since differentiated organoids can remain spherical or acquire folded morphologies that seem to have different cell composition (chapter 3.4), I performed the same experiments and analysis detailed in sections 5.2, 5.3, and 5.4, on differentiated folded organoids and compared them to spherical ones. The complexity of these morphologies poses an additional challenge, requiring more manual intervention throughout the processing and analysis protocols. The results discussed in this section are therefore preliminary and more experiments and analysis are needed to further explore these observations. With the help of a master student in our group, I am currently working on more movies to quantify the wound and tissue dynamics of folded organoids.

5.5.1 Junctional tension and cell packing

Instant recoil of junctional ablations in differentiated organoids with a folded morphology (DM 12d - F) reveal that tension is lower than in spherical ones (DM 12d – S), comparable to progenitor organoids (figures 5.5a and 5.1a"). However, actin localisation and packing distribution of folded organoids resemble those of differentiated spherical organoids. Actin stainings show it is localised at the cell junctions rather than forming a mesh network (figures 5.5b

and 5.1b) and cell packing is also hexagonal (figure 5.5c), yet tension is low.

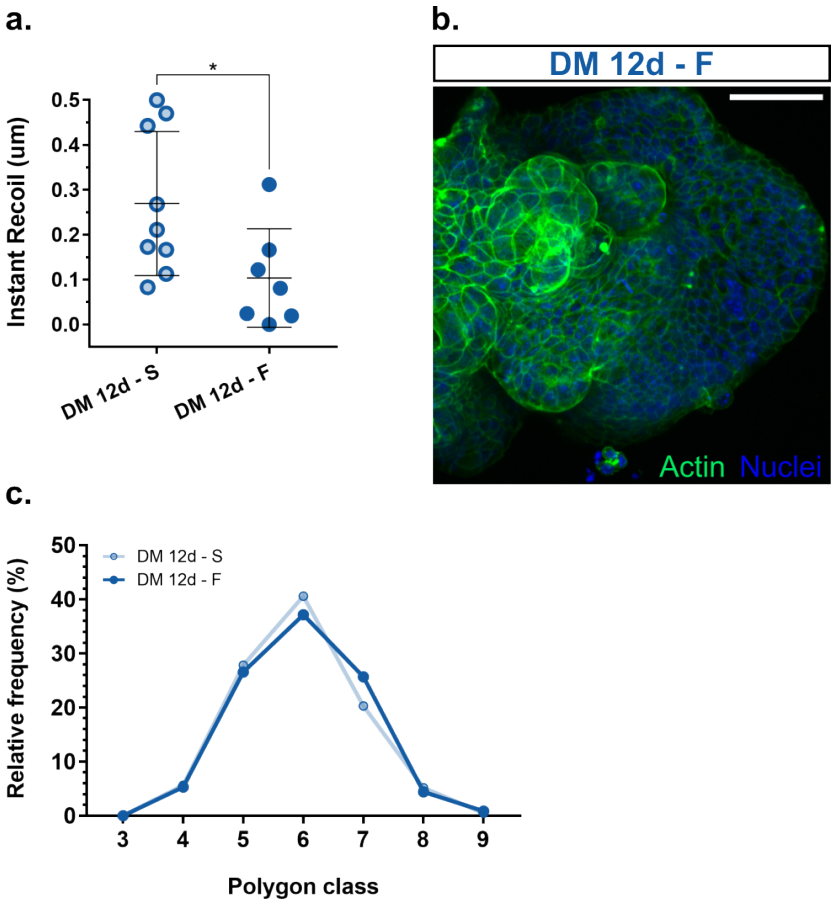

Figure 5.5: Tension and cell packing of folded organoids. (a.) Instant recoil of ablated junctions. n=9 for DM 12d - S. n=7 for DM 12d - F. Error bars represent mean and s.d. Unpaired two-tailed t-test to compare S against F. p-values * <0.05. **(b.)** Representative confocal image of actin staining in folded organoids. 50 μm scale bar. **(c.)** Cell packing (polygon class) distribution. n=212 cells for DM 12d - S, mean=5.929. n=113 for DM 12d - F, mean=6.

As all organoids start with a spherical morphology, it is possible that increased cell tension due to differentiation is released through folding without drastically affecting actin localisation and cell packing. Moreover, given that hepatocytes tend to have multiple smaller apical and lateral domains (see section 1.4.3), it is probable that junctional actin does not contribute to higher tension as in ductal cells with a larger apico-lateral domain. Regarding polygon shape

distribution, its limitations have been discussed in section 5.3 and should therefore be cautiously interpreted.

5.5.2 Wound closure time

The mean closure time of folded organoids is lower than spherical ones, although the difference is not statistically significant with closure times varying from ∼55 to 95 min. This could also be due to variations of the initial wound area and, more likely, due to cell heterogeneity within and across organoids, as discussed in section 5.4.

Folded organoids acquire their complex morphology in a seemingly random manner. Even though they all share similar features at a whole organoid scale (see methods 2.6 and section 3.2), they are highly heterogeneous regarding cell size, composition, organisation, and the structures cells form within each organoid (figure 3.2). Their complexity makes folded organoids difficult to image, ablate (for tension measurements and inducing injury), and analyse. Thus, most (if not all) tension measurements and injury experiments were done on the flattest region available, which is usually facing a big lumen and has a more 'ductal-like' phenotype (chapter 3.4).

The morphological characteristics of the injured region, *i.e.* flat facing a big lumen, a region with a small or no lumen, or a folded section with cell layers and bridge like structures (figure 3.2), will inevitably impact how cells respond to injury. It is therefore even more important for folded organoids to keep injury conditions (*e.g.* wound size, organoid size, injured region characteristics, etc.) as consistent as possible before drawing any conclusive interpretations.

Apical vs. basal wound closure

Earlier wound closure at the basal surface before apical closure was also observed in folded organoids, supporting previous observations of uncoupled apical and basal cell behaviours that would be worth studying further (see section 5.4.1 and [205]).

5.5.3 Tissue dynamics

A simple preliminary analysis of the number of cells around the wound at specific timepoints throughout wound closure (figure 5.6b) shows the wound edge cell intercalation trend for spherical and folded differentiated organoids (in light and dark blue, respectively) in addition to progenitor organoids (in orange). Even though a more thorough analysis is needed, in addition to the limitations of the wounding assay described in section 5.4.1, interesting differences can already be noticed. Progenitor organoids intercalate faster and down to ∼50% of the starting number of wound edge cells at the time of injury. Unlike differentiated spherical organoids, where only ∼25% of the wound edge cells slowly intercalate and the other ∼75% remain in contact once the wound has closed.

Finally, folded organoids (DM 12d - F) fall in between, with ∼40% of the wound edge cells intercalating faster than DM 12d - S but slower than EM 0d. These trends are consistent with tension measurements and the results described in previous sections (in particular section 5.4.2) regarding progenitor mICOs being in a more fluid state and differentiated organoids in a solid state. Furthermore, the differences between differentiated mICOs with different morphologies (S and F) suggest spherical organoids behave even more as a solid tissue compared to folded organoids. Since spherical morphologies seem to correspond to ductal-like organoids and folded morphologies to hepatocyte-like mICOs (results from chapter 3), these dynamic behaviours would help

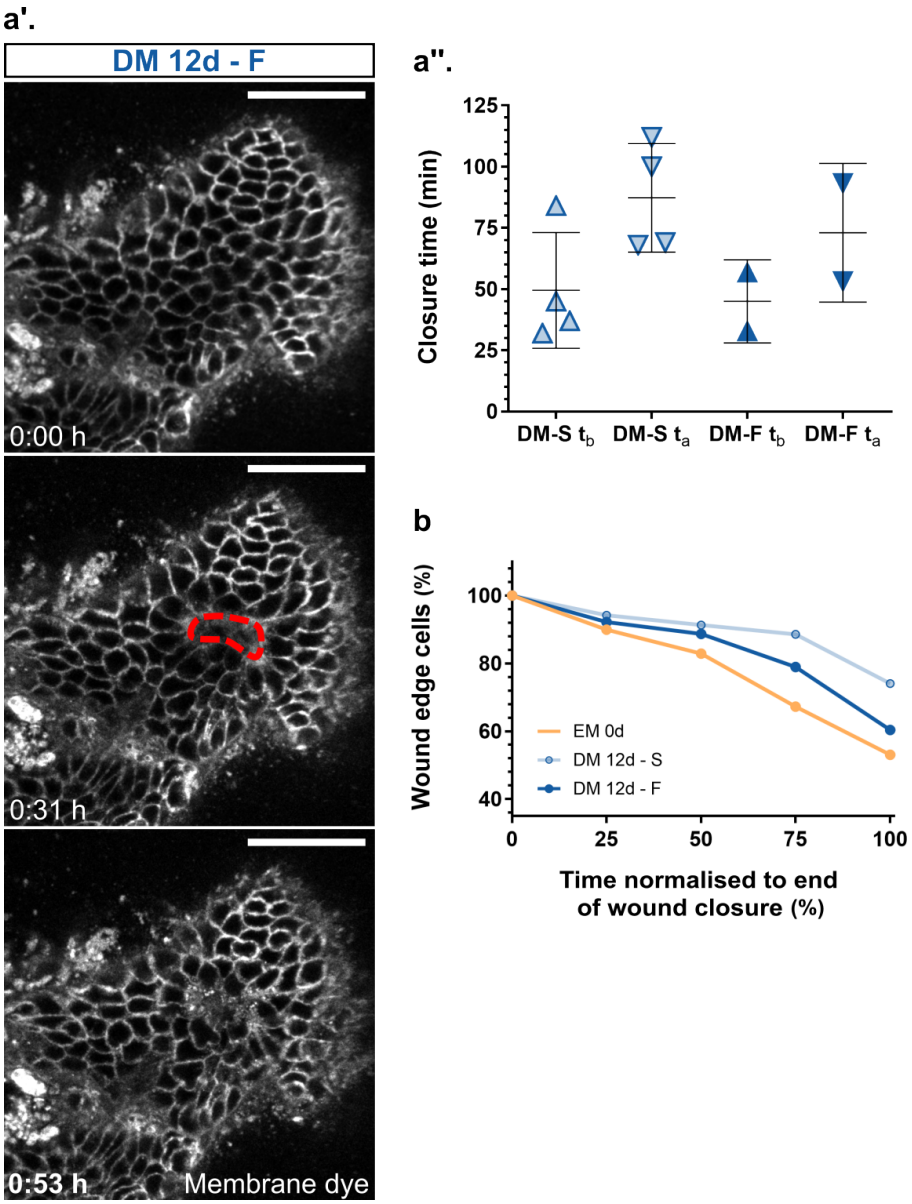

Figure 5.6: Injury of folded organoids and wound closure times. (a'.) Confocal images of spherical organoids before injury (top), 31 min into wound closure (middle), and after repair (bottom). 50 μm scale bars. **(a".)** Apical (t_a) and basal (t_b) closure times. n=4 for DM 12d - S. n=2 for DM 12d - F. One-way ANOVA analysis with False Discovery Rate approach (FDR using the two-stage linear step-up procedure of Benjamini, Krieger and Yekutieli, with Q=1%) to compare t_a and t_b closure across all conditions against each other (EM 0d in figure 5.3 and DM 12d - S and F in this figure). Error bars represent mean and s.d. p-values n.s., not shown. **(b)** Preliminary analysis of wound edge cell intercalations Manual quantification of number of cells around the wound. Time in X axis corresponds to quarters of the total closure time for each movie, *i.e.* 50 means half way through wound closure for all organoids regardless of how many minutes each took to heal. This was done in order to be able to compare all organoids across all 3 conditions. n=5 for EM 0d. n=4 for DM 12d - S. n=3 for DM 12d - F. Error bars are not shown for clarity.

understand from a mechanics perspective what has been described *in vivo*, where hepatocytes are the first main response to most damage (see section 1.8).

5.6 Discussion

In this last chapter I characterised tension levels in progenitor and differentiated organoids of spherical morphologies, determining that they transition from a fluid to solid state with higher junctional tension, actin localisation at the cell junctions, and cell packing acquiring a hexagonal polygon distribution (sections 5.2 and 5.3). These differences in the mechanical status of mICOs raised the question of whether organoids would respond differently to injury, potentially reflecting some of the repair responses that have been observed *in vivo* (covered in section 1.4.1).

To investigate this, I performed live-imaging of liver organoids to induce targeted injury using a 2-photon laser and capture the repair response of progenitor and differentiated mICOs. At a first glance, there were no significant differences in the time it takes organoids from each condition to close the wound. I have discussed possible explanations for this result and suggested alternatives to improve these experiments. Nonetheless, two intriguing observations surfaced when analysing injury movies in more detail (section 5.4).

While closure times showed no significant differences across conditions, all wounds healed basally first before closing apically. As discussed in section 5.4.1, it would be worth exploring these differences further and the cell behaviours taking place during wound closure a the basal and apical domains. As a first step, analysis of cell behaviours on the apical surface reveal that pro-

genitor organoids with lower tension exhibit a more fluid response to injury with the wound edge cells intercalating as the wound closes. Unlike differentiated organoids with higher tension and a more solid-like state in which cells respond collectively to reduce wound area, intercalating only at the end of the repair process when the wound is nearly closed and the wound edge cells are much closer to each other (figure 5.4). These observations agree with what was previously shown by Tetley *et al*, 2019 [23].

In the last section of this chapter I also explored tension levels and repair times of differentiated organoids with folded morphologies, as these are likely to be composed of mostly hepatocytes over ductal cells (from chapter 3) and thus must have different characteristics and responses to injury. Interestingly, folded organoids seem to have lower tension than spherical ones despite presenting junctional actin and a clear hexagonal polygon distribution (figure 5.5). While analysis of more folded organoids is necessary, this reduction in junctional tension could be due to its release through folding and buckling of the tissue.

Furthermore, an initial quantification of injured folded organoids suggests they heal faster (although not significantly) than spherical differentiated and even progenitor organoids. Another simple analysis of wound edge cells shows that folded organoids are also able to intercalate more easily during wound closure than spherical differentiated but not progenitor organoids. These results are very preliminary and more analyses are currently being done to conclusively prove any differences. If these trends are correct, this would be a powerful system to understand the cell behaviours and tissue dynamics that take place during different repair responses reported in the liver tissue *in vivo*; as it is known that hepatocytes are the first main response to injury (see section 1.4.1).

Chapter 6

General discussion and outlook

6.1 General discussion

This work aimed to characterise the morphological changes that occur in liver organoids recapitulating regenerative morphogenesis *in vitro* and their correlation with cell identities (6.1.1); to describe how this is affected by the properties of the mechanoenvironment (6.1.2); and finally, to characterise the mechanical changes of liver organoids at the tissue level and the effect this might have in subsequent damage (6.1.3). In the following sections I recapitulate the main conclusions from the evidence and/or preliminary results detailed in previous chapters with the purpose of addressing the questions and aims of this dissertation.

6.1.1 Morphological changes and cell composition in liver organoid regenerative morphogenesis

I first examined the morphological differences between progenitor and differentiated organoids, showing that the first ones normally have a very clear spherical or cystic morphology while differentiated organoids acquire more complex and more varied morphologies, which I refer to as folded or non-spherical (to

include those in between spherical and folded phenotypes) (figure 3.1).

I then found that similar morphologies appear even without actively inducing chemical differentiation for 12 days and only letting organoids grow for the time period in progenitor conditions (referred to as old cultures, figure 3.3). By examining organoids from old cultures, I observed they are less proliferative and express hepatocyte markers, which means they are differentiating (to an extent) in a passive or spontaneous manner without any specific chemical signals (figure 3.4). This is further investigated in chapter 4 and discussed in section 6.1.2.

Specific features of spherical organoids resemble characteristics of cholangiocytes/ductal cells, whereas features of folded organoids look very similar to 3D hepatocyte cultures (figures 3.2 and 3.5). These observations, together with evidence from other groups ([176] and section 3.4.1), suggest cell composition of spherical organoids is of ductal identity and that of folded organoids is of hepatocyte (or at least hepatocyte-like) identity.

To confirm this correlation between organoid morphology and cell composition, I looked at expression levels of specific cell markers in manually sorted spherical and folded organoids from chemically differentiated and older culture conditions. Differences in gene expression are not clearly observed for older cultures, probably due to higher variability of passive differentiation and several other reasons discussed in chapter 3. However, it is clear that in chemically differentiated cultures, folded organoids have a more hepatocyte-like profile than spherical organoids (figure 3.6).

6.1.2 Effects of substrate mechano-chemical properties

A lot of studies have provided evidence that the mechanical properties of a substrate can induce and regulate differentiation (covered in section 1.3.2). To determine what non-chemical signals are causing older cultures to differentiate and change their spherical morphology, I cultured mICOs in synthetic PEG hydrogels [202, 9] in order to independently vary substrate stiffness and adhesiveness.

By exploring a set of 9 gel conditions with low, medium, and high levels of both variables (figure 4.2) I found that organoid survival and growth are severely compromised in substrates with low adhesiveness without being significantly affected by its stiffness (figure 4.3). Organoid morphology is also affected by substrate adhesiveness but mainly by stiffness. Spherical organoids require high adhesive and stiffness levels while non-spherical morphologies are dominant in soft gels. This can be due to cell-substrate interactions and adhesion being facilitated in gels with high stiffness or adhesiveness (the first potentially compensating for the lack of the latter [234], see section 4.2.3 for more detail), promoting establishment of apico-basal polarity and forming ductal-like morphologies [169, 213, 186, 129]. In soft gels cell-cell adhesion are favoured, enabling them to form complex structures [186].

To test whether cell composition is also changing along with morphology, I looked at gene expression of liver cell markers in organoids grown in gels with high adhesiveness and 3 stiffness levels. Even though these results are not conclusive, they hint towards early gene expression changes taking place. It is likely that organoids in soft gels, abundant in folded morphologies, start expressing a marker for hepatocyte specification (figure 4.4). While further confirmation of these results is required, these observations could be evidence for shape changes taking place before any clear changes in gene expression.

Independently, the hydrogel matrix has provided substrate conditions with reproducible mechano-chemical features that result in organoids with less morphological variability. Moreover, since these organoid cultures are even younger than chemically differentiated ones (8 vs 12 days), it worth further exploring gel conditions together with chemical differentiation (DM) in order to improve and homogenise hepatocyte differentiation of mICOs.

6.1.3 Mechanical properties of liver organoids and repair responses

While the effects of the mechanoenvironment are important and interesting, tissue mechanical properties are also relevant as tissues undergo morphological changes and differentiation processes. Therefore, I characterised tissue tension of progenitor and differentiated organoids by examining several outputs (figures 5.1 and 5.2), discovering that organoids transition from a fluid-like to solid-like state even though their morphology remains spherical.

Given that mICOs grown *in vitro* are replicating a regenerative liver response [63], and that fluid to solid transitions are known to influence how a tissue might respond to injury [23], I examined how organoids respond to injury and if there are any differences in cell behaviours during repair. Closure times were similar between progenitor and differentiated organoids (figure 5.3). However, cell behaviours taking place in progenitor organoids correspond to those observed in more fluid tissues, *i.e.* gradual wound edge cell intercalations as the wound closes. On the contrary, differentiated organoids behave like solid tissues with wound edge cell intercalations only taking place towards the end when the wound is almost closed (figure 5.4). Similar to what was shown before in the *Drosophila* wing disc by Tetley *et al*, 2019 [23].

Finally, I also provided preliminary results on tension, closure times, and tissue

dynamics of differentiated folded organoids. While definite conclusions cannot be drawn yet, these hepatocyte-like organoids have lower tension and seem to close slightly faster that spherical organoids (although not significantly, figures 5.5 and 5.6) while undergoing more wound edge intercalations, a hallmark of more fluid tissues (see section 1.1.1). More detailed analysis are needed but the repair response of all these different conditions are worth studying in more detail as they can provide some insights into the varied regenerative mechanisms that have been described in the liver.

6.2 Outlook

While there is no conclusive answer yet for all of the questions asked at the beginning of this work (section 1.6), there is enough progress and evidence to confirm some aspects and re-direct experiments to further investigate and understand the others. The next steps that are currently being worked on and some new ones are discussed in detail in each chapter and summarised here.

To confidently say that spherical and folded organoids are of ductal and hepatocyte composition (1) more RT-qPCR repeats are needed, testing a larger set of genes; and (2) electron microscopy images would confirm which organoids and/or organoid regions are composed of ductal cells and hepatocytes. These experiments are currently being carried out for older and chemically differentiated cultures, as well as for PEG hydrogel conditions to confirm if folded morphologies are in fact differentiated in these synthetic substrates.

Immunostainings for polarity markers could help test the hypothesis of PEG gels favouring cell-cell or cell-substrate interactions, depending on their stiffness and adhesiveness, and whether this results in folded or spherical organoids. Additionally, it would be worth exploring gel conditions that are even stiffer

and more adhesive to try and replicate the abundance of spherical morphologies observed in matrigel. Finding hydrogel conditions that can grow organoids in a reproducible manner is a highly valuable tool with many potential applications in basic and applied research; for example, it can facilitate the use and further study of 3D culture systems and the role of the mechanoenvironment, as well as enabling their therapeutic use in humans in a more controlled way.

Regarding injury experiments, more movies are being analysed to extract more information on cell behaviours during wound closure of progenitor and differentiated organoids (spherical and folded), despite being difficult to process and segment. Moreover, the difference in wound closure times between apical and basal surfaces is very interesting and it should definitely be investigated as it would provide information on 3D cell behaviours during repair.

In general, all organoid systems have similar limitations. They can be highly variable and they are a simplified version of any given organ, replicating the epithelium but lacking other non-epithelial components such as mesenchymal and immune cells that would normally be present *in vivo*. Nonetheless, collective progress is being made to overcome this limitations and improve organoid culture (*e.g.* single-cell studies, development of synthetic substrates and co-culture systems [240], discussed in the relevant sections throughout this thesis). Furthermore, organoids are closer to replicating the architecture and 3D context of a tissue compared to 2D cell culture. Their reductionist nature is still useful to focus, in this case, on the mechanical properties of the system and its environment; to test them without the influence of other components that could mask their importance.

mICOs are a great tool to examine the role of mechanics of liver repair since they inherently recapitulate a regenerative response from mature ductal cells, which is triggered through the isolation process [63]. As a result, studying

mICO formation, growth, and differentiation (chapters 3 and 4) can already contribute to our understanding of these processes in the context of liver regeneration. The additional injury induced by laser ablation can help us understand the wound healing response of liver cells in the context of micro damage (chapter 5). This targeted laser ablation technique, together with the synthetic hydrogels I have used, are a powerful combination to investigate liver organoids in the context of chronic disease. Repeated controlled injury can be performed to test the effect of long-term damage and how the liver epithelium manages or fails to cope with it; whereas stiff PEG gels can be used to mimic fibrotic conditions [232].

Other models that would complement the observations from this work are hepatocyte derived organoids (see [176] and section 1.5) in order to compare them to the non-spherical hepatocyte-like organoids described in chapter 3. It would also be interesting to investigate the mechanical properties of organoids isolated from diseased livers (*e.g.* fibrotic) and how they form, grow, and respond to injury in comparison to the healthy mICOs I have used for this project. Regarding the mechanoenvironment, synthetic hydrogels with different characteristics could be tested to explore the role of other parameters, including viscoelasticity [143], and even control substrate stiffness and ligand patterns in a more precise manner [228, 229, 230].

Studying the mechanical properties of mICOs (progenitor vs. differentiated of different morphologies) and how they relate to their different responses to injury is a powerful tool that can contribute to a better understanding of the liver repair responses that have been observed *in vivo*. It can also help understand what happens in diseased conditions, such as fibrosis, and shed some light on how and why liver cells respond in diverse manners to different types of damage; an intriguing characteristic that makes the liver one of the most regenerative organs.

Appendix A

Tables of p-values for relevant experiments

A.1 Morphology classification

	Adjusted p-value	Significant
Spherical		
EM 0d vs. EM 12d	<0.0001	****
EM 0d vs. DM 12d	<0.0001	****
EM 12d vs. DM 12d	0.0101	*
Intermediate		
EM 0d vs. EM 12d	0.0003	***
EM 0d vs. DM 12d	<0.0001	****
EM 12d vs. DM 12d	0.0011	**
Folded		
EM 0d vs. EM 12d	0.0782	ns
EM 0d vs. DM 12d	0.2256	ns
EM 12d vs. DM 12d	0.8037	ns
Dead		
EM 0d vs. EM 12d	0.8287	ns
EM 0d vs. DM 12d	0.8708	ns
EM 12d vs. DM 12d	0.9948	ns

Table A.1: Organoid morphology frequencies in EM 0d, EM 12d, and DM 12d. Two-way ANOVA analysis with Tukey's multiple comparisons test to compare morphologies of all culture conditions against each other (EM 0d n=4, EM 12d n=7, and DM 12d n=7). Data corresponds to figures 3.1 and 3.3.

	0% adhesiveness		25% adhesiveness		50% adhesiveness	
	Adjusted p-value	Significant	Adjusted p-value	Significant	Adjusted p-value	Significant
Spherical						
M+ vs. M-	0.9926	ns	0.0311	*	-	-
M+ vs. 0.5 kPa	<0.0001	****	<0.0001	****	<0.0001	****
M+ vs. 1.6 kPa	<0.0001	****	<0.0001	****	0.0005	***
M+ vs. 4 kPa	<0.0001	****	<0.0001	****	0.0051	**
Intermediate						
M+ vs. M-	0.7064	ns	0.2278	ns	-	-
M+ vs. 0.5 kPa	0.0001	***	0.0001	***	0.107	ns
M+ vs. 1.6 kPa	0.019	*	0.0007	***	0.9604	ns
M+ vs. 4 kPa	0.0024	**	0.3678	ns	0.4944	ns
Folded						
M+ vs. M-	0.9733	ns	0.782	ns	-	-
M+ vs. 0.5 kPa	0.2339	ns	<0.0001	****	<0.0001	****
M+ vs. 1.6 kPa	0.0002	***	<0.0001	****	0.0008	***
M+ vs. 4 kPa	<0.0001	****	<0.0001	****	0.1603	ns
Dead						
M+ vs. M-	>0.9999	ns	>0.9999	ns	-	-
M+ vs. 0.5 kPa	0.9871	ns	0.9977	ns	0.7552	ns
M+ vs. 1.6 kPa	0.9976	ns	0.9997	ns	0.8535	ns
M+ vs. 4 kPa	>0.9999	ns	>0.9999	ns	0.9472	ns
Unclear						
M+ vs. M-	0.9985	ns	0.9999	ns	-	-
M+ vs. 0.5 kPa	0.001	**	0.8231	ns	0.9952	ns
M+ vs. 1.6 kPa	0.0096	**	0.7384	ns	>0.9999	ns
M+ vs. 4 kPa	0.3113	ns	0.5964	ns	>0.9999	ns

Table A.2: Organoid morphology frequencies in PEG hydrogels and matrigel controls. Two-way ANOVA analysis with Dunnett's multiple comparisons to compare morphologies of gel conditions against positive matrigel controls (M+) within each set of experiments (0% n=2, 25% n=2, and 50% n=3). Data corresponds to figure 4.3.

References

[1] M. Huch and B.-K. Koo. Modeling mouse and human development using organoid cultures. *Development*, 142(18):3113–3125, 2015.

[2] Senthil K. Muthuswamy. Bringing together the organoid field: from early beginnings to the road ahead. *Development*, 144(6):963–967, 2017.

[3] Mijo Simunovic and Ali H. Brivanlou. Embryoids, organoids and gastruloids: new approaches to understanding embryogenesis. *Development*, 144(6):976–985, 2017.

[4] Marta Kapałczyńska, Tomasz Kolenda, Weronika Przybyła, Maria Zajączkowska, Anna Teresiak, Violetta Filas, Matthew Ibbs, Renata Bliźniak, Łukasz Łuczewski, and Katarzyna Lamperska. 2D and 3D cell cultures - a comparison of different types of cancer cell cultures. *Archives of medical science : AMS*, 14(4):910–919, jun 2018.

[5] Giuliana Rossi, Andrea Manfrin, and Matthias P Lutolf. Progress and potential in organoid research. *Nature Reviews Genetics*, 19(11):671–687, 2018.

[6] Matthias P. Lutolf, Penney M. Gilbert, and Helen M. Blau. Designing materials to direct stem-cell fate. *Nature*, 462(7272):433–441, 2009.

[7] Steven R. Caliari and Jason A. Burdick. A practical guide to hydrogels for cell culture. *Nature Methods*, 13(5):405–414, 2016.

[8] Nathalie Brandenberg, Sylke Hoehnel, Fabien Kuttler, Krisztian Homicsko, Camilla Ceroni, Till Ringel, Nikolce Gjorevski, Gerald Schwank, George Coukos, Gerardo Turcatti, and Matthias P. Lutolf. High-throughput auto-

mated organoid culture via stem-cell aggregation in microcavity arrays. *Nature Biomedical Engineering*, 2020.

[9] Michael D.A. Norman, Silvia A. Ferreira, Geraldine M. Jowett, Laurent Bozec, and Eileen Gentleman. Measuring the elastic modulus of soft culture surfaces and three-dimensional hydrogels using atomic force microscopy. *Nature Protocols*, 16(5):2418–2449, 2021.

[10] Thomas Lecuit, Pierre-François Lenne, and Edwin Munro. Force generation, transmission, and integration during cell and tissue morphogenesis. *Annual Review of Cell and Developmental Biology*, 27(1):157–184, 2011. PMID: 21740231.

[11] Monirosadat Sadati, Nader Taheri Qazvini, Ramaswamy Krishnan, Chan Young Park, and Jeffrey J. Fredberg. Collective migration and cell jamming. *Differentiation*, 86(3):121–125, 2013.

[12] Sham Tlili, Cyprien Gay, François Graner, Philippe Marcq, François Molino, and Pierre Saramito. Colloquium: Mechanical formalisms for tissue dynamics. *The European Physical Journal E*, 38(5):33, 2015.

[13] Dominik Eder, Christof Aegerter, and Konrad Basler. Forces controlling organ growth and size. *Mechanisms of Development*, 144:53 – 61, 2017. Roles of physical forces in development.

[14] Jonathan B. Freund, Jacky G. Goetz, Kent L. Hill, and Julien Vermot. Fluid flows and forces in development: functions, features and biophysical principles. *Development*, 139(7):1229–1245, 04 2012.

[15] Thomas Iskratsch, Haguy Wolfenson, and Michael P Sheetz. Appreciating force and shape — the rise of mechanotransduction in cell biology. *Nature Reviews Molecular Cell Biology*, 15(12):825–833, 2014.

[16] J. Matthew Barnes, Laralynne Przybyla, and Valerie M. Weaver. Tissue mechanics regulate brain development, homeostasis and disease. *Journal of Cell Science*, 130(1):71–82, 2017.

[17] Valerie Marie Weaver. Cell and tissue mechanics: the new cell biology frontier. *Molecular Biology of the Cell*, 28(14):1815–1818, 2017.

[18] Pierre-François Lenne and Vikas Trivedi. Sculpting tissues by phase transitions. *Nature Communications*, 13(1):664, 2022.

[19] G. Wayne Brodland. The differential interfacial tension hypothesis (dith): A comprehensive theory for the self-rearrangement of embryonic cells and tissues. *Journal of Biomechanical Engineering*, 124(2):188 – 197, 2002. Cited by: 189.

[20] Reza Farhadifar, Jens-Christian Röper, Benoit Aigouy, Suzanne Eaton, and Frank Jülicher. The influence of cell mechanics, cell-cell interactions, and proliferation on epithelial packing. *Current Biology*, 17(24):2095–2104, 2007.

[21] Dapeng Bi, J H Lopez, J M Schwarz, and M Lisa Manning. A density-independent rigidity transition in biological tissues. *Nature Physics*, 11(12):1074–1079, 2015.

[22] Jin-Ah Park, Jae Hun Kim, Dapeng Bi, Jennifer A Mitchel, Nader Taheri Qazvini, Kelan Tantisira, Chan Young Park, Maureen McGill, Sae-Hoon Kim, Bomi Gweon, Jacob Notbohm, Robert Steward Jr, Stephanie Burger, Scott H Randell, Alvin T Kho, Dhananjay T Tambe, Corey Hardin, Stephanie A Shore, Elliot Israel, David A Weitz, Daniel J Tschumperlin, Elizabeth P. Henske, Scott T Weiss, M Lisa Manning, James P Butler, Jeffrey M Drazen, and Jeffrey J Fredberg. Unjamming and cell shape in the asthmatic airway epithelium. *Nature Materials*, 14(10):1040–1048, 2015.

[23] Robert J. Tetley, Michael F. Staddon, Davide Heller, Andreas Hoppe, Shiladitya Banerjee, and Yanlan Mao. Tissue fluidity promotes epithelial wound healing. *Nature Physics*, 15(11):1195–1203, 2019.

[24] K. Venkatesan Iyer, Romina Piscitello-Gómez, Joris Paijmans, Frank Jülicher, and Suzanne Eaton. Epithelial Viscoelasticity Is Regulated by Mechanosensitive E-cadherin Turnover. *Current Biology*, 29(4):578–591.e5, feb 2019.

[25] Nabila Founounou, Reza Farhadifar, Giovanna M. Collu, Ursula Weber, Michael J. Shelley, and Marek Mlodzik. Tissue fluidity mediated by adherens

junction dynamics promotes planar cell polarity-driven ommatidial rotation. *Nature Communications*, 12(1):6974, 2021.

[26] Yanlan Mao, Alexander L Tournier, Andreas Hoppe, Lennart Kester, Barry J Thompson, and Nicolas Tapon. Differential proliferation rates generate patterns of mechanical tension that orient tissue growth. *The EMBO Journal*, 32(21):2790–2803, 2013.

[27] Sangbum Park, David G. Gonzalez, Boris Guirao, Jonathan D. Boucher, Katie Cockburn, Edward D. Marsh, Kailin R. Mesa, Samara Brown, Panteleimon Rompolas, Ann M. Haberman, Yohanns Bellaïche, and Valentina Greco. Tissue-scale coordination of cellular behaviour promotes epidermal wound repair in live mice. *Nature Cell Biology*, 19(2):155–163, 2017.

[28] Natalie J. Kirkland, Alice C. Yuen, Melda Tozluoglu, Nancy Hui, Ewa K. Paluch, and Yanlan Mao. Tissue mechanics regulate mitotic nuclear dynamics during epithelial development. *Current Biology*, 30(13):2419–2432.e4, 2020.

[29] Alessandro Mongera, Payam Rowghanian, Hannah J Gustafson, Elijah Shelton, David A Kealhofer, Emmet K Carn, Friedhelm Serwane, Adam A Lucio, James Giammona, and Otger Campàs. A fluid-to-solid jamming transition underlies vertebrate body axis elongation. *Nature*, 561(7723):401–405, 2018.

[30] Matteo Rauzi, Pascale Verant, Thomas Lecuit, and Pierre François Lenne. Nature and anisotropy of cortical forces orienting Drosophila tissue morphogenesis. *Nature Cell Biology*, 10(12):1401–1410, 2008.

[31] Robert J. Tetley and Yanlan Mao. The same but different: Cell intercalation as a driver of tissue deformation and fluidity. *Philosophical Transactions of the Royal Society B: Biological Sciences*, 373(1759), 2018.

[32] Anna Haeger, Marina Krause, Katarina Wolf, and Peter Friedl. Cell jamming: Collective invasion of mesenchymal tumor cells imposed by tissue confinement. *Biochimica et Biophysica Acta (BBA) - General Subjects*, 1840(8):2386–2395, 2014. Matrix-mediated cell behaviour and properties.

[33] Steve Pawlizak, Anatol W Fritsch, Steffen Grosser, Dave Ahrens, Tobias Thalheim, Stefanie Riedel, Tobias R Kießling, Linda Oswald, Mareike Zink, M Lisa

Manning, and Josef A Käs. Testing the differential adhesion hypothesis across the epithelialmesenchymal transition. *New Journal of Physics*, 17(8):083049, aug 2015.

[34] Adrian F. Pegoraro, Jeffrey J. Fredberg, and Jin Ah Park. Problems in biology with many scales of length: Cell-cell adhesion and cell jamming in collective cellular migration. *Experimental Cell Research*, 343(1):54–59, apr 2016.

[35] William Wood, Antonio Jacinto, Richard Grose, Sarah Woolner, Jonathan Gale, Clive Wilson, and Paul Martin. Wound healing recapitulates morphogenesis in Drosophila embryos. *Nature Cell Biology*, 4(11):907–912, 2002.

[36] Paul Martin and Susan M. Parkhurst. Parallels between tissue repair and embryo morphogenesis. *Development*, 131(13):3021–3034, 07 2004.

[37] Iswar K. Hariharan and Florenci Serras. Imaginal disc regeneration takes flight. *Current Opinion in Cell Biology*, 48:10–16, 2017.

[38] Alejandra Guzmán-Herrera and Yanlan Mao. Polarity during tissue repair, a multiscale problem. *Current Opinion in Cell Biology*, 62:31–36, 2020.

[39] V Velnar, T Bailey, T Smrkolj. The Wound Healing Process : an Overview of the Cellular and Molecular Mechanisms. *J Int Med Res*, 37(5):1528–1542, 2009.

[40] M. T. Abreu-Blanco, J. M. Verboon, R. Liu, J. J. Watts, and S. M. Parkhurst. Drosophila embryos close epithelial wounds using a combination of cellular protrusions and an actomyosin purse string. *Journal of Cell Science*, 125(24):5984–5997, 2012.

[41] Kate MacCord and Jane Maienschein. Understanding regeneration at different scales. *eLife*, 8, mar 2019.

[42] Rachel E. Stephenson, Tomohito Higashi, Ivan S. Erofeev, Torey R. Arnold, Marcin Leda, Andrew B. Goryachev, and Ann L. Miller. Rho Flares Repair Local Tight Junction Leaks. *Developmental Cell*, 48(4):445–459.e5, 2019.

[43] Michael Levin. Endogenous bioelectrical networks store non-genetic patterning information during development and regeneration. *The Journal of Physiology*, 592(11):2295–2305, jun 2014.

[44] Sera M Busse, Patrick T McMillen, and Michael Levin. Cross-limb communication during Xenopus hindlimb regenerative response: non-local bioelectric injury signals. *Development*, 145(19):dev164210, oct 2018.

[45] Fallon Durant, Johanna Bischof, Chris Fields, Junji Morokuma, Joshua LaPalme, Alison Hoi, and Michael Levin. The Role of Early Bioelectric Signals in the Regeneration of Planarian Anterior/Posterior Polarity. *Biophysical Journal*, 116(5):948–961, 2019.

[46] Alejandro Sánchez Alvarado and Panagiotis A Tsonis. Bridging the regeneration gap: genetic insights from diverse animal models. *Nature Reviews Genetics*, 7(11):873–884, 2006.

[47] Geoffrey C. Gurtner, Sabine Werner, Yann Barrandon, and Michael T. Longaker. Wound repair and regeneration. *Nature*, 453(7193):314–321, 2008.

[48] Hitoshi Yokoyama. Initiation of limb regeneration: The critical steps for regenerative capacity. *Development, Growth & Differentiation*, 50(1):13–22, jan 2008.

[49] Alexandra E. Bely and Kevin G. Nyberg. Evolution of animal regeneration: re-emergence of a field. 25(3):161–170, mar 2010.

[50] Brigitte Galliot and Luiza Ghila. Cell plasticity in homeostasis and regeneration. *Molecular Reproduction and Development*, 77(10):837–855, oct 2010.

[51] Nathaniel P. Hoyle, Estere Seinkmane, Marrit Putker, Kevin A. Feeney, Toke P. Krogager, Johanna E. Chesham, Liam K. Bray, Justyn M. Thomas, Ken Dunn, John Blaikley, and John S. O'Neill. Circadian actin dynamics drive rhythmic fibroblast mobilization during wound healing. *Science Translational Medicine*, 9(415):eaal2774, 2017.

[52] Abijeet S. Mehta and Amit Singh. Insights into regeneration tool box: An animal model approach. *Developmental Biology*, apr 2019.

[53] Ada Repiso, Cora Bergantiños, and Florenci Serras. Cell fate respecification and cell division orientation drive intercalary regeneration in Drosophila wing discs. *Development*, 140(17):3541 LP – 3551, sep 2013.

[54] Rachel Smith-Bolton. Drosophila Imaginal Discs as a Model of Epithelial Wound Repair and Regeneration. *Advances in Wound Care*, 5(6):251–261, 2016.

[55] Luigi Aloia, Mikel Alexander McKie, and Meritxell Huch. Cellular plasticity in the adult liver and stomach. *Journal of Physiology*, 594(17):4815–4825, 2016.

[56] Steffen Werner, Hanh Thi Kim Vu, and Jochen C. Rink. Self-organization in development, regeneration and organoids. *Current Opinion in Cell Biology*, 44:102–109, 2017.

[57] William Razzell, Will Wood, and Paul Martin. Recapitulation of morphogenetic cell shape changes enables wound re-epithelialisation. *Development*, 141(9):1814–1820, 2014.

[58] Rebecca Richardson, Manuel Metzger, Philipp Knyphausen, Thomas Ramezani, Krasimir Slanchev, Christopher Kraus, Elmon Schmelzer, and Matthias Hammerschmidt. Re-epithelialization of cutaneous wounds in adult zebrafish combines mechanisms of wound closure in embryonic and adult mammals. *Journal of Cell Science*, 129(13):e1.1–e1.1, 2016.

[59] Rebecca Richardson and Matthias Hammerschmidt. The role of Rho kinase (Rock) in re-epithelialization of adult zebrafish skin wounds. *Small GTPases*, 9(3):230–236, 2018.

[60] Paula Santabárbara-Ruiz, Mireya López-Santillán, Irene Martínez-Rodríguez, Anahí Binagui-Casas, Lídia Pérez, Marco Milán, Montserrat Corominas, and Florenci Serras. Ros-induced jnk and p38 signaling is required for unpaired cytokine activation during drosophila regeneration. *PLOS Genetics*, 11(10):1–26, 10 2015.

[61] Melanie I. Worley, Linda Setiawan, and Iswar K. Hariharan. Regeneration and Transdetermination in Drosophila Imaginal Discs. *Annual Review of Genetics*, 46(1):289–310, 2012.

[62] Jorge V. Beira and Renato Paro. The legacy of Drosophila imaginal discs. *Chromosoma*, 125(4):573–592, 2016.

[63] Luigi Aloia, Mikel Alexander McKie, Grégoire Vernaz, Lucía Cordero-Espinoza, Niya Aleksieva, Jelle van den Ameele, Francesco Antonica, Berta Font-Cunill, Alexander Raven, Riccardo Aiese Cigliano, German Belenguer, Richard L. Mort, Andrea H. Brand, Magdalena Zernicka-Goetz, Stuart J. Forbes, Eric A. Miska, and Meritxell Huch. Epigenetic remodelling licences adult cholangiocytes for organoid formation and liver regeneration. *Nature Cell Biology*, 21(11):1321–1333, 2019.

[64] Agustí Brugués, Ester Anon, Vito Conte, Jim H. Veldhuis, Mukund Gupta, Julien Colombelli, José J. Muñoz, G. Wayne Brodland, Benoit Ladoux, and Xavier Trepat. Forces driving epithelial wound healing. *Nature Physics*, 10(9):683–690, 2014.

[65] Sri Ram Krishna Vedula, Grégoire Peyret, Ibrahim Cheddadi, Tianchi Chen, Agustí Brugués, Hiroaki Hirata, Horacio Lopez-Menendez, Yusuke Toyama, Luís Neves De Almeida, Xavier Trepat, Chwee Teck Lim, and Benoit Ladoux. Mechanics of epithelial closure over non-adherent environments. *Nature Communications*, 6:1–10, 2015.

[66] Charlène Guillot and Thomas Lecuit. Mechanics of epithelial tissue homeostasis and morphogenesis. *Science*, 340(6137):1185–1189, 2013.

[67] Sandra B. Lemke and Celeste M. Nelson. Dynamic changes in epithelial cell packing during tissue morphogenesis. *Current Biology*, 31(18):R1098–R1110, 2021.

[68] Giulia Paci and Yanlan Mao. Forced into shape: Mechanical forces in drosophila development and homeostasis. *Seminars in Cell Developmental Biology*, 120:160–170, 2021. Special issue: The mechanics of development by Timothy Saunders and Ivo Telley.

[69] D Kaspar, W Seidl, C Neidlinger-Wilke, A Ignatius, and L Claes. Dynamic cell stretching increases human osteoblast proliferation and cicp synthesis but decreases osteocalcin synthesis and alkaline phosphatase activity. *Journal of Biomechanics*, 33(1):45 – 51, 2000.

[70] Thomas Schluck, Ulrike Nienhaus, Tinri Aegerter-Wilmsen, and Christof M. Aegerter. Mechanical Control of Organ Size in the Development of the Drosophila Wing Disc. *PLoS ONE*, 8(10), 2013.

[71] Geoffrey C. Gurtner, Reinhold H. Dauskardt, Victor W. Wong, Kirit A. Bhatt, Kenneth Wu, Ivan N. Vial, Karine Padois, Joshua M. Korman, and Michael T. Longaker. Improving cutaneous scar formation by controlling the mechanical environment: Large animal and phase i studies. *Annals of Surgery*, 254(2):217–225, 2011.

[72] Leandra A. Barnes, Clement D. Marshall, Tripp Leavitt, Michael S. Hu, Alessandra L. Moore, Jennifer G. Gonzalez, Michael T. Longaker, and Geoffrey C. Gurtner. Mechanical Forces in Cutaneous Wound Healing: Emerging Therapies to Minimize Scar Formation. *Advances in Wound Care*, 7(2):47–56, jan 2018.

[73] Anna B. Kobb, Teresa Zulueta-Coarasa, and Rodrigo Fernandez-Gonzalez. Tension regulates myosin dynamics during Drosophila embryonic wound repair . *Journal of Cell Science*, 130(4):689–696, 2017.

[74] Simon Begnaud, Tianchi Chen, Delphine Delacour, René-marc Mège, and Benoit Ladoux. Mechanics of epithelial tissues during gap closure. *Current opinion in cell biology*, 42:52–62, 2016.

[75] Akanksha Jain, Vladimir Ulman, Arghyadip Mukherjee, Mangal Prakash, Marina B Cuenca, Lokesh G Pimpale, Stefan Münster, Robert Haase, Kristen A Panfilio, Florian Jug, Stephan W Grill, Pavel Tomancak, and Anastasios Pavlopoulos. Regionalized tissue fluidization is required for epithelial gap closure during insect gastrulation. *Nature Communications*, 11(1):5604, 2020.

[76] D. Kuipers, A. Mehonic, M. Kajita, L. Peter, Y. Fujita, T. Duke, G. Charras, and J. E. Gale. Epithelial repair is a two-stage process driven first by dying

cells and then by their neighbours. *Journal of Cell Science*, 127(6):1229–1241, 2014.

[77] Asako Shindo, Anastasia Audrey, Maki Takagishi, Masahide Takahashi, John B. Wallingford, and Makoto Kinoshita. Septin-dependent remodeling of cortical microtubule drives cell reshaping during epithelial wound healing. *Journal of Cell Science*, 2018.

[78] Lara Carvalho, Pedro Patricio, Susana Ponte, Carl Philipp Heisenberg, Luis Almeida, André S. Nunes, Nuno A.M. Araújo, and Antonio Jacinto. Occluding junctions as novel regulators of tissue mechanics during wound repair. *Journal of Cell Biology*, 217(12):4267–4283, 2018.

[79] Paul Martin and Julian Lewis. Actin cables and epidermal movement in embryonic wound healing. *Nature*, 360(6400):179–183, 1992.

[80] J Brock, K Midwinter, J Lewis, and P Martin. Healing of incisional wounds in the embryonic chick wing bud: characterization of the actin purse-string and demonstration of a requirement for Rho activation. *The Journal of Cell Biology*, 135(4):1097 LP – 1107, nov 1996.

[81] W M Bement, P Forscher, and M S Mooseker. A novel cytoskeletal structure involved in purse string wound closure and cell polarity maintenance. *The Journal of Cell Biology*, 121(3):565 LP – 578, may 1993.

[82] Nivetha Kannan and Vivian W. Tang. Myosin-1c promotes E-cadherin tension and force-dependent recruitment of α-actinin to the epithelial cell junction. *Journal of cell science*, 131(12):jcs211334, 2018.

[83] Tomohito Higashi and Ann L Miller. Tricellular junctions: how to build junctions at the TRICkiest points of epithelial cells. *Molecular Biology of the Cell*, 28(15):2023–2034, jul 2017.

[84] Julie Salomon, Cécile Gaston, Jérémy Magescas, Boris Duvauchelle, Danielle Canioni, Lucie Sengmanivong, Adeline Mayeux, Grégoire Michaux, Florence Campeotto, Julie Lemale, Jérôme Viala, Françoise Poirier, Nicolas Minc,

Jacques Schmitz, Nicole Brousse, Benoit Ladoux, Olivier Goulet, and Delphine Delacour. Contractile forces at tricellular contacts modulate epithelial organization and monolayer integrity. *Nature Communications*, 8, 2017.

[85] Bipul R. Acharya, Alexander Nestor-Bergmann, Xuan Liang, Shafali Gupta, Kinga Duszyc, Estelle Gauquelin, Guillermo A. Gomez, Srikanth Budnar, Philippe Marcq, Oliver E. Jensen, Zev Bryant, and Alpha S. Yap. A Mechanosensitive RhoA Pathway that Protects Epithelia against Acute Tensile Stress. *Developmental Cell*, 47(4):439–452.e6, 2018.

[86] Maria Duda, Natalie J. Kirkland, Nargess Khalilgharibi, Melda Tozluoglu, Alice C. Yuen, Nicolas Carpi, Anna Bove, Matthieu Piel, Guillaume Charras, Buzz Baum, and Yanlan Mao. Polarization of Myosin II Refines Tissue Material Properties to Buffer Mechanical Stress. *Developmental Cell*, 48(2):245–260.e7, 2019.

[87] Nargess Khalilgharibi, Jonathan Fouchard, Nina Asadipour, Ricardo Barrientos, Maria Duda, Alessandra Bonfanti, Amina Yonis, Andrew Harris, Payman Mosaffa, Yasuyuki Fujita, Alexandre Kabla, Yanlan Mao, Buzz Baum, José J Muñoz, Mark Miodownik, and Guillaume Charras. Stress relaxation in epithelial monolayers is controlled by the actomyosin cortex. *Nature Physics*, 2019.

[88] Antoine Ducuing and Stéphane Vincent. The actin cable is dispensable in directing dorsal closure dynamics but neutralizes mechanical stress to prevent scarring in the Drosophila embryo. *Nature Cell Biology*, 18(11):1149–1160, 2016.

[89] Tommi Anttonen, Ilya Belevich, Maarja Laos, Anni Herranen, Eija Jokitalo, Cord Brakebusch, and Ulla Pirvola. Cytoskeletal Stability in the Auditory Organ In Vivo : RhoA Is Dispensable for Wound Healing but Essential for Hair Cell Development . *Eneuro*, 4(5):ENEURO.0149–17.2017, 2017.

[90] George T. Eisenhoffer and Jody Rosenblatt. Bringing balance by force: live cell extrusion controls epithelial cell numbers. *Trends in Cell Biology*, 23(4):185–192, 2013.

[91] Ian G. Macara, Richard Guyer, Graham Richardson, Yongliang Huo, and Syed M. Ahmed. Epithelial homeostasis. *Current Biology*, 24(17):R815–R825, 2014.

[92] Enrique Rodriguez-Boulan, Geri Kreitzer, and Anne Müsch. Organization of vesicular trafficking in epithelia. *Nature Reviews Molecular Cell Biology*, 6(3):233–247, 2005.

[93] Daniel St Johnston and Julie Ahringer. Cell polarity in eggs and epithelia: Parallels and diversity. *Cell*, 141(5):757–774, 2010.

[94] Fernando Martin-Belmonte and Keith Mostov. Regulation of cell polarity during epithelial morphogenesis. *Current Opinion in Cell Biology*, 20(2):227–234, 2008. Cell regulation.

[95] Daniel St Johnston and Bénédicte Sanson. Epithelial polarity and morphogenesis. *Current Opinion in Cell Biology*, 23(5):540–546, 2011. Cell-to-cell contact and extracellular matrix.

[96] Ulrich Tepass. The apical polarity protein network in drosophila epithelial cells: Regulation of polarity, junctions, morphogenesis, cell growth, and survival. *Annual Review of Cell and Developmental Biology*, 28(1):655–685, 2012. PMID: 22881460.

[97] Amalia Riga, Victoria G. Castiglioni, and Mike Boxem. New insights into apical-basal polarization in epithelia. *Current Opinion in Cell Biology*, 62:1–8, 2020.

[98] Carolina Epifano and Mirna Perez-Moreno. Crossroads of integrins and cadherins in epithelia and stroma remodeling. *Cell adhesion migration*, 6:261–73, 05 2012.

[99] Adam C. Martin, Michael Gelbart, Rodrigo Fernandez-Gonzalez, Matthias Kaschube, and Eric F. Wieschaus. Integration of contractile forces during tissue invagination. *Journal of Cell Biology*, 188(5):735–749, 03 2010.

[100] Buzz Baum and Marios Georgiou. Dynamics of adherens junctions in epithelial establishment, maintenance, and remodeling. *Journal of Cell Biology*, 192(6):907–917, 03 2011.

[101] Yu-Chiun Wang, Zia Khan, Matthias Kaschube, and Eric F Wieschaus. Differential positioning of adherens junctions is associated with initiation of epithelial folding. *Nature*, 484(7394):390–393, 2012.

[102] Jean-Léon Maître and Carl-Philipp Heisenberg. Three functions of cadherins in cell adhesion. *Current Biology*, 23(14):R626–R633, 2013.

[103] Shinji Hirano, Naomi Kimoto, Yutaka Shimoyama, Setsuo Hirohashi, and Masatoshi Takeichi. Identification of a neural -catenin as a key regulator of cadherin function and multicellular organization. *Cell*, 70(2):293–301, 1992.

[104] Michael A. Davis, Renee C. Ireton, and Albert B. Reynolds. A core function for p120-catenin in cadherin turnover . *Journal of Cell Biology*, 163(3):525–534, 11 2003.

[105] Sylvie Dufour, René-Marc Mège, and Jean Paul Thiery. -catenin, vinculin, and f-actin in strengthening e-cadherin cell–cell adhesions and mechanosensing. *Cell Adhesion & Migration*, 7(4):345–350, 2013. PMID: 23739176.

[106] D.E. Leckband and J. de Rooij. Cadherin adhesion and mechanotransduction. *Annual Review of Cell and Developmental Biology*, 30(1):291–315, 2014. PMID: 25062360.

[107] Ekaterina Papusheva and Carl-Philipp Heisenberg. Spatial organization of adhesion: force-dependent regulation and function in tissue morphogenesis. *The EMBO Journal*, 29(16):2753–2768, 2010.

[108] Charlène Guillot and Thomas Lecuit. Adhesion disengagement uncouples intrinsic and extrinsic forces to drive cytokinesis in epithelial tissues. *Developmental Cell*, 24(3):227–241, 2013.

[109] David Garrod and Martyn Chidgey. Desmosome structure, composition and function. *Biochimica et Biophysica Acta (BBA) - Biomembranes*, 1778(3):572–587, 2008. Apical Junctional Complexes Part I.

[110] Caezar Al-Jassar, Hennie Bikker, Michael Overduin, and Martyn Chidgey. Mechanistic basis of desmosome-targeted diseases. *Journal of Molecular Biology*, 425(21):4006–4022, 2013. Understanding Molecular Effects of Naturally Occurring Genetic Differences.

[111] Meghan A. Morrissey and David R. Sherwood. An active role for basement membrane assembly and modification in tissue sculpting. *Journal of Cell Science*, 128(9):1661–1668, 2015.

[112] Aleksandra N. Kozyrina, Teodora Piskova, and Jacopo Di Russo. Mechanobiology of epithelia from the perspective of extracellular matrix heterogeneity. *Frontiers in Bioengineering and Biotechnology*, 8, 2020.

[113] W. P. Daley, S. B. Peters, and M. Larsen. Extracellular matrix dynamics in development and regenerative medicine. *Journal of Cell Science*, 121(3):255–264, 2008.

[114] Achilleas D Theocharis, Spyros S Skandalis, Chrysostomi Gialeli, and Nikos K Karamanos. Extracellular matrix structure. *Advanced Drig Delivery Reviews*, 97:4–27, 2016.

[115] Fiona M Watt and Wilhelm T S Huck. Role of the extracellular matrix in regulating stem cell fate. *Nature Reviews Molecular Cell Biology*, 14(8):467–473, 2013.

[116] Jay D Humphrey, Eric R Dufresne, and Martin A Schwartz. Mechanotransduction and extracellular matrix homeostasis. *Nature Reviews Molecular Cell Biology*, 15(12):802–812, 2014.

[117] Adam J. Engler, Shamik Sen, H. Lee Sweeney, and Dennis E. Discher. Matrix Elasticity Directs Stem Cell Lineage Specification. *Cell*, 126(4):677–689, 2006.

[118] Matthew J. Paszek, Nastaran Zahir, Kandice R. Johnson, Johnathon N. Lakins, Gabriela I. Rozenberg, Amit Gefen, Cynthia A. Reinhart-King, Susan S. Margulies, Micah Dembo, David Boettiger, Daniel A. Hammer, and Valerie M. Weaver. Tensional homeostasis and the malignant phenotype. *Cancer Cell*, 8(3):241 – 254, 2005.

[119] Kelly C Clause and Thomas H Barker. Extracellular matrix signaling in morphogenesis and repair. *Current Opinion in Biotechnology*, 24(5):830–833, 2013.

[120] John G. Lock, Bernhard Wehrle-Haller, and Staffan Strömblad. Cell-matrix adhesion complexes: Master control machinery of cell migration. *Seminars in Cancer Biology*, 18(1):65–76, 2008.

[121] Yoshikazu Takada, Xiaojing Ye, and Scott Simon. The integrins. *Genome Biology*, 8(5), 2007.

[122] Jianghai Zhu, Bing-Hao Luo, Tsan Xiao, Chengzhong Zhang, Noritaka Nishida, and Timothy A. Springer. Structure of a complete integrin ectodomain in a physiologic resting state and activation and deactivation by applied forces. *Molecular Cell*, 32(6):849–861, 2008.

[123] Aidan P. Maartens, Jutta Wellmann, Emma Wictome, Benjamin Klapholz, Hannah Green, and Nicholas H. Brown. Drosophila vinculin is more harmful when hyperactive than absent, and can circumvent integrin to form adhesion complexes. *Journal of Cell Science*, 129(23):4354–4365, 12 2016.

[124] Mithila Burute and Manuel Thery. Spatial segregation between cell–cell and cell–matrix adhesions. *Current Opinion in Cell Biology*, 24(5):628–636, 2012. Cell-to-cell contact and extracellular matrix.

[125] Yanlan Mao and Buzz Baum. Tug of war-The influence of opposing physical forces on epithelial cell morphology. *Developmental Biology*, 401(1):92–102, 2015.

[126] Liyuan Sui, Silvanus Alt, Martin Weigert, Natalie Dye, Suzanne Eaton, Florian Jug, Eugene W Myers, Frank Jülicher, Guillaume Salbreux, and Christian Dahmann. Differential lateral and basal tension drive folding of Drosophila wing discs through two distinct mechanisms. *Nature Communications*, 9(1):4620, 2018.

[127] Kim S. Midwood, Leyla Valenick Williams, and Jean E. Schwarzbauer. Tissue repair and the dynamics of the extracellular matrix. *International Journal of Biochemistry and Cell Biology*, 36(6):1031–1037, 2004.

[128] Janna K Mouw, Guanqing Ou, and Valerie M Weaver. Extracellular matrix assembly: a multiscale deconstruction. *Nature Reviews Molecular Cell Biology*, 15(12):771–785, 2014.

[129] Nargess Khalilgharibi and Yanlan Mao. To form and function: on the role of basement membrane mechanics in tissue development, homeostasis and disease. *Open Biology*, 11(2):200360, 2021.

[130] Patricia Murray and David Edgar. Regulation of Programmed Cell Death by Basement Membranes in Embryonic Development. *Journal of Cell Biology*, 150(5):1215–1221, 09 2000.

[131] Lucy Erin O'Brien, Tzuu-Shuh Jou, Anne L Pollack, Qihang Zhang, Steen H Hansen, Peter Yurchenco, and Keith E Mostov. Rac1 orientates epithelial apical polarity through effects on basolateral laminin assembly. *Nature Cell Biology*, 3(9):831–838, 2001.

[132] Jeffrey P. Rasmussen, Sowmya Somashekar Reddy, and James R. Priess. Laminin is required to orient epithelial polarity in the C. elegans pharynx. *Development*, 139(11):2050–2060, 06 2012.

[133] Saori L. Haigo and David Bilder. Global tissue revolutions in a morphogenetic movement controlling elongation. *Science*, 331(6020):1071–1074, 2011.

[134] Jill S. Harunaga, Andrew D. Doyle, and Kenneth M. Yamada. Local and global dynamics of the basement membrane during branching morphogenesis require protease activity and actomyosin contractility. *Developmental Biology*, 394(2):197–205, 2014.

[135] José Carlos Pastor-Pareja and Tian Xu. Shaping cells and organs in drosophila by opposing roles of fat body-secreted collagen iv and perlecan. *Developmental Cell*, 21(2):245–256, 2011.

[136] Yukihiko Kubota, Kayo Nagata, Asako Sugimoto, and Kiyoji Nishiwaki. Tissue Architecture in the Caenorhabditis elegans Gonad Depends on Interactions Among Fibulin-1, Type IV Collagen and the ADAMTS Extracellular Protease. *Genetics*, 190(4):1379–1388, 04 2012.

[137] Kandice R. Levental, Hongmei Yu, Laura Kass, Johnathon N. Lakins, Mikala Egeblad, Janine T. Erler, Sheri F.T. Fong, Katalin Csiszar, Amato Giaccia, Wolfgang Weninger, Mitsuo Yamauchi, David L. Gasser, and Valerie M. Weaver. Matrix crosslinking forces tumor progression by enhancing integrin signaling. *Cell*, 139(5):891–906, 2009.

[138] Pierre Bedossa and Valérie Paradis. Liver extracellular matrix in health and disease. *The Journal of Pathology*, 200(4):504–515, 2003.

[139] Andrea Baiocchini, Claudia Montaldo, Alice Conigliaro, Alessio Grimaldi, Virginia Correani, Francesco Mura, Fabiola Ciccosanti, Nicolina Rotiroti, Alessia Brenna, Marzia Montalbano, Gianpiero D'Offizi, Maria Rosaria Capobianchi, Riccardo Alessandro, Mauro Piacentini, Maria Eugenia Schininà, Bruno Maras, Franca Del Nonno, Marco Tripodi, and Carmine Mancone. Extracellular matrix molecular remodeling in human liver fibrosis evolution. *PLOS ONE*, 11(3):1–14, 03 2016.

[140] Sayaka Higuchi, Qingsong Lin, Jigang Wang, Teck Kwang Lim, Shashikant B. Joshi, Ganesh Srinivasan Anand, Maxey C M Chung, Michael P. Sheetz, and Hideaki Fujita. Heart extracellular matrix supports cardiomyocyte differentiation of mouse embryonic stem cells. *Journal of Bioscience and Bioengineering*, 115(3):320–325, 2013.

[141] L F Tapias and H C Ott. Decellularized Scaffolds as a Platform for Bioengineered Organs. *Current Opinion in Organ Transplantation*, 19(2):145–152, 2014.

[142] Lucas R. Smith, Sangkyun Cho, and Dennis E. Discher. Stem cell differentiation is regulated by extracellular matrix mechanics. *Physiology*, 33(1):16–25, 2018. PMID: 29212889.

[143] Alberto Elosegui-Artola. The extracellular matrix viscoelasticity as a regulator of cell and tissue dynamics. *Current Opinion in Cell Biology*, 72:10–18, 2021.

[144] Jonna Petzold and Eileen Gentleman. Intrinsic Mechanical Cues and Their Impact on Stem Cells and Embryogenesis. *Frontiers in Cell and Developmental Biology*, 9(November), 2021.

[145] Jianping Fu, Yang-Kao Wang, Michael T Yang, Ravi A Desai, Xiang Yu, Zhijun Liu, and Christopher S Chen. Mechanical regulation of cell function with geometrically modulated elastomeric substrates. *Nature Methods*, 7(9):733–736, 2010.

[146] Nathaniel Huebsch, Praveen R Arany, Angelo S Mao, Dmitry Shvartsman, Omar A Ali, Sidi A Bencherif, José Rivera-Feliciano, and David J Mooney. Harnessing traction-mediated manipulation of the cell/matrix interface to control stem-cell fate. *Nature Materials*, 9(6):518–526, 2010.

[147] Amnon Buxboim, Jerome Irianto, Joe Swift, Avathamsa Athirasala, Jae-Won Shin, Florian Rehfeldt, and Dennis E. Discher. Coordinated increase of nuclear tension and lamin-a with matrix stiffness outcompetes lamin-b receptor that favors soft tissue phenotypes. *Molecular Biology of the Cell*, 28(23):3333–3348, 2017. PMID: 28931598.

[148] N. Gjorevski, M. Nikolaev, T. E. Brown, O. Mitrofanova, N. Brandenberg, F. W. DelRio, F. M. Yavitt, P. Liberali, K. S. Anseth, and M. P. Lutolf. Tissue geometry drives deterministic organoid patterning. *Science*, 375(6576):eaaw9021, 2022.

[149] Sharona Even-Ram, Vira Artym, and Kenneth M. Yamada. Matrix control of stem cell fate. *Cell*, 126(4):645–647, 2006.

[150] Christopher J Hindley, Gianmarco Mastrogiovanni, and Meritxell Huch. The plastic liver : differentiated cells , stem cells , every cell ? *The Journal of Clinical Investigation*, 124(12):5099–5102, 2014.

[151] Shani Ben-Moshe and Shalev Itzkovitz. Spatial heterogeneity in the mammalian liver. *Nature Reviews Gastroenterology Hepatology*, 16(7):395–410, 2019.

[152] Lauren Tomlinson, Lauren Hyndman, James W. Firman, Robert Bentley, Jonathan A. Kyffin, Steven D. Webb, Sean McGinty, and Parveen Sharma. In vitro liver zonation of primary rat hepatocytes. *Frontiers in Bioengineering and Biotechnology*, 7, 2019.

[153] Andrew W Duncan, Matthew H Taylor, Raymond D Hickey, Amy E Hanlon Newell, Michelle L Lenzi, Susan B Olson, Milton J Finegold, and Markus Grompe. The ploidy conveyor of mature hepatocytes as a source of genetic variation. *Nature*, 467(7316):707–710, 2010.

[154] Bruce Wang, Ludan Zhao, Matt Fish, Catriona Y Logan, and Roel Nusse. Self-renewing diploid Axin2+ cells fuel homeostatic renewal of the liver. *Nature*, 524(7564):180–185, 2015.

[155] Shengda Lin, Elisabete M. Nascimento, Chandresh R. Gajera, Lu Chen, Patrick Neuhöfer, Alina Garbuzov, Sui Wang, and Steven E. Artandi. Distributed hepatocytes expressing telomerase repopulate the liver in homeostasis and injury. *Nature*, 556(7700):244–248, 2018.

[156] Branden D. Tarlow, Carl Pelz, Willscott E. Naugler, Leslie Wakefield, Elizabeth M. Wilson, Milton J. Finegold, and Markus Grompe. Bipotential adult liver progenitors are derived from chronically injured mature hepatocytes. *Cell Stem Cell*, 15(5):605–618, 2014.

[157] Joan Font-Burgada, Shabnam Shalapour, Suvasini Ramaswamy, Brian Hsueh, David Rossell, Atsushi Umemura, Koji Taniguchi, Hayato Nakagawa, Mark A. Valasek, Li Ye, Janel L. Kopp, Maike Sander, Hannah Carter, Karl Deisseroth, Inder M. Verma, and Michael Karin. Hybrid periportal hepatocytes regenerate the injured liver without giving rise to cancer. *Cell*, 162(4):766–779, 2015.

[158] Craig Dorrell, Laura Erker, Jonathan Schug, Janel L. Kopp, Pamela S. Canaday, Alan J. Fox, Olga Smirnova, Andrew W. Duncan, Milton J. Finegold, Maike Sander, Klaus H. Kaestner, and Markus Grompe. Prospective isolation of a bipotential clonogenic liver progenitor cell in adult mice. *Genes Development*, 25(11):1193–1203, 2011.

[159] Soona Shin, Gabriel Walton, Reina Aoki, Karrie Brondell, Jonathan Schug, Alan Fox, Olga Smirnova, Craig Dorrell, Laura Erker, Andrew S. Chu, Rebecca G. Wells, Markus Grompe, Linda E. Greenbaum, and Klaus H. Kaestner. Foxl1-cre-marked adult hepatic progenitors have clonogenic and bilineage differentiation potential. *Genes Development*, 25(11):1185–1192, 2011.

[160] Regina Español–Suñer, Rodolphe Carpentier, Noémi Van Hul, Vanessa Legry, Younes Achouri, Sabine Cordi, Patrick Jacquemin, Frédéric Lemaigre, and Isabelle A. Leclercq. Liver progenitor cells yield functional hepatocytes in response to chronic liver injury in mice. *Gastroenterology*, 143(6):1564–1575.e7, 2012.

[161] Meritxell Huch, Craig Dorrell, Sylvia F. Boj, Johan H. Van Es, Vivian S.W. Li, Marc Van De Wetering, Toshiro Sato, Karien Hamer, Nobuo Sasaki, Milton J. Finegold, Annelise Haft, Robert G. Vries, Markus Grompe, and Hans Clevers. In vitro expansion of single Lgr5 + liver stem cells induced by Wnt-driven regeneration. *Nature*, 494(7436):247–250, 2013.

[162] Craig Dorrell, Branden Tarlow, Yuhan Wang, Pamela S. Canaday, Annelise Haft, Jonathan Schug, Philip R. Streeter, Milton J. Finegold, Lincoln T. Shenje, Klaus H. Kaestner, and Markus Grompe. The organoid-initiating cells in mouse pancreas and liver are phenotypically and functionally similar. *Stem Cell Research*, 13(2):275 – 283, 2014.

[163] Meritxell Huch, Helmuth Gehart, Ruben Van Boxtel, Karien Hamer, Francis Blokzijl, Monique M.A. Verstegen, Ewa Ellis, Martien Van Wenum, Sabine A. Fuchs, Joep De Ligt, Marc Van De Wetering, Nobuo Sasaki, Susanne J. Boers, Hans Kemperman, Jeroen De Jonge, Jan N.M. Ijzermans, Edward E.S. Nieuwenhuis, Ruurdtje Hoekstra, Stephen Strom, Robert R.G. Vries, Luc J.W. Van Der Laan, Edwin Cuppen, and Hans Clevers. Long-term culture of genome-stable bipotent stem cells from adult human liver. *Cell*, 160(1-2):299–312, 2015.

[164] Wei-Yu Lu, Thomas G Bird, Luke Boulter, Atsunori Tsuchiya, Alicia M Cole, Trevor Hay, Rachel V Guest, Davina Wojtacha, Tak Yung Man, Alison Mackinnon, Rachel A Ridgway, Timothy Kendall, Michael J Williams, Thomas Jamieson, Alex Raven, David C Hay, John P Iredale, Alan R Clarke, Owen J Sansom, and Stuart J Forbes. Hepatic progenitor cells of biliary origin with liver repopulation capacity. *Nature Cell Biology*, 17(8):971–983, 2015.

[165] C. Bart Rountree, Lopa Mishra, and Holger Willenbring. Stem cells in liver diseases and cancer: Recent advances on the path to new therapies. *Hepatology*, 55(1):298–306, 2012.

[166] Ramón Bataller and David A. Brenner. Liver fibrosis. *The Journal of Clinical Investigation*, 115(2):209–218, 2 2005.

[167] Kim E. Barrett. *Chapter 10. Functional Anatomy of the Liver and Biliary System.* The McGraw-Hill Companies, New York, NY, 2014.

[168] Kyo-Sang Yoo, Woo Taek Lim, and Ho Soon Choi. Biology of Cholangiocytes: From Bench to Bedside. *Gut and Liver*, 10(5):687–698, sep 2016.

[169] Chen Liu and James M. Crawford. Liver, anatomy. In Leonard R. Johnson, editor, *Encyclopedia of Gastroenterology*, pages 510–515. Elsevier, New York, 2004.

[170] Anne Müsch. The unique polarity phenotype of hepatocytes. *Experimental Cell Research*, 328(2):276–283, 2014.

[171] Angélique Gougelet, Cyril Torre, Philippe Veber, Chiara Sartor, Laura Bachelot, Pierre-Damien Denechaud, Cécile Godard, Marthe Moldes, Anne-Françoise Burnol, Céline Dubuquoy, Benoit Terris, François Guillonneau, Tao Ye, Michael Schwarz, Albert Braeuning, Christine Perret, and Sabine Colnot. T-cell factor 4 and -catenin chromatin occupancies pattern zonal liver metabolism in mice. *Hepatology*, 59(6):2344–2357, 2014.

[172] Qiuyuan Yang, Shuping Zhang, Juan Ma, Sijin Liu, and Shuguang Chen. In Search of Zonation Markers to Identify Liver Functional Disorders. *Oxidative Medicine and Cellular Longevity*, 2020:9374896, 2020.

[173] Regeant Panday, Chase P. Monckton, and Salman R. Khetani. The Role of Liver Zonation in Physiology, Regeneration, and Disease. *Seminars in Liver Disease*, 42(1):1–16, 2022.

[174] Y. Sasai, M. Eiraku, and H. Suga. In vitro organogenesis in three dimensions: self-organising stem cells. *Development*, 139(22):4111–4121, 2012.

[175] Yoshiki Sasai. Cytosystems dynamics in self-organization of tissue architecture. *Nature*, 493(7432):318–326, 2013.

[176] Ary Marsee, Floris J.M. Roos, Monique M.A. Verstegen, Floris Roos, Monique Verstegen, Hans Clevers, Ludovic Vallier, Takanori Takebe, Meritxell Huch, Weng Chuan Peng, Stuart Forbes, Frédéric Lemaigre, Eelco de Koning, Helmuth Gehart, Luc van der Laan, Bart Spee, Sylvia Boj, Pedro Baptista, Kerstin Schneeberger, Carol Soroka, Markus Heim, Sandro Nuciforo, Kenneth Zaret, Yoshimasa Saito, Matthias Lutolf, Vincenzo Cardinale, Ben Simons, Sven van IJzendoorn, Akihide Kamiya, Hiromi Chikada, Shuyong Wang, Seon Ju Mun, Myung Jin Son, Tamer Tevfik Onder, James Boyer, Toshiro Sato, Nikitas Georgakopoulos, Andre Meneses, Laura Broutier, Luke Boulter, Dominic Grün, Jan IJzermans, Benedetta Artegiani, Ruben van Boxtel, Ewart Kuijk, Guido Carpino, Gary Peltz, Jesus Banales, Nancy Man, Luigi Aloia, Nicholas LaRusso, Gregory George, Casey Rimland, George Yeoh, Anne Grappin-Botton, Daniel Stange, Nicole Prior, Janina E.E. Tirnitz-Parker, Emma Andersson, Chiara Braconi, Nicholas Hannan, Wei Yu Lu, Stephen Strom, Pau Sancho-Bru, Shinichiro Ogawa, Vincenzo Corbo, Madeline Lancaster, Huili Hu, Sabine Fuchs, Delilah Hendriks, Stuart J. Forbes, and Luc J.W. van der Laan. Building consensus on definition and nomenclature of hepatic, pancreatic, and biliary organoids. *Cell Stem Cell*, 28(5):816–832, 2021.

[177] Caleb Jensen and Yong Teng. Is it time to start transitioning from 2d to 3d cell culture? *Frontiers in Molecular Biosciences*, 7, 2020.

[178] Svend Dahl-Jensen and Anne Grapin-Botton. The physics of organoids: a biophysical approach to understanding organogenesis. *Development*, 144(6):946–951, 2017.

[179] Meritxell Huch, Juergen A. Knoblich, Matthias P. Lutolf, and Alfonso Martinez-Arias. The hope and the hype of organoid research. *Development*, 144(6):938–941, 2017.

[180] Silvia Benito-Kwiecinski, Stefano L. Giandomenico, Magdalena Sutcliffe, Erlend S. Riis, Paula Freire-Pritchett, Iva Kelava, Stephanie Wunderlich, Ulrich

Martin, Gregory A. Wray, Kate McDole, and Madeline A. Lancaster. An early cell shape transition drives evolutionary expansion of the human forebrain. *Cell*, 184(8):2084–2102.e19, 2021.

[181] Jorge Lázaro, Maria Costanzo, Marina Sanaki-Matsumiya, Charles Girardot, Masafumi Hayashi, Katsuhiko Hayashi, Sebastian Diecke, Thomas B. Hildebrandt, Giovanna Lazzari, Jun Wu, Stoyan Petkov, Rüdiger Behr, Vikas Trivedi, Mitsuhiro Matsuda, and Miki Ebisuya. A stem cell zoo uncovers intracellular scaling of developmental tempo across mammals. *Cell Stem Cell*, 30(7):938–949.e7, jul 2023.

[182] Yorick Post, Jens Puschhof, Joep Beumer, Harald M. Kerkkamp, Merijn A.G. de Bakker, Julien Slagboom, Buys de Barbanson, Nienke R. Wevers, Xandor M. Spijkers, Thomas Olivier, Taline D. Kazandjian, Stuart Ainsworth, Carmen Lopez Iglesias, Willine J. van de Wetering, Maria C. Heinz, Ravian L. van Ineveld, Regina G.D.M. van Kleef, Harry Begthel, Jeroen Korving, Yotam E. Bar-Ephraim, Walter Getreuer, Anne C. Rios, Remco H.S. Westerink, Hugo J.G. Snippert, Alexander van Oudenaarden, Peter J. Peters, Freek J. Vonk, Jeroen Kool, Michael K. Richardson, Nicholas R. Casewell, and Hans Clevers. Snake venom gland organoids. *Cell*, 180(2):233–247.e21, 2020.

[183] Mitsuhiro Matsuda, Hanako Hayashi, Jordi Garcia-Ojalvo, Kumiko Yoshioka-Kobayashi, Ryoichiro Kageyama, Yoshihiro Yamanaka, Makoto Ikeya, Junya Toguchida, Cantas Alev, and Miki Ebisuya. Species-specific segmentation clock periods are due to differential biochemical reaction speeds. *Science*, 369(6509):1450–1455, 2020.

[184] Atsushi Miyajima, Minoru Tanaka, and Tohru Itoh. Stem/progenitor cells in liver development, homeostasis, regeneration, and reprogramming. *Cell Stem Cell*, 14(5):561–574, 2014.

[185] Lucía Cordero Espinoza. *The mesenchymal regulation of ductal-driven liver regeneration*. Doctoral thesis, University of Cambridge, 2018.

[186] Lenka Belicova, Urska Repnik, Julien Delpierre, Elzbieta Gralinska, Sarah Seifert, José Ignacio Valenzuela, Hernán Andrés Morales-Navarrete, Christian

Franke, Helin Räägel, Evgeniya Shcherbinina, Tatiana Prikazchikova, Victor Koteliansky, Martin Vingron, Yannis L. Kalaidzidis, Timofei Zatsepin, and Marino Zerial. Anisotropic expansion of hepatocyte lumina enforced by apical bulkheads. *Journal of Cell Biology*, 220(10), 07 2021. e202103003.

[187] Jing Shan, Robert E Schwartz, Nathan T Ross, David J Logan, David Thomas, Stephen A Duncan, Trista E North, Wolfram Goessling, Anne E Carpenter, and Sangeeta N Bhatia. Identification of small molecules for human hepatocyte expansion and iPS differentiation. *Nature Chemical Biology*, 9(8):514–520, 2013.

[188] Arif Ibrahim Ardisasmita, Imre F Schene, Indi P Joore, Gautam Kok, Delilah Hendriks, Benedetta Artegiani, Michal Mokry, Edward E S Nieuwenhuis, and Sabine A Fuchs. A comprehensive transcriptomic comparison of hepatocyte model systems improves selection of models for experimental use. *Communications Biology*, 5(1):1094, 2022.

[189] Qin Meng. Three-dimensional culture of hepatocytes for prediction of drug-induced hepatotoxicity. *Expert Opinion on Drug Metabolism & Toxicology*, 6(6):733–746, 2010. PMID: 20380484.

[190] Huili Hu, Helmuth Gehart, Benedetta Artegiani, Carmen LÖpez-Iglesias, Florijn Dekkers, Onur Basak, Johan van Es, Susana M. Chuva de Sousa Lopes, Harry Begthel, Jeroen Korving, Maaike van den Born, Chenhui Zou, Corrine Quirk, Luis Chiriboga, Charles M. Rice, Stephanie Ma, Anne Rios, Peter J. Peters, Ype P. de Jong, and Hans Clevers. Long-term expansion of functional mouse and human hepatocytes as 3d organoids. *Cell*, 175(6):1591–1606.e19, 2018.

[191] Weng Chuan Peng, Catriona Y. Logan, Matt Fish, Teni Anbarchian, Francis Aguisanda, Adrián Álvarez Varela, Peng Wu, Yinhua Jin, Junjie Zhu, Bin Li, Markus Grompe, Bruce Wang, and Roel Nusse. Inflammatory cytokine tnf promotes the long-term expansion of primary hepatocytes in 3d culture. *Cell*, 175(6):1607–1619.e15, 2018.

[192] Laura Broutier, Amanda Andersson-Rolf, Christopher J. Hindley, Sylvia F. Boj, Hans Clevers, Bon Kyoung Koo, and Meritxell Huch. Culture and establishment of self-renewing human and mouse adult liver and pancreas 3D organoids and their genetic manipulation. *Nature Protocols*, 11(9):1724–1743, 2016.

[193] Rowena McBeath, Dana M Pirone, Celeste M Nelson, Kiran Bhadriraju, and Christopher S Chen. Cell shape, cytoskeletal tension, and rhoa regulate stem cell lineage commitment. *Developmental Cell*, 6(4):483–495, 2004.

[194] Irena L. Ivanovska, Joe Swift, Kyle Spinler, Dave Dingal, Sangkyun Cho, and Dennis E. Discher. Cross-linked matrix rigidity and soluble retinoids synergize in nuclear lamina regulation of stem cell differentiation. *Molecular Biology of the Cell*, 28(14):2010–2022, 2017. PMID: 28566555.

[195] Elisabeth E Charrier, Katarzyna Pogoda, Rebecca G Wells, and Paul A Janmey. Control of cell morphology and differentiation by substrates with independently tunable elasticity and viscous dissipation. *Nature Communications*, 9(1):449, 2018.

[196] Aina Ollé-Vila, Salva Duran-Nebreda, Núria Conde-Pueyo, Raúl Montañez, and Ricard Solé. A morphospace for synthetic organs and organoids: the possible and the actual. *Integrative Biology*, 8(4):485–503, 04 2016.

[197] Michael A. Borten, Sameer S. Bajikar, Nobuo Sasaki, Hans Clevers, and Kevin A. Janes. Automated brightfield morphometry of 3D organoid populations by OrganoSeg. *Scientific Reports*, 8(1):1–10, 2018.

[198] Denis Jabaudon and Madeline Lancaster. Exploring landscapes of brain morphogenesis with organoids. *Development*, 145(22), 11 2018. dev172049.

[199] Denise Serra, Urs Mayr, Andrea Boni, Ilya Lukonin, Markus Rempfler, Ludivine Challet Meylan, Michael B Stadler, Petr Strnad, Panagiotis Papasaikas, Dario Vischi, Annick Waldt, Guglielmo Roma, and Prisca Liberali. Self-organization and symmetry breaking in intestinal organoid development. *Nature*, 569(7754):66–72, 2019.

[200] Lauren E. Beck, Jasmine Lee, Christopher Coté, Margaret C. Dunagin, Ilya Lukonin, Nikkita Salla, Marcello K. Chang, Alex J. Hughes, Joseph D. Mornin, Zev J. Gartner, Prisca Liberali, and Arjun Raj. Systematically quantifying morphological features reveals constraints on organoid phenotypes. *Cell Systems*, 13(7):547–560.e3, 2022.

[201] Tzer Han Tan, Jifeng Liu, and Anne Grapin-Botton. Mapping and exploring the organoid state space using synthetic biology. *Seminars in Cell Developmental Biology*, 141:23–32, 2023. Special Issue: Synthetic developmental biology.

[202] Geraldine M. Jowett, Michael D.A. Norman, Tracy T.L. Yu, Patricia Rosell Arévalo, Dominique Hoogland, Suzette T. Lust, Emily Read, Eva Hamrud, Nick J. Walters, Umar Niazi, Matthew Wai Heng Chung, Daniele Marciano, Omer S. Omer, Tomasz Zabinski, Davide Danovi, Graham M. Lord, Jöns Hilborn, Nicholas D. Evans, Cécile A. Dreiss, Laurent Bozec, Oommen P. Oommen, Christian D. Lorenz, Ricardo M.P. da Silva, Joana F. Neves, and Eileen Gentleman. ILC1 drive intestinal epithelial and matrix remodelling. *Nature Materials*, 20(2):250–259, 2021.

[203] Johannes Schindelin, Ignacio Arganda-Carreras, Erwin Frise, Verena Kaynig, Mark Longair, Tobias Pietzsch, Stephan Preibisch, Curtis Rueden, Stephan Saalfeld, Benjamin Schmid, Jean-Yves Tinevez, Daniel James White, Volker Hartenstein, Kevin Eliceiri, Pavel Tomancak, and Albert Cardona. Fiji: an open-source platform for biological-image analysis. *Nature Methods*, 9(7):676–682, 2012.

[204] RStudio Team. *RStudio: Integrated Development Environment for R*. RStudio, PBC, Boston, MA, 2022.

[205] Pedro Gómez-Gálvez, Pablo Vicente-Munuera, Antonio Tagua, Cristina Forja, Ana M Castro, Marta Letrán, Andrea Valencia-Expósito, Clara Grima, Marina Bermúdez-Gallardo, Óscar Serrano-Pérez-Higueras, Florencia Cavodeassi, Sol Sotillos, María D Martín-Bermudo, Alberto Márquez, Javier Buceta, and Luis M Escudero. Author Correction: Scutoids are a geometrical solution to

three-dimensional packing of epithelia. *Nature Communications*, 9(1):4210, 2018.

[206] Christoph Sommer, Christoph N. Straehle, Ullrich Köthe, and Fred A. Hamprecht. ilastik: Interactive learning and segmentation toolkit. In *Eighth IEEE International Symposium on Biomedical Imaging (ISBI 2011).Proceedings*, pages 230–233, 2011. 1.

[207] Davide Heller, Andreas Hoppe, Simon Restrepo, Lorenzo Gatti, Alexander L. Tournier, Nicolas Tapon, Konrad Basler, and Yanlan Mao. EpiTools: An Open-Source Image Analysis Toolkit for Quantifying Epithelial Growth Dynamics. *Developmental Cell*, 36(1):103–116, 2016.

[208] Sébastien Herbert, Léo Valon, Laure Mancini, Nicolas Dray, Paolo Caldarelli, Jérôme Gros, Elric Esposito, Spencer L Shorte, Laure Bally-cuif, Nathalie Aulner, Romain Levayer, and Jean-yves Tinevez. LocalZProjector and DeProj : a toolbox for local 2D projection and accurate morphometrics of large 3D microscopy images. pages 1–13, 2021.

[209] Benoît Aigouy, Reza Farhadifar, Douglas B. Staple, Andreas Sagner, Jens-Christian Röper, Frank Jülicher, and Suzanne Eaton. Cell flow reorients the axis of planar polarity in the wing epithelium of drosophila. *Cell*, 142(5):773–786, 2010.

[210] Benoit Aigouy, Daiki Umetsu, and Suzanne Eaton. *Segmentation and Quantitative Analysis of Epithelial Tissues*, pages 227–239. Springer New York, New York, NY, 2016.

[211] Jeffrey D. Axelrod. Cell shape in proliferating epithelia: A multifaceted problem. *Cell*, 126(4):643–645, 2006.

[212] Matthew C Gibson, Ankit B Patel, Radhika Nagpal, and Norbert Perrimon. The emergence of geometric order in proliferating metazoan epithelia. *Nature*, 442(7106):1038–1041, 2006.

[213] Noushin Dianat, Hélène Dubois-Pot-Schneider, Clara Steichen, Christophe Desterke, Philippe Leclerc, Aurélien Raveux, Laurent Combettes, Anne Weber, Anne Corlu, and Anne Dubart-Kupperschmitt. Generation of functional

cholangiocyte-like cells from human pluripotent stem cells and heparg cells. *Hepatology*, 60(2):700–714, 2014.

[214] Yilan Li, Jennifer S. Ross-Viola, Neil F. Shay, David D. Moore, and Marie-Louise Ricketts. Human cyp3a4 and murine cyp3a11 are regulated by equol and genistein via the pregnane x receptor in a species-specific manner, ,. *The Journal of Nutrition*, 139(5):898–904, 2009.

[215] Ying Wen, Dengjie Ouyang, Qiongyan Zou, Qitong Chen, Na Luo, Hongye He, Munawar Anwar, and Wenjun Yi. A literature review of the promising future of trop2 : a potential drug therapy target. *Annals of Translational Medicine*, 10(24), 2022.

[216] Sára Lenárt, Peter Lenárt, Jan Šmarda, Ján Remšík, Karel Souček, and Petr Beneš. Trop2: Jack of all trades, master of none. *Cancers*, 12(11), 2020.

[217] Yuan Guan, Dan Xu, Phillip M. Garfin, Ursula Ehmer, Melissa Hurwitz, Greg Enns, Sara Michie, Manhong Wu, Ming Zheng, Toshihiko Nishimura, Julien Sage, and Gary Peltz. Human hepatic organoids for the analysis of human genetic diseases. *JCI Insight*, 2(17), 9 2017.

[218]

[219] Eléanor Luce and Anne Dubart-Kupperschmitt. Chapter 4 - pluripotent stem cell-derived cholangiocytes and cholangiocyte organoids. In Jason R. Spence, editor, *Human Pluripotent Stem Cell Derived Organoid Models*, volume 159 of *Methods in Cell Biology*, pages 69–93. Academic Press, 2020.

[220] Muhammad Nadzim Bin Ramli, Yee Siang Lim, Chwee Tat Koe, Deniz Demircioglu, Weiquan Tng, Kevin Andrew Uy Gonzales, Cheng Peow Tan, Iwona Szczerbinska, Hongqing Liang, Einsi Lynn Soe, Zhiping Lu, Chaiyaboot Ariyachet, Ka Man Yu, Shu Hui Koh, Lai Ping Yaw, Nur Halisah Binte Jumat, John Soon Yew Lim, Graham Wright, Asim Shabbir, Yock Young Dan, Huck-Hui Ng, and Yun-Shen Chan. Human pluripotent stem cell-derived organoids as models of liver disease. *Gastroenterology*, 159(4):1471–1486.e12, 2020.

[221] Monique M A Verstegen, Floris J M Roos, Ksenia Burka, Helmuth Gehart, Myrthe Jager, Maaike de Wolf, Marcel J C Bijvelds, Hugo R de Jonge, Arif I

Ardisasmita, Nick A van Huizen, Henk P Roest, Jeroen de Jonge, Michael Koch, Francesco Pampaloni, Sabine A Fuchs, Imre F Schene, Theo M Luider, Hubert P J van der Doef, Frank A J A Bodewes, Ruben H J de Kleine, Bart Spee, Gert-Jan Kremers, Hans Clevers, Jan N M IJzermans, Edwin Cuppen, and Luc J W van der Laan. Human extrahepatic and intrahepatic cholangiocyte organoids show region-specific differentiation potential and model cystic fibrosis-related bile duct disease. *Scientific Reports*, 10(1):21900, 2020.

[222] Casey A. Rimland, Samantha G. Tilson, Carola M. Morell, Rute A. Tomaz, Wei-Yu Lu, Simone E. Adams, Nikitas Georgakopoulos, Francisco Otaizo-Carrasquero, Timothy G. Myers, John R. Ferdinand, Richard L. Gieseck III, Fotios Sampaziotis, Olivia C. Tysoe, Alexander Ross, Judith M. Kraiczy, Brandon Wesley, Daniele Muraro, Matthias Zilbauer, Gabriel C. Oniscu, Nicholas R.F. Hannan, Stuart J. Forbes, Kourosh Saeb-Parsy, Thomas A. Wynn, and Ludovic Vallier. Regional differences in human biliary tissues and corresponding in vitro–derived organoids. *Hepatology*, 73(1):247–267, 2021.

[223] Nduka O. Enemchukwu, Ricardo Cruz-Acuña, Tom Bongiorno, Christopher T. Johnson, José R. García, Todd Sulchek, and Andrés J. García. Synthetic matrices reveal contributions of ECM biophysical and biochemical properties to epithelial morphogenesis. *Journal of Cell Biology*, 212(1):113–124, 2016.

[224] Shauheen S. Soofi, Julie A. Last, Sara J. Liliensiek, Paul F. Nealey, and Christopher J. Murphy. The elastic modulus of matrigel™ as determined by atomic force microscopy. *Journal of Structural Biology*, 167(3):216–219, 2009.

[225] Katie Slater, Jeff Partridge, and Himabindu Nandivada. Tuning the Elastic Moduli of Corning ® Matrigel ® and Collagen I 3D Matrices by Varying the Protein Concentration Application Note. *Corning Incorporated, Life Sciences*, 1(I):1–8, 2018.

[226] M. L. Oyen. Mechanical characterisation of hydrogel materials. *International Materials Reviews*, 59(1):44–59, 2014.

[227] Suzette T. Lust, Dominique Hoogland, Michael D. A. Norman, Caoimhe Kerins, Jasmin Omar, Geraldine M. Jowett, Tracy T. L. Yu, Ziqian Yan,

Jessie Z. Xu, Daniele Marciano, Ricardo M. P. da Silva, Cécile A. Dreiss, Pablo Lamata, Rebecca J. Shipley, and Eileen Gentleman. Selectively cross-linked tetra-peg hydrogels provide control over mechanical strength with minimal impact on diffusivity. *ACS Biomaterials Science & Engineering*, 7(9):4293–4304, 2021. PMID: 34151570.

[228] Katarzyna A. Mosiewicz, Laura Kolb, André J. van der Vlies, and Matthias P. Lutolf. Microscale patterning of hydrogel stiffness through light-triggered uncaging of thiols. *Biomater. Sci.*, 2:1640–1651, 2014.

[229] Matthew G. Ondeck and Adam J. Engler. Mechanical Characterization of a Dynamic and Tunable Methacrylated Hyaluronic Acid Hydrogel. *Journal of Biomechanical Engineering*, 138(2), 01 2016. 021003.

[230] Lisa A Sawicki and April M Kloxin. Light-mediated Formation and Patterning of Hydrogels for Cell Culture Applications. *JoVE*, (115):e54462, 2016.

[231] Meng Yin, John Woollard, Xiaofang Wang, Vicente E. Torres, Peter C. Harris, Christopher J. Ward, Kevin J. Glaser, Armando Manduca, and Richard L. Ehman. Quantitative assessment of hepatic fibrosis in an animal model with magnetic resonance elastography. *Magnetic Resonance in Medicine*, 58(2):346–353, 2007.

[232] Giovanni Sorrentino, Saba Rezakhani, Ece Yildiz, Sandro Nuciforo, Markus H Heim, Matthias P Lutolf, and Kristina Schoonjans. Mechano-modulatory synthetic niches for liver organoid derivation. *Nature Communications*, 11(1):3416, 2020.

[233] Sebastian Mueller and Laurent Sandrin. Liver stiffness: a novel parameter for the diagnosis of liver disease. *Hepatic medicine: evidence and research*, pages 49–67, 2010.

[234] Samuel J.I. Blackford, Tracy T.L. Yu, Michael D.A. Norman, Adam M. Syanda, Michail Manolakakis, Dariusz Lachowski, Ziqian Yan, Yunzhe Guo, Elena Garitta, Federica Riccio, Geraldine M. Jowett, Soon Seng Ng, Santiago Vernia, Armando E. del Río Hernández, Eileen Gentleman, and S. Tamir

Rashid. Rgd density along with substrate stiffness regulate hpsc hepatocyte functionality through yap signalling. *Biomaterials*, 293:121982, 2023.

[235] Richard M Giadone, Derek C Liberti, Taylor M Matte, Jessica D Rosarda, Celia Torres-Arancivia, Sabrina Ghosh, Jolene K Diedrich, Sandra Pankow, Nicholas Skvir, J C Jean, John R Yates III, Andrew A Wilson, Lawreen H Connors, Darrell N Kotton, R Luke Wiseman, and George J Murphy. Expression of Amyloidogenic Transthyretin Drives Hepatic Proteostasis Remodeling in an Induced Pluripotent Stem Cell Model of Systemic Amyloidxa0;Disease. *Stem Cell Reports*, 15(2):515–528, aug 2020.

[236] Asma Nusrat, Charlene Delp, JamesL Madara, et al. Intestinal epithelial restitution. characterization of a cell culture model and mapping of cytoskeletal elements in migrating cells. *The Journal of clinical investigation*, 89(5):1501–1511, 1992.

[237] Visar Ajeti, A. Pasha Tabatabai, Andrew J. Fleszar, Michael F. Staddon, Daniel S. Seara, Cristian Suarez, M. Sulaiman Yousafzai, Dapeng Bi, David R. Kovar, Shiladitya Banerjee, and Michael P. Murrell. Wound healing coordinates actin architectures to regulate mechanical work. *Nature Physics*, 15(7):696–705, 2019.

[238] Gloria M. Slattum and Jody Rosenblatt. Tumour cell invasion: An emerging role for basal epithelial cell extrusion. *Nature Reviews Cancer*, 14(7):495–501, 2014.

[239] Zijun Sun, Christopher Amourda, Murat Shagirov, Yusuke Hara, Timothy E. Saunders, and Yusuke Toyama. Basolateral protrusion and apical contraction cooperatively drive Drosophila germ-band extension. *Nature Cell Biology*, 19(4):375–383, 2017.

[240] Anna M. Dowbaj, Timo N. Kohler, Lucía Cordero-Espinoza, Florian Hollfelder, and Meritxell Huch. Generation of liver mesenchyme and ductal cell organoid co-culture using cell self-aggregation and droplet microfluidics. *STAR Protocols*, 4(2):102333, 2023.